PB 204 011

Catalytic Control of NO_x Emissions from Mobile Sources

FINAL REPORT

by
M. I. Seegall
J. C. Napier
W. A. Coughlin

Prepared for
Environmental Protection Agency
Office of Air Programs
Division of Emission Control Technology

Reproduced by
NATIONAL TECHNICAL
INFORMATION SERVICE
Springfield, Va. 22151

STANDARD TITLE PAGE FOR TECHNICAL REPORTS

1. Report No. EPA-EHS-70-114

2. Govt. Accession No.

3. Recipient's Catalog No.

4. Title and Subtitle

Catalytic Control of NO_x Emissions from Mobile Sources

5. Report Date December 1971

6. Performing Organization Code

7. Author(s) Manfred I. Seegall, James C. Napier, and William A. Compton

8. Performing Organization Rept. No.

9. Performing Organization Name and Address

Solar
Division of International Harvester
2200 Pacific Highway
San Diego, California 92112

10. Project/Task/Work Unit No.

11. Contract/Grant No. EHS-70-114

12. Sponsoring Agency Name and Address

Environmental Protection Agency
Office of Air Programs
2565 Plymouth Road
Ann Arbor, Michigan 48105

13. Type of Report & Period Covered 6/70 to 11/71

14. Sponsoring Agency Code

15. Supplementary Notes

16. Abstracts

This project investigated the use of various catalytic media to control nitrogen oxide emissions from motor vehicles. Laboratory tests of various compounds were conducted. The compounds tested included rare earth oxides, platinum, palladium, copper dichromate, and modified monels.

The modified Monel compounds were found most effective in reducing nitrogen oxides. The ammonia formulation of all these catalysts was also measured and was frequently found significant.

17. Key Words and Document Analysis. (a). Descriptors

Nitrogen oxides
Air Pollution
Catalysts
Motor Vehicle Pollution

17b. Identifiers/Open-Ended Terms

17c. COSATI Field/Group

18. Distribution Statement

Public distribution -no restrictions

19. Security Class (This Report) UNCLASSIFIED

20. Security Class. (This Page) UNCLASSIFIED

21. No. of Pages

22. Price

FORM NBS-867(1-70)

Catalytic Control of NO_x Emissions from Mobile Sources

FINAL REPORT

by

M. I. Seegall
J. C. Napier
W. A. Compton

Details of illustrations in
this document may be better
studied on microfiche

Prepared for
Environmental Protection Agency
Office of Air Programs
Division of Emission Control Technology

IH SOLAR
DIVISION OF INTERNATIONAL HARVESTER COMPANY
2200 PACIFIC HIGHWAY · SAN DIEGO, CALIFORNIA 92112

RDR 1700
December 1971

FOREWORD

This Final Report covers the work performed for the Environmental Protection Agency during the work period July 1, 1970 to July 31, 1971.

The contract with the Research Laboratories of Solar Division of International Harvester Company, San Diego, California, was initiated by EPA under contract number EHS 70-114 and monitored at the start by Mr. Steve Quick, and since November 1970, by Dr. Joseph H. Somers.

The program was under the direction of Mr. W. A. Compton, Assistant Director-Research, who served as Program Director. Mr. M. I. Seegall, Senior Research Engineer, was the principal investigator at Solar. Mr. J. C. Napier, Research Engineer, conducted the catalytic gas reaction tests and collected the material for the ammonia testing. The Reaction Kinetics program was conducted by Dynamic Science, a Division of Marshall Industries. Mr. Edward Fort, Staff Engineer, Engineering Research, International Harvester (Hinsdale, Illinois) acted as a consultant throughout the program, providing valuable data on Otto cycle exhaust composition and general guidance on emission monitoring. Mr. T. E. Duffy, set up and built the apparatus for the measurement of the catalyst surface area and Mr. J. F. Nachman, Chief of Applied Science, wrote most of Appendix E. Special gratitude is due to Mr. J. V. Long, Director-Research, who supported the project and encouraged the research team throughout the entire program.

This report is identified by Solar as RDR 1700.

BLANK PAGE

ABSTRACT

This is a program studying the catalytic approach toward the control of NO_x emissions from motor vehicle exhaust. An investigation of rare earth oxide catalysts and a comparison with selected transition metal and noble metal catalysts for the promotion of the reaction

$$2\,NO + 2\,CO \longrightarrow N_2 + 2\,CO_2$$

was made. The initial criteria for the catalyst were:

a. to have high effectivity for NO reduction;

b. not to be permanently damaged by lead oxide and lead bromide compounds in the exhaust;

c. to be physically stable for long periods in exhaust gases - to last an equivalent of about 50,000 miles of engine operation;

d. to be economical.

Point b, on the compatibility of the catalyst with lead, became less important with the probability that unleaded fuel for catalytic systems will be widely available in 1975.

The study involved the design of experimental equipment for the gas reaction process and for the investigation of physical and chemical properties of the rare earth oxide catalysts. Also included were a theoretical nitric oxide equilibrium analysis, a reaction kinetics study, and a study in concentration of NO, CO, and CO_2 as a function of several reaction parameters of the catalytical gas reaction. The data were analyzed by the non-dispersive infrared (NDIR) analysis method for the concentration of these three gases, and by titration for the measurement of ammonia generated.

The following catalysts were investigated in the course of the program:

- Catalyst RE(23)75-P
- Catalyst RE(M3)75

- Monel 400
- Solar Monel 400 Mod
- Solar Monel 400 Core
- Copper Dichromate, $CuCr_2O_7$
- Palladium Catalyst, 0.5% Pd on Al_2O_3 pellets
- Platinum Catalyst, 0.5% Pt on Al_2O_3 pellets.

The first two catalysts listed represent rare earth oxide formulations.

Although the effectiveness of the rare earth oxide catalysts was less than desired, the goals listed under points b, c and d, were met. The other catalysts evaluated by comparison have been found to possess a higher effectivity, but they fall far short of goals b and c.

The Monel 400 catalysts were found to be substantially more efficient than all others for NO reduction and minimum ammonia formation. The noble metal and copper dichromate catalysts were in the same NO reduction efficiency range, however, ammonia formation for Pt and Pd catalysts were well beyond acceptable limits.

CONTENTS

Section — Page

1 INTRODUCTION 1

1.1 Background 1
1.2 Goals of Solar Program 3

2 THEORETICAL ANALYSIS 5

2.1 Definition of Concepts 5
2.2 Equilibrium Composition Analysis 5
2.3 Study of CO-NO Reaction Kinetics 16

2.3.1 Catalytic Reactor Program -- Thermochemical Calculations 16

2.4 Significance of Theoretical Study of Experimental Work 19

3 EXPERIMENTAL PROCEDURE 21

3.1 Rare Earth Oxide Catalyst Study 21

3.1.1 Catalyst Composition Selection and Screening 21

3.2 Experimental Study With Other Catalysts 29
3.3 The Catalytic Gas Reaction Experiment 29

3.3.1 Gas Flow Apparatus 29
3.3.2 The Synthetic Exhaust Gas Mixture 35
3.3.3 Description of Analytical Apparatus for Emissions Monitoring 40
3.3.4 Procedure for Conducting Experiment 43
3.3.5 Reduction of Data 46

4 EXPERIMENTAL RESULTS 47

4.1 Catalysts and Catalytical Reaction Parameters Investigated 47

4.1.1 Catalysts Considered in the Program 47
4.1.2 Parameters Considered in the Program 47
4.1.3 Parametric Investigation of the NO-Reducing Efficiency of the Catalysts in This Program 48

CONTENTS (Contd)

Section Page

4.2 NO Reduction Efficiency of the Catalysts Tested 50

4.2.1 Experimental Data for Rare Earth Oxide Catalysts 50
4.2.2 Experimental Data for Transition Metal and Noble Metal Catalysts 55

4.3 The Ammonia Generating Factor for all Catalysts Tested 57

5 EVALUATION OF DATA AND DISCUSSION 61

5.1 Evaluation of Experimental Data 61

5.1.1 Graphical Presentation of Catalytical Efficiency Parameters 61

5.1.2 Comparison of Ammonia-Generating Factor E for all Catalysts Tested 70

5.2 Parametric Design Charts for Catalyst Formula RE(23)75-P 72

6 SUMMARY AND CONCLUSIONS 77

REFERENCES 81

APPENDIX A 85

APPENDIX B 95

APPENDIX C 105

APPENDIX D 113

APPENDIX E 127

APPENDIX F 137

ILLUSTRATIONS

Figure		Page
1	Equilibrium Concentration of NO (Y) Vs. Temperature (T)	11
2	Effect of CO/NO Concentration Ratios on NO Equilibrium Concentration Normalized for Y at Ratio of 2	12
3	Effect of Pressure on NO Equilibrium Concentration, Normalized for Y at 1 Atmosphere	13
4	Dependence of NO Equilibrium Concentration of Either N_2 or CO_2	14
5	Influence of Initial Reaction Product Concentration on NO Equilibrium Concentration Normalized to NO Initial Product Concentration	15
6	Rare Earth Oxides as Raw Material for Solar Catalyst Formulas	23
7	Exhibit of Solar Sponsored Catalyst Development Program, Covering Five Formulations, Poisoning Studies, and Raw Materials Utilized	25
8	View of Newly Pelletized REO Catalysts, Segregated by Formula and Preparation Parameters, Prior to Sintering	26
9	Catalyst Samples of Figure 8 After Sintering	28
10	Schematic of Catalytic Gas Reaction Apparatus for Experimentation With Synthetic Exhaust Gas Mixtures	30
11	Detailed Sketch of Catalyst Bed	33
12	Gas Temperature Profile in Catalyst Bed	33
13	General View of Catalytic Gas Reaction Apparatus in Final Version	34
14	Researcher Rolls Safety Screen in Front of Gas Accumulator Underneath Gas Manifold Section of Catalytic Gas Reaction Apparatus	35

ILLUSTRATIONS (Contd)

Figure		Page
15	Main Part of Gas Reaction Apparatus With Flow-Monitoring Section, Catalyst Furnace, Heat Exchanger, and Dynamic and Static Gas Sampling Stations Located in Front of and Behind the Catalyst Furnace	36
16	NO in Exhaust Gas	38
17	Exhaust Gas Composition Typical of S.I. Engine Using Fuel With H/C: 1.9	39
18A	The Non-Dispersive Infrared Radiation Detector and Readout Recorder of the Beckman Gas Analyzer	41
18B	Total View of Beckman Gas Analyzer Including the Flame Ionization Detector for the Measurement of HC Shown at Left	41
19	Principle of Operation of Infrared Analyzers	42
20	The Gas Chromatograph for Static Measurements of Gas Exhaust Components	43
21	Three-Dimensional Schematic Representation of Experimental Conditions for the Testing of Catalysts Noted	49
22	Three-Dimensional Schematic Representation of Experimental Conditions for the Testing of Rare Earth Catalyst Noted	50
23	Three-Dimensional Schematic Representation of Experimental Conditions of Transition Metal and Noble Metal Catalysts	51
24	NO Reducing Efficiency η Versus Flowrate φ for RE(23)75-P	62
25	NO Reducing Efficiency η of Catalyst RE(23)75-P Versus Temperature T, Averaged Over Four Gas Compositions Tested	64
26	NO Reducing Efficiency η of Catalyst RE(23)75-P Versus Temperature T, for Various NO Concentration and CO/NO Ratios R	64
27	Mapping of Catalyst Efficiency η Versus Space Velocity ν Within a Given Temperature and Flowrate Region	65
28	NO-Reducing Efficiency η Versus Flowrate φ	67
29	NO-Reducing Efficiency η Versus Temperature T, for Various NO Concentrations and CO/NO Ratios R	67

ILLUSTRATIONS (Contd)

Figure		Page
30	NO Reducing Efficiency η For the Empty Bed Versus Temperature T, for Various NO Concentrations and CO/NO Ratios R, in the Catalyst Bed in Absence of Catalyst	68
31	Comparison of the NO Reducing Efficiency η as a Function of T for the Various Catalysts Tested	69
32	Version of Parametric Design Chart for RE(23)75-P in Nomograph Form	73
33	Revised Version of Parametric Design Chart for RE(23)75-P	74
B-1	Schematic Diagram of the Apparatus Used for the Determination of Adsorption Isotherms	100
B-2	Adsorption Isotherm for BET Surface Area Measurement of $CuCr_2O_7$ Catalyst	101
B-3	View of BET Surface Area Measurement Apparatus	103
C-1	Solar Catalyst Formulas as they Appeared Before Spalling Test	108
C-2	Components of the Humidity Chamber	109
C-3	Catalyst Formulas Inserted into Humidity Chamber	109
C-4	Solar Catalyst Formulas as they Appeared After Spalling Test	111
D-1	Solar Catalyst RE(23)75-P and Standard Catalyst $CuCr_2O_7$ Before Lead Poisoning Test	116
D-2	The Retort and its Components for the Lead Poisoning Test of the Catalyst	116
D-3	The Boat With the $2PbO-PbBr_2$ is Inserted into the Retort	117
D-4	The Catalyst Boat is Placed on Top of the Boat Containing the Lead Oxide-Lead Bromide, and the Retort is then Covered With the Ceramic Block at Left	118
D-5	Operator Places Retort into Furnace to Melt the Lead Compounds	119
D-6	Retort and Its Contents After the Lead Poisoning Test	120
D-7A	Close-Up of Lead Poisoned Solar Catalyst Formula RE(23)75-P	121
D-7B	Close-Up of Lead Poisoned Standard Catalyst $CuCr_2O_7$	121

ILLUSTRATIONS (Contd)

Figure		Page
D-8	Both Catalysts are Immersed in Dilute Nitric Acid (Dilution 1:1) to Wash Off Poisoning Lead Deposits	122
D-9	Symbolic Representation of Heating Step For Washing of Poisoned Catalysts	123
D-10	Results of Restoration of Poisoned Catalysts	124
D-11	Close-Up of Restored Solar Catalyst Formula RE(23)75-P at Conclusion of Test	125
E-1	Cost of Catalytic Agents of Varying Purity	131
E-2	Economics of Catalysts	134

TABLES

Table		Page
I	Concentration Quantities for Computer Equilibrium Analysis	8
II	Values of the CO-NO Reaction Equilibrium Constant at Constant Pressures Vs. Temperature	9
III	Coding of Rare Earth Oxide Catalyst Formulas	23
IV	Certified Contents of Synthetic Exhaust Gas Components	36
V	Preheater Temperatures Used in Restoring Mixture Values of CO and NO	37
VI	Actually Used Synthetic Exhaust Gas Mixtures for Catalyst NO Reduction Efficiency Experimentation	40
VII	Definition of Gas Mixture Denoted "A"	40
VIII	Flowrate Range	48
IX	The NO-Reducing Efficiency, and Percent Loss of CO, for Catalyst RE(23)75-P at a Flowrate of 9000 cc/min	52
X	NO Reducing Efficiency, and Percent Loss of CO, as a Function of Flowrate for Catalyst RE(23)75-P, at T = 1200° F, Gas Mixture A	53
XI	The NO Reducing Efficiency, and Percent Loss of CO, for Catalyst RE(M3)75 at a flowrate of 9000 cc/min	54
XII	NO Reducing Efficiency, and Percent Loss of CO, as a Function of Flowrate, for Catalyst RE(M3)75, at T = 1200° F, Gas Mixture A	55
XIII	Percent Loss of NO and CO, Versus Gas Mixture and Temperature, for Empty Catalyst Bed, at a Gas Flowrate of 9000 cc/min	56
XIV	Percent Loss of NO and CO, as a Function of Flowrate for Empty Catalyst Bed at T = 1200° F, Gas Mixture A	57

TABLES (Contd)

Table		Page
XV	NO Reducing Efficiency of Selected Transition Metal and Noble Metal Catalysts, Versus Temperature, in Synthetic Exhaust Gas Apparatus	58
XVI	NO Reducing Efficiency of Monel 400 Catalyst in Different Structural Configuration	59
XVII	Ammonia Formation for All Catalysts Studied in this Program at T = 1400° F (Except Where Noted Otherwise), and Gas Flowrate of 9.0 ℓ/min	60
XVIII	Comparison of Ammonia Generation Factor E (in % of NO Re Reduced) for the Various Catalysts Tested and With Preheater Plus Empty Bed Only	71
XIX	State of Art in NO Reducing Catalysts	79
A-I	Iso-Octane/Air Equilibrium Exhaust Composition	88
A-II	Iso-Octane/Air Equilibrium Exhaust Composition	89
A-III	Iso-Octane/Air Equilibrium Exhaust Composition	90
A-IV	Iso-Octane/Air Equilibrium Exhaust Composition	91
A-V	Iso-Octane/Air Equilibrium Exhaust Composition	92
A-VI	Iso-Octane/Air Equilibrium Exhaust Composition	93
B-I	Results of Beta Surface Area Measurements of Catalysts	104
C-I	Weights of Catalysts Before, During and After Spalling Test	110
D-I	Catalyst Weights During Poisoning and Regeneration Experiments, in Grams	121
F-I	Catalyst Effectiveness	141
F-II	Catalyst Effectiveness	142
F-III	NH_3 Production Over Solar Catalysts	143

1

INTRODUCTION

1.1 BACKGROUND

The deterioration of the quality of the air we breathe, and the increase in air pollution, is caused to a significant extent by the emissions of the internal combustion engine, which among other things, powers our automobiles. These mobile sources emit about

- 40 percent of the oxides of nitrogen
- 60 percent of the unburned hydrocarbons, and
- 64 percent of the carbon monoxide,

released daily into the atmosphere within the USA (Ref. 1).

The oxides of nitrogen, in the form of nitric oxide and nitrogen dioxide, absorb ultraviolet radiation from the sun and generate ozone and more nitric oxide, which in turn later oxidizes to nitrogen dioxide again. The ozone oxidizes the unburned hydrocarbons, and thus yields aldehydes and carboxylic acids. Further oxidation of the aldehydes which then combine with NO_2 generates the very noxious peroxyacyl nitrates (PAN) (Ref. 2), and thus all the principal elements of photochemical smog have come into being. Meantime, the oxides of nitrogen, regenerated early in the cycle, produce more ozone, the chemical reactions form a closed loop, and the smog multiplies and spreads.

In order to control this problem, the obvious solution is to eliminate the precursor materials from the engine exhaust, namely NO_x and HC. Since the mobile source population is increasing at a faster rate than the general population, a marked reduction (EPA standards are for 90%) in the emission values of carbon monoxide, oxides of nitrogen, and hydrocarbons will be needed in the next few years in order to prevent further increases in atmospheric contamination. This means that new methods will be required, both for the actual removal of pollutants from the exhaust gases and for preventing the formation of pollutants in the internal combustion engine. It is expected that a combination of these two approaches will be required in order for the existing vehicle power plants to meet the new 1975 Federal standards for exhaust emissions.

The work discussed in this report concerns itself solely with the control of the emission of the oxides of nitrogen, which is created as NO in the internal combustion engine, and oxidized to NO_2 in the air. The mixture of NO plus NO_2 is commonly referred to as NO_x.

Several possible approaches exist for the control of NO_x in the emission gases from mobile sources. The two main ones are the prevention of the formation of NO in the engine, and the decomposition of the NO gas formed, either by dissociation, by recycling, or by catalytic reduction. The Solar program concentrates on the reduction of NO by CO under the action of rare earth based catalysts.

The catalytic reaction under consideration is

$$2NO + 2CO \xrightarrow{\text{catalyst}} N_2 + 2CO_2 + 173\ \text{kcal}$$

This reaction proceeds essentially in two steps, as follows:

$$2NO + 2CO \xrightarrow{\text{catalyst}} CO_2 + 2N$$

$$2N + M \xrightarrow[\text{catalyst}]{} N_2 + M_{\text{catalyst}}$$

with the second reaction being rate controlling. The literature (Ref. 3) describes various iron, copper, and noble metal based oxide catalysts, which take three steps to reduce NO by CO, as follows:

$$2NO + CO \xrightarrow{\text{catalyst}} N_2O + CO_2$$

$$N_2O + CO \xrightarrow{\text{catalyst}} 2N + CO_2$$

$$2N + M \xrightarrow[\text{catalyst}]{} N_2 + M_{\text{catalyst}}$$

The rate controlling step is a function of catalyst temperature, at lower temperatures it is step 2, at higher ones, step 3. Solar's studies of rare earth based catalysts have shown that the three step reduction process of most commercial catalysts does not occur, the two step process is the one controlling the gas reaction.

In addition, since the rare earth based catalyst material has refractory properties, unlike the copper, nickel and iron based ones, it can be reclaimed from lead poisoning by chemical means.

For these reasons, the use of rare earth based catalysts in the control of NO_x emissions from mobile sources has promised to show certain advantages over the conventional commercial catalysts. It is the purpose of this program to demonstrate these advantages, so that this catalyst, either by itself or in combined formulations with other catalysts, can be considered by EPA to reduce NO emissions from motor vehicles.

The use of a catalyst to remove NO from mobile sources is particularly promising since it requires no modification to the engine and might function to control NO emissions while extensive engine modifications and redesigning (or conversion to a different type of power plant) are carried out. In addition, if very low emission levels are required, a system incorporating both low emissions from a properly modified engine and reaction of the exhaust after it leaves the cylinder has practical interest.

1.2 GOALS OF SOLAR PROGRAM

The objectives of this program are limited to the selection of a rare earth oxide catalyst or catalysts from a group of the lighter rare earth oxides, to be used either singly or in certain mixtures, and the study of the nitric oxide reducing efficiency of this catalyst as a function of various parameters. The program goals do not include life tests, road tests and studies of catalyst warm-up times, as has been done in other catalytic investigations described in the literature (Ref. 4, 5, 6, 7).

The study of the efficiency of the rare earth oxide catalyst or catalysts in the reduction of the NO by CO and in part by the hydrogen in the exhaust, includes the initial NO concentration for which two initial levels have been decided upon, namely, concentrations of 1000 and 500 parts per million. The second parameter is the ratio of the CO to the NO concentration. This ratio is related to the air to fuel ratio in an actual exhaust gas mixture. The air to fuel ratio selected for all original testing is close to 14 which gives us a CO/NO ratio of 10. This parameter is varied downward to 5 in order to obtain a true measure of the NO reduction efficiency of the catalyst. As shall be shown in the theoretical section, the equilibrium concentration of NO is a function of the CO/NO ratio and decreases with an increase in the CO/NO ratio. Therefore, a large excess of carbon monoxide aids in the reduction of the nitric oxide to nitrogen and carbon dioxide. The third parameter of importance for the parametric study of the efficiency of the catalyst is the temperature range. The temperature range selected lies between 600 and 1600° F. Finally, the flow rates selected lie between 460 and 18,000 cc per minute, which corresponds for our catalyst bed configuration to automobile flow rates of between 5 to 200 cubic feet per minute.

One of the secondary parameters in the catalytic reduction reaction is the catalyst surface, whereby we are using the maximum surface obtainable under the conditions and methods of the preparation of the catalyst. The goal is to be in the neighborhood of 10 square meters per gram. Another parameter is the effect of competing reactions on our main catalytical reaction. This competing reaction consists of the oxidation of carbon monoxide by the oxygen present in the exhaust gas under the fuel-rich conditions. Thus the "effective" CO/NO ratio is decreased by the oxygen. Another parameter includes the effect of the water vapor on the overall gas reaction kinetics. Another competing reaction is the generation of ammonia by the free hydrogen in the exhaust gas. For our purposes we have introduced pure hydrogen, mixed with nitrogen into our synthetic gas exhaust mixture, in order to see whether the catalyst will generate an appreciable amount of ammonia from the reduced nitric oxide. Experience has shown in the literature cited that the ammonia will be oxidized back to nitric oxide in the oxidizing stage of the double catalyst bed and therefore, a generation of ammonia will reduce the overall NO removing efficiency of the catalyst.

These are the parameters studied in the present program. In the following section we shall introduce the theoretical analysis describing the CO/NO equilibrium conditions and their dependence upon the various parameters defined above and the CO/NO reaction kinetics. This section is followed by the experimental procedure section, which summarizes the studies made on the rare earth oxide catalyst as such and the catalytic gas reaction experiment, including the analytical apparatus and the procedures used to obtain the data. Section 4 discusses the experimental results, first as the function of parameters investigated, second as a reduction efficiency for each of the catalysts selected, and finally the ammonia generation factor for each of the catalysts. Then follows the discussion which will show the relationship of this catalyst to some of the others on the basis of our data. Section 6 concludes this report. The economics of the rare earth oxide catalysts, as well as results of secondary studies regarding their physical and chemical properties, are discussed in the Appendices.

2

THEORETICAL ANALYSIS

In this chapter we shall derive the equilibrium concentration of nitric oxide as a function of various reaction parameters, and calculate the reaction kinetics of our equation $2NO + 2CO \longrightarrow N_2 + CO_2$ using a simulated catalyst.

2.1 DEFINITION OF CONCEPTS

The main concept to be defined is the one of catalytic efficiency. The efficiency can be denoted as the ability of the catalyst to obtain the equilibrium concentration of the reaction rapidly. It is thus a measure of the reduction below the initial NO concentration and toward the equilibrium NO concentration. The catalyst is 100 percent efficient if within a short time (a few seconds) it will reduce the NO concentration down to equilibrium. The equilibrium concentration in turn is defined as the chemically lowest possible concentration of the reagent left after the reaction. It itself is a function of various parameters, as shall be seen in the next section.

Another concept entering into the calculation of the efficiency is the one of the reaction kinetics. This can be defined as a measure of the time rate of progress of the reaction toward equilibrium. The catalytic reaction rate therefore is the difference in the progress of the reaction in the presence and absence of the catalyst. If in the absence of the catalyst the reaction does not proceed at all, as in the case with the NO-CO reaction, then the catalyst determines by itself the reaction kinetics. This concept will be analyzed for a simulated catalyst in Section 2.3.

The conclusion of the chapter will summarize the results and their significance for the experimental determination of reaction efficiency of the rare earth oxide catalysts considered in this program.

2.2 EQUILIBRIUM COMPOSITION ANALYSIS

The equilibrium constant K_p for the reaction

$$CO + NO \longrightarrow \frac{1}{2} N_2 + CO_2 \qquad (1)$$

may be derived in terms of the equilibrium constants with respect to the elements in their standard states. The three equilibrium expressions pertinent to Equation (1) are the following:

$$\frac{1}{2} N_2 + \frac{1}{2} O_2 \rightleftharpoons NO \qquad (P-6)$$

$$C(g) + \frac{1}{2} O_2 \rightleftharpoons CO \qquad (P-9)$$

$$C(g) + O_2 \rightleftharpoons CO_2 \qquad (P-10)$$

where the three elemental reactions are labelled according to Penner's Table of Equilibrium constants (Ref. 8) $K_{P,\#}$, which are constants based on equilibrium pressures, the temperature dependence of which are tabulated in the above reference.

In particular, the following equilibrium constants are tabulated as a function of temperature, which corresponds to the above three equilibrium expressions: (graphite, C(g), which is not a gas, and does not have a partial pressure, thus does not appear in $K_{P,\#}$):

$$K_{P,6} = P_{NO}/(P_{N_2} P_{O_2})^{1/2}, \qquad (2)$$

$$K_{P,9} = P_{CO}/P_{O_2}^{1/2}, \qquad (3)$$

$$K_{P,10} = P_{CO_2}/P_{O_2}. \qquad (4)$$

Combining Equations (2), (3) and (4) yields an expression for K_P, i.e.,

$$K_P = K_{P,10}/K_{P,9}K_{P,6} = (P_{N_2})^{1/2} P_{CO_2}/P_{CO} P_{NO}. \qquad (5)$$

For this analysis it is preferable to work with mole fractions (or percent by volume) instead of partial pressures since the experimental data is in parts per million. The mole fraction of species i is defined as

$$X_i = P_i/P_T, \qquad (6)$$

where P_i is the partial pressure of species i and P_T is the total pressure, i.e.,

$$P_T = \Sigma_i P_i \, . \tag{7}$$

Mole fraction values can be easily converted to parts per million by the relation

$$PPM = X_i \times 10^6 \, . \tag{8}$$

Introducing Equation (6) into Equation (5) leads to the equation

$$P_T^{1/2} K_P = X_{N_2}^{1/2} X_{CO_2} / X_{CO} X_{NO} \, . \tag{9}$$

When equilibrium is reached according to Equation (1), the following mole fractions of each component will be present:

$$\begin{aligned} X_{NO} &= X^{\circ}_{NO} - \zeta, \\ X_{CO} &= X^{\circ}_{CO} - \zeta, \\ X_{N_2} &= X^{\circ}_{N_2} + 1/2\zeta, \\ X_{CO_2} &= X^{\circ}_{CO_2} + \zeta, \end{aligned} \tag{10}$$

where X°_{NO}, X_{CO}, X_{N_2}, and X_{CO_2} represent, respectively, the initial mole fractions of NO, CO, N_2, and CO_2. The above equations indicate that for every ζ mole fraction CO_2 formed, $1/2\zeta$ mole fraction of N_2 is formed, and ζ mole fraction of each, NO and CO, disappears. From Equation (9) it now follows that

$$P_T^{1/2} K_P = (X^{\circ}_{N_2} + 1/2\zeta)^{1/2} (X^{\circ}_{CO_2} + \zeta) \Big/ (X^{\circ}_{NO} - \zeta)(X^{\circ}_{CO} - \zeta) \tag{11}$$

It is evident that, for given values of the total pressure and the equilibrium constant K_P, the value of ζ can be calculated readily for given initial mole fractions of the four reactants.

A computer program has been written for several values of K_P, P, and initial reagent and reactant compositions, over the temperature range between 600 and 1600° F, and a pressure range between 1.0 and 2.0 atmospheres. Table I summarizes the quantities of Equation (10) as they are redefined for the computer program, to simplify the expression in Equation (11).

TABLE I

CONCENTRATION QUANTITIES FOR COMPUTER EQUILIBRIUM ANALYSIS

Quantity	Symbol in Equation (10)	Symbol for Computer Analysis
NO Equilibrium Mole Reaction	X_{NO}	Y
Initial CO Mole Fraction	X°_{CO}	β_1
Initial NO Mole Fraction	X°_{NO}	β_2
Initial N_2 Mole Fraction	$X^{\circ}_{N_2}$	α_1
Initial CO_2 Mole Fraction	$X^{\circ}_{CO_2}$	α_2
Mole Fraction of NO Reduced	ζ	X

Thus, from Equation (11) we obtain, in the new terminology,

$$\left[X^2 + \beta_1\beta_2 - X(\beta_1 + \beta_2)\right] P_T^{1/2} K_P = (\alpha_1 + 1/2X)^{1/2}(\alpha_2 + X) \qquad (12)$$

and $$-Y = X - \beta_2.$$

The expression $X = \beta_2$ is very close to the solution, i.e., the equilibrium concentration of NO approaches zero, therefore

$$(X - \beta_1)(X - \beta_2) = \frac{(\alpha_1 + 1/2\beta_2)^{1/2}(\alpha_2 + \beta_2)}{P_T^{1/2} K_P} = D \qquad (13)$$

If $\beta_1 = \beta_2$,

$$(X - \beta_2)^2 = D; \; -Y = X - \beta_2 = -\sqrt{D}$$

If $\beta_1 \neq \beta_2$,

$$-Y = X - \beta_2 = \frac{-D}{\beta_2 - \beta_1}$$

The temperature dependence of Equation (13) is given by the equilibrium constant K_p, which is listed in Table II in 200° F increments, starting from 600° F and ending at 1600° F. The constant K_p has dimensions of inverse pressure to the 1/2 power and is therefore called K_p for pressure. Equation (13) has been solved for various parameters, as follows:

TABLE II

VALUES OF THE CO-NO REACTION EQUILIBRIUM CONSTANT AT CONSTANT PRESSURES VS. TEMPERATURE

Temperature (° F)	K_p
600	1.688×10^{33}
800	4.28×10^{22}
1000	9.88×10^{18}
1200	1.70×10^{16}
1400	1.54×10^{14}
1600	1.155×10^{12}

The temperature changes from 600 to 1600° F in accordance with the values of Table II for K_p. Pressure values selected are 1 atmosphere, 1.5 atmospheres, 2 atmospheres. The original CO concentration are defined as 0.001 mole fraction, 0.003, 0.006, and 0.010. The original NO concentrations considered is 1,000 parts per million and 500 parts per million. Original concentrations of CO_2, the reaction product, is none and 0.002 mole fraction; the original nitrogen concentrations, another product of the reaction, is in 0, 0.002, and 0.2 mole fractions. The equilibrium concentration has been calculated by means of a computer for all combinations of these points at each temperature, so that the total of 648 points was obtained. The data were then analyzed according to the various parameters introduced. During this analysis, no regard was taken of the fact that the equilibrium concentration computed was negligibly small, which was due to the value of the equilibrium constant K_p. From the tabulation set up by the computer, data were collected for equilibrium concentration Y versus temperature, with all the other parameters held constant. In further analysis it was shown that the value of the NO equilibrium concentration Y was independent for each parameter, and the effect of all the parameters was merely to multiply their total factors to obtain the actual equilibrium concentration in mole fraction for a given set of parameters. Therefore, it was possible to plot the data separately for each parameter varied and this has been done in the following figures.

Figure 1 shows the temperature dependence of the equilibrium NO concentration between 600 and 1600° F. As can be observed from Figure 1, the curve is of a parabolic type; increasing from utmost small numbers in the low temperature range, rapidly at first and slower later, to still very small numbers at the higher temperature range, reaching, for a given set of parameters, the value of 10^{-12} mole fraction for 1600° F. The normalizing set of parameters used is a CO-NO ratio of 2, a gas pressure of 1 atmosphere, and the absence of any initial N_2 and CO_2 concentrations.

After eliminating the effect of the temperature on the NO equilibrium concentration, the factor Y, which is the equilibrium NO concentration, has been normalized to the parameters given above, and the effect of the remaining parameters on it has been plotted out in the following figures.

Figure 2 shows the effect of the CO-NO ratio on the NO equilibrium concentration. Since the CO-NO ratio effect is independent of the temperature, pressure, or any other equilibrium parameter effect, it has been normalized and the change of Y_N, the normalized NO equilibrium concentration versus the CO-NO ratio has been plotted. As can be seen, the CO-NO ratio reduces the NO equilibrium concentration rapidly at first and slower later. It looks similar to an exponential curve. We have had also data for a CO-NO ratio of one, however, in terms of normalized Y_N, the amount is orders of magnitude greater for the CO-NO ratio of one than it is for values of two and higher. In addition, a slight temperature dependence of the CO-NO ratio value of one has been found. However, this temperature dependence disappears for higher values of the ratio, so that a division of the parametric influences could safely be made.

The effect of pressure on the NO equilibrium concentration is shown in Figure 3. As can be seen, with increased pressure the equilibrium concentration is reduced and it decreases to about 70 percent of the value of the pressure data point at 1 atmosphere by the time it reaches 2 atmospheres. This effect, however, is not as pronounced as was the CO-NO ratio effect.

After considering the pressure, temperature, and ratio parameters, the effect of reactant concentrations on the CO-NO reaction and the equilibrium concentration of NO was evaluated. Figure 4 shows the data for NO concentrations between 10^{-3} mole fraction and 0.7 mole fraction of N_2. Similarly, the data for CO_2 go from

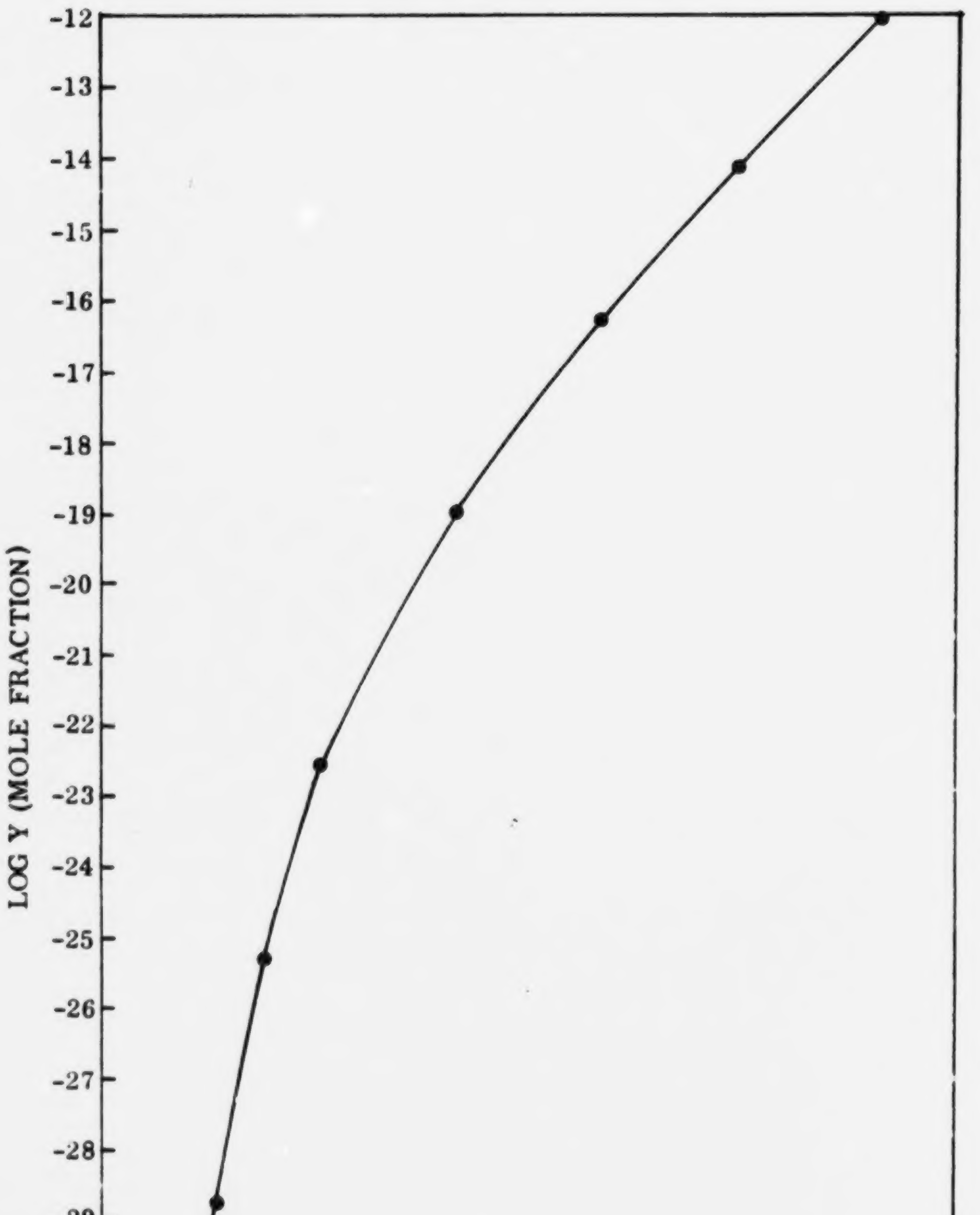

FIGURE 1. EQUILIBRIUM CONCENTRATION OF NO (Y) VS. TEMPERATURE (T)

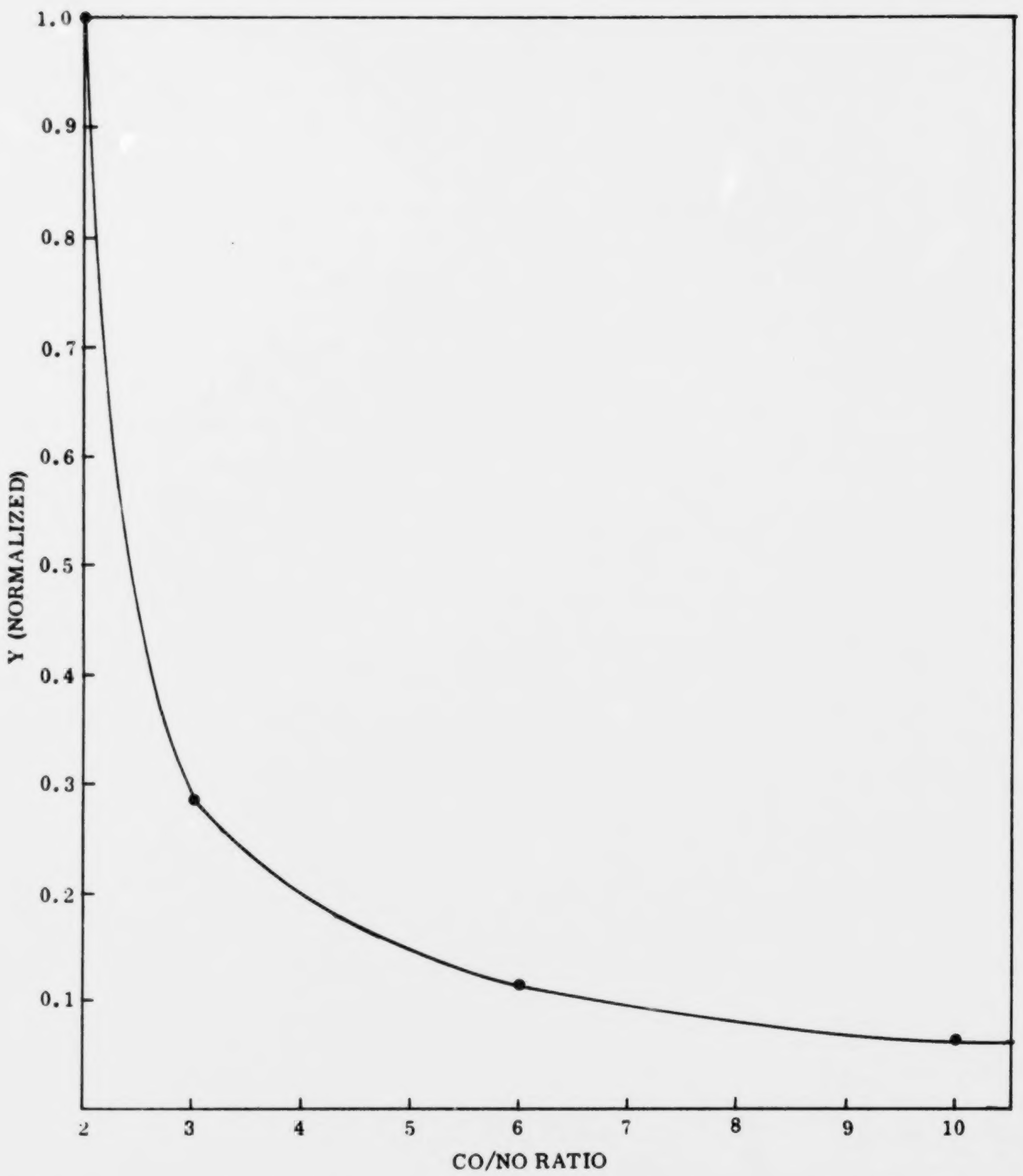

FIGURE 2. EFFECT OF CO/NO CONCENTRATION RATIOS ON NO EQUILIBRIUM CONCENTRATION NORMALIZED FOR Y AT RATIO OF 2

a mole fraction of 10^{-3} to mole fraction of 0.2 with an extension to 0.7 also. In normal conditions, the N_2 concentration would be 0.7 mole, or 70 percent of nitrogen in the exhaust gas; the initial CO_2 concentration would be about 14 percent or 0.14 mole. Figure 4 shows the increase in the NO equilibrium concentration normalized to zero CO_2 and zero N_2, with increases in N_2, but CO_2 remaining constant at zero, which is the top curve; and increase in CO_2 concentration with N_2 remaining a constant at zero in the bottom curve. As can be seen, the N_2 concentration has a bigger effect

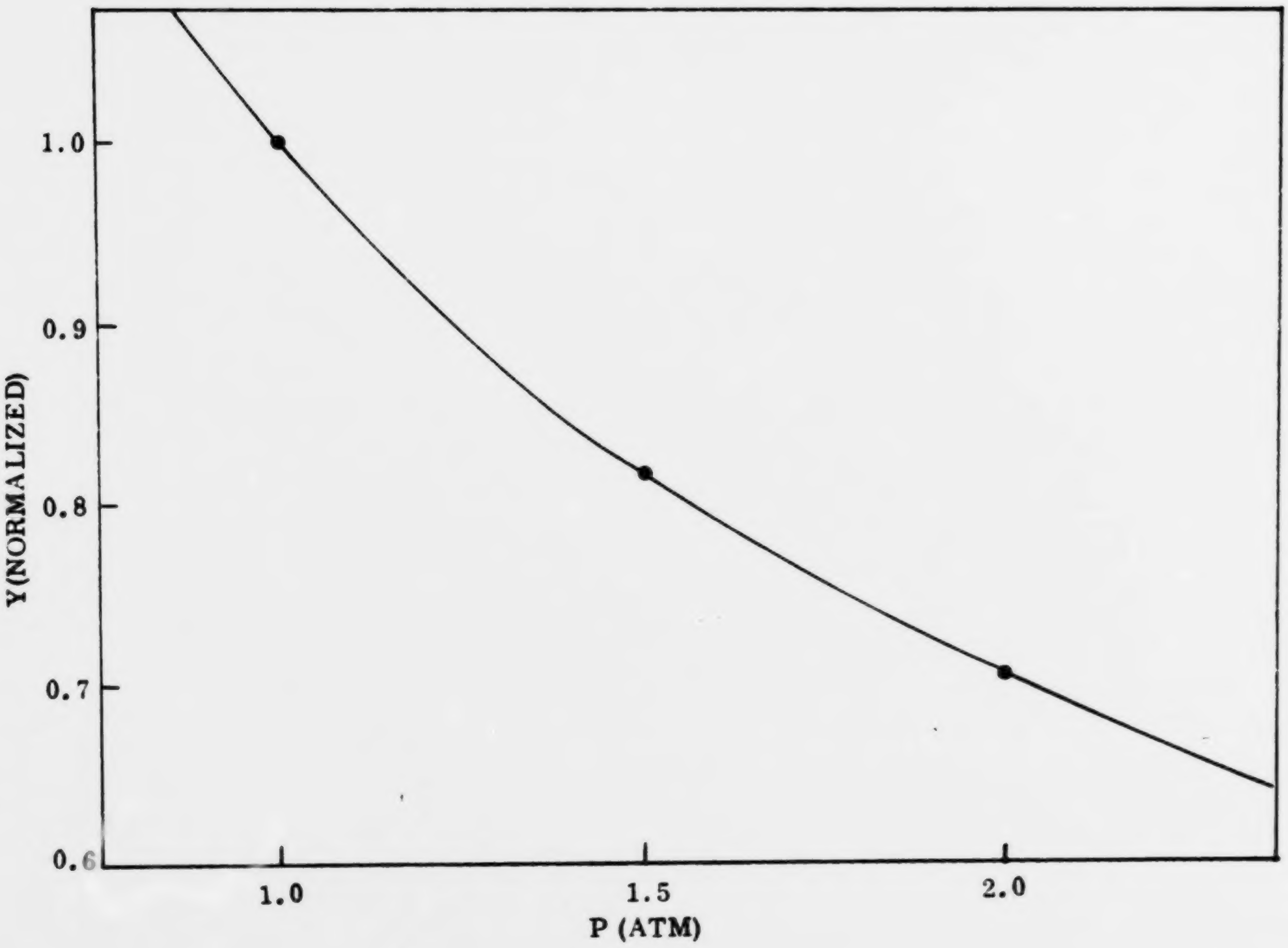

FIGURE 3. EFFECT OF PRESSURE ON NO EQUILIBRIUM CONCENTRATION, NORMALIZED FOR Y AT 1 ATMOSPHERE

on the NO equilibrium concentrations than the CO_2 concentration. From the observation that the effect of the combined N_2 and CO_2 the concentrations on Y_N equals the product of both parameters taken separately, several graphs have been selected for Figure 5, where the NO equilibrium concentration is shown as a function of initial N_2 and initial CO_2 concentration. The N_2 concentration ranges continuously from 10^{-3} to 0.7 mole fraction. Selected values for the CO_2 concentration from zero to 0.1 mole fraction have been chosen.

This analysis shows that, in order to obtain the equilibrium NO concentration at a given set of parameters, the value from Figure 1 for the temperature is multiplied by the Y_N value for the ratio effect in Figure 2, the pressure effect in Figure 3, the initial nitrogen concentration effect and the CO_2 concentration effects in Figure 4, and thus for any given set, the NO equilibrium concentration Y is obtained. We shall give some examples of this below.

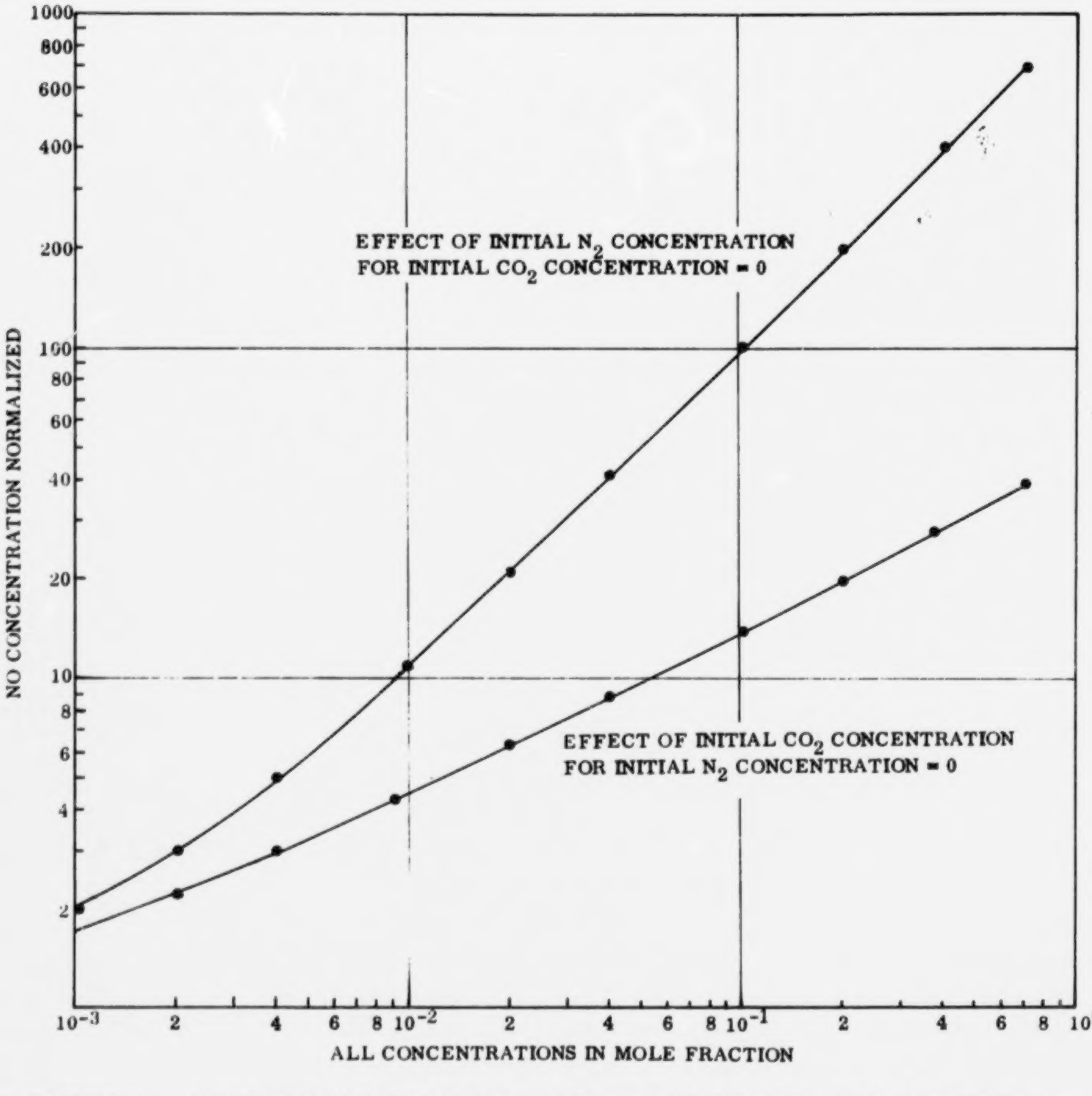

FIGURE 4. DEPENDENCE OF NO EQUILIBRIUM CONCENTRATION OF EITHER N_2 OR CO_2

As our discussion has shown, the equilibrium concentration of NO for various values of T, P, R, N_2, and CO_2 initially is given by:

$$NO_{[equil.]} = Y(T)Y_N(P)Y_N(R)Y_N(N_2)Y_N(CO_2)$$

These values are given in Figures 1 through 4. We shall demonstrate this on the following examples:

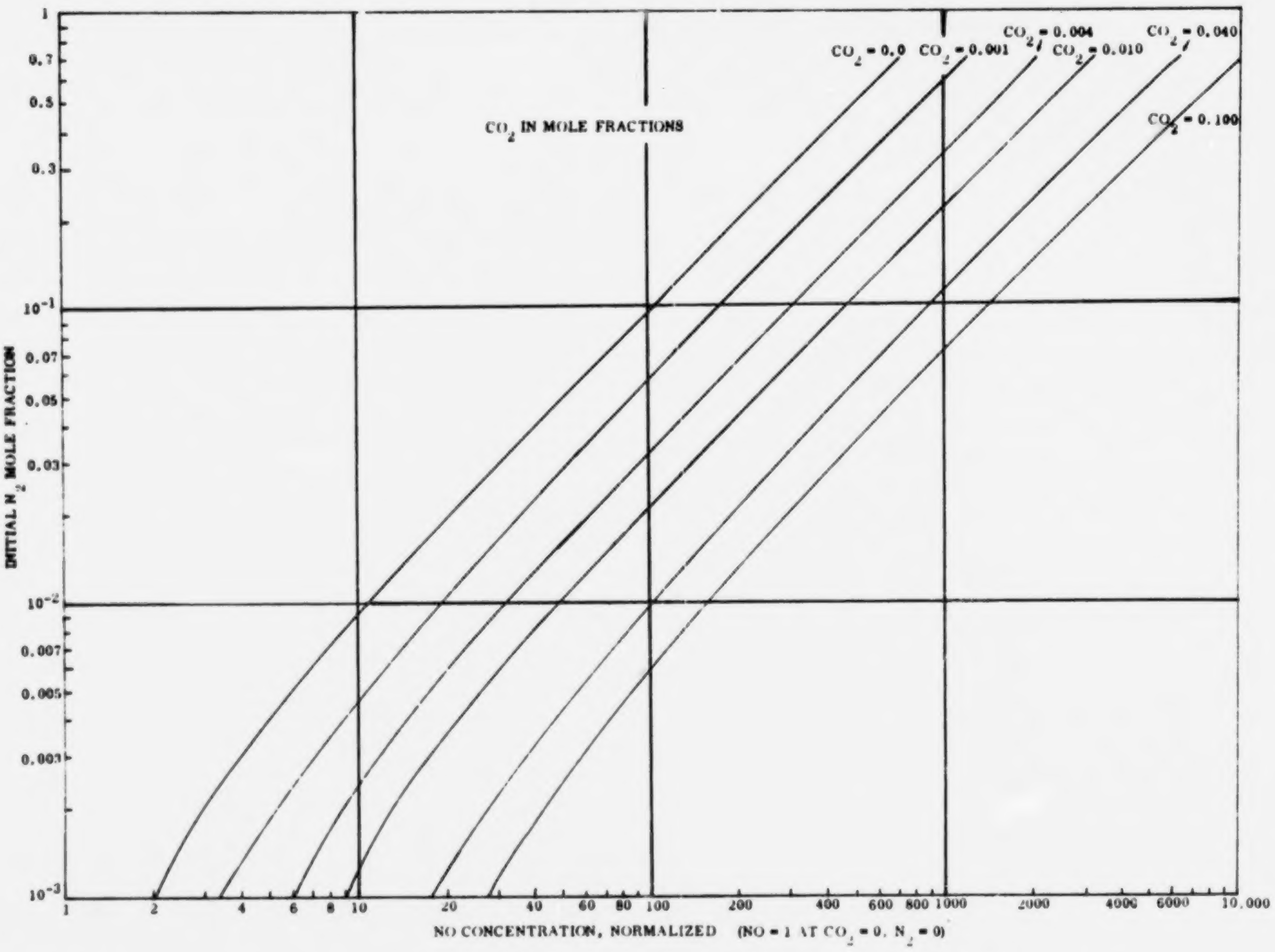

FIGURE 5. INFLUENCE OF INITIAL REACTION PRODUCT CONCENTRATION ON NO EQUILIBRIUM CONCENTRATION NORMALIZED TO NO INITIAL PRODUCT CONCENTRATION

1. At T = 1000° F, R = 3, P = 1 atm., CO_2 = 0 moles, N_2 = 0 moles.

   From the figures we find mole fraction of

   $Y(T) = 10^{-19}$

   $Y_N(R) = 0.29$

   $Y_N(P) = 1$

   $Y_N(N_2) = 1$

   $Y_N(CO_2) = 1$

Therefore, the mole fraction of

$$NO_{[equil.]} = 10^{-19} \times 0.29 \times 1 \times 1 \times 1 = 2.9 \times 10^{-20}.$$

2. In the above example, we have an initial concentration of $CO_2 = 0.01$, and $N_2 = 0.70$ mole fraction. Then $Y_N(N_2) = 700$, $Y_N(CO_2) = 4.6$, and the mole fraction of

$$NO_{[equil.]} = 10^{-19} \times 0.29 \times 1 \times 700 \times 4.6 = 9.3 \times 10^{-17}.$$

3. At T = 1600° F, P = 1.25 atm., R = 2, $CO_2 = 0.02$, $N_2 - 0.70$. Here we find mole fraction of

$$Y(T) = 10^{-12}$$

$$Y_N(P) = 0.89$$

$$Y_N(R) = 1$$

$$Y_N(N_2) = 700$$

$$Y_N(CO_2) = 6.4$$

and the mole fraction of

$$NO_{[equil.]} = 10^{-12} \times 0.89 \times 1 \times 700 \times 6.4 = 3.987 \times 10^{-9}$$

or about 4 parts per billion.

It may be observed that for the conditions of Example 3, the NO equilibrium concentration no longer is significantly small, and for a CO/NO ratio of 1 will grow into the ppm range.

2.3 STUDY OF CO-NO REACTION KINETICS

2.3.1 Catalytic Reactor Program -- Thermochemical Calculations

The work accomplished has centered on estimating the effect of the preheater located upstream of the catalytic reactor on the composition of a simulated exhaust gas mixed at room temperature. The variables are initial concentration, preheater temperature, and residence time at temperature. The procedure then was to use the Dynamic Science Generalized Kinetics Program to predict the change in equilibrium concentration of a gas mixture when heated to automotive exhaust temperatures.

The initial effort was to gather data representative of the range of automotive exhaust emissions. This provided a realistic basis for the simulation of automobile exhaust in terms of the trace contaminant species (CO, NO_x, HC). Most of the data presented in Volume 6 and 12 of the SAE Technical Progress Series on exhaust emissions were compiled. Several distinct operating modes were recognized; these being: idle, cruise at 30, 50 and 60 mph, acceleration and deceleration from low velocity (30 mph) and high velocity (50 mph).

Generally CO decreases as automobile speed increases. During acceleration and deceleration, CO reaches levels near those at idle (nearly 10% of entire exhaust composition). NO generally increases with velocity but is very low ($\approx$50 ppm) on deceleration and at idle. Unburned hydrocarbon measurements show that the trend is generally toward decreasing HC with velocity. Increases are noted during acceleration. HC measurements during deceleration from high velocity are an order of magnitude higher than all the others (Ref. 9). These results then represent a rather large scale summary of existing measured emission levels. To assess preheater effects, it is necessary to define the rest of the chemical system, i.e., major species concentrations.

A series of chemical equilibrium calculations was made for two reasons:

1. To determine the major species concentrations in the exhaust which are at or very near equilibrium values.

2. Determine the degree of departure of the measured emission data from equilibrium concentrations; for if the measured values are in equilibrium at the exhaust temperature, no conversion can occur in the reactor.

A scattering of computer runs, designed to look at the range of exhaust conditions, were made with the Generalized Kinetics Program. The results, in tabular form, are given in Appendix A. Since a wide scattering of conditions were run, the presentation of these restults in graphical format was difficult, and the tabular form (Table A-I) preferred. In summary, the results show, however, that:

1. Nonequilibrium CO and NO are "frozen" in the exhaust gases at temperatures and times representative of the preheater in the absence of oxygen.

2. At temperatures higher than approximately 1600° F, trace amounts of oxygen can oxidize from 10-50 percent of the initial CO to CO_2.

3. The addition of oxygen has no effect on the NO and only affects CO.

4. At A/F ratio of 14 ammonia generation is limited to the lower temperatures and does not exceed 20 ppm. At richer A/F ratios, NH_3 concentration may reach up to 30 ppm.

2.3.2 Effect of Gas Phase Reactions on Simulated Catalytic Conversion of NO

A crude attempt was made to assess whether gas phase reactions would effect the catalytic conversion of NO. For this evaluation, the catalytic process was first modeled by assuming the catalyst affected only the reaction:

$$NO + CO \xrightarrow{k} CO_2 + N \qquad (14)$$

The rate constant k was determined by integrating, in closed form, the rate expression for [NO].

$$\frac{d[NO]}{dt} = -[NO][CO]\,k$$

which gives

$$k = \frac{1}{t[CO]} \log \frac{[NO]_{initial}}{[NO]_{final}} \qquad (15)$$

It was then assumed that the catalytic reactor would reduce [NO] to approximately 10 percent of its initial value in 0.1 sec, i.e., $[NO]_{final}/[NO]_{initial} \approx 0.1$ for t = 100 msec. Using these values, an effective rate constant k was computed. This k was then the input into the kinetics program for the reaction $NO + CO \rightarrow CO_2 + N$, along with the other gas phase reactions and the program was then run for 100 milliseconds. The calculated concentration of NO after this time interval for an initial NO concentration of 7.12×10^{15} molecule/cc(~1000 ppm) was 1.58×10^{14} molecule/cc as compared to an NO concentration of 8.47×10^{14} molecule/cc computed using Equation (16). This result was somewhat surprising, since it indicates that the gas phase reactions accelerate the catalytic NO conversion process.

In order to evaluate whether this conclusion was valid or only a result of the constraints on the chemistry due to the input catalytic reaction, a second set of calculations were made. For these calculations, the reaction

$$2NO + 2CO \xrightarrow{k^1} 2CO_2 + N_2 \qquad (16)$$

was used to represent the catalytic reaction, thereby eliminating the production of free N atoms (which could reduce the NO concentration by reactions such as $N + NO = N_2 + O$). The rate constant for this reaction k^1 was similarly evaluated by a closed form integration for $[NO]_{final}/[NO]_{initial} \approx 0.1$, at t = 100 msec. This constant and reaction (16) were input into the final kinetics program using the same initial conditions used previously. This calculation yielded an NO concentration of 2.12×10^{14} molecule/cc compared to 3.78×10^{14} molecule/cc for the closed form calculation. Again the kinetic NO concentration is lower, indicating a gas phase enhancement of the NO conversion.

2.4 SIGNIFICANCE OF THEORETICAL STUDY OF EXPERIMENTAL WORK

The data of the theoretical analysis in the previous two sections make it possible to practically define the reaction efficiency of the catalyst studied experimentally. Regarding the equilibrium concentration of the nitric oxide, it is zero on our scale, which is in the parts per million range. The catalytic efficiency therefore can be defined as the ratio of the difference of the initial minus the final concentration of the nitric oxide with the initial concentration of nitric oxide, multiplied by 100 percent.

As far as the reaction kinetics is concerned, there is none without the catalyst for the reaction under study. Therefore, the catalyst is the sole determining factor of the reaction kinetics, and can be evaluated accordingly. Finally, regarding the competing reactions, the analysis showed that some of the secondary reactions are supporting our basic relation and some are hindering the catalytic action. This particular result is important, since no single reaction component experiments were being run, but the experiment was run in the total synthetic exhaust gas mixture containing all the components of such a mixture. The effect of the ammonium generation as a fraction of the nitric oxide reduced, which is another competing reaction, was not considered in the reaction kinetic program as such.

We shall now proceed with the discussion of the experimental phase of the program.

BLANK PAGE

3

EXPERIMENTAL PROCEDURE

The experimental part of the program was divided essentially into two phases: the rare earth oxide catalyst study and the study of the gas reaction. Therefore, this chapter will discuss first the screening and selection of the rare earth catalyst, briefly summarize its properties, and then pass on to the description of the experimental procedure and apparatus. The actual data obtained from the catalytical gas reaction study, as well as the ammonia generation factor, will be discussed in the next chapter, headed Experimental Results.

3.1 RARE EARTH OXIDE CATALYST STUDY

3.1.1 Catalyst Composition Selection and Screening

In selecting a catalyst for the reduction of NO by CO, the following criteria originally were used by Solar:

The catalyst should be stable and refractory

The catalyst should be able to be regenerated after poisoning.

Based on these criteria, the best class of catalyst material suited under these conditions appeared to be the class of the rare earth oxide catalysts. In the following sections, we shall describe our choice of the rare earth oxide catalysts, the way we coded the catalyst formulas, the narrowing down of the selection of the REO catalyst, and the economics of the REO catalyst compared with other standard catalytical materials.

(a) Choice of Rare Earth Oxides

In the group of rare earth oxides, the light rare earth oxides are of special interest because they contain two elemental oxides which are highly unstable and therefore very well suited for catalytic action. The instability is a phase change between various of the oxidation stages, i.e., as a function of temperature and oxygen pressure, the element increases its valence for oxygen or decreases it. The two elements of interest are cerium and praseodymium. Especially in the case of

Preceding page blank

praseodymium, various phase changes can be noted, whereby the degree of oxidation of the praseodymium varies from PrO_2 to Pr_2O_3. The change from one to the other does not occur in one step but in several steps (Ref. 10). The change from PrO_2 to $PrO_{1.5}$ occurs in nine steps or nine phases, which are designated in order from the original PrO_2 phase, which is the alpha-phase, along the Greek alphabet as beta, gamma, delta, epsilon, phi, sigma, pi, and theta. Pi and theta are two forms of $PrO_{1.5}$. Due to these various phase changes, the praseodymium oxide is very often denoted PrO_x, where the x can have any value between 1.5 and 2. Most common is the value of $x = 1.833$, which is also written as Pr_6O_{11}. Other values of x are 1.8, 1.78, 1.71, 1.70, 1.67, and 1.5. In a similar fashion, but not quite as complicated, the cerium oxide switches its oxygen content between CeO_2 and Ce_2O_3. The Ce_2O_3 oxide is white in color, while the CeO_2 is a light yellow. Similarly, the Pr_6O_{11} is a black powder and the Pr_2O_3 is a light green one. The neighboring oxides, including those of lanthanum and neodymium, and the combination of praseodymium and neodymium known as didymium, have also been studied in this connection.

The raw materials from which our catalysts are formulated, are shown in Figure 6. The upper row shows the pure rare earth oxides of 99 percent purity, namely, from left to right, the white La_2O_3, the light yellow CeO_2, the black Pr_6O_{11}, and the light blue Nd_2O_3. The bottom row shows commercially available mixed oxides which we are also using due to their economy, namely the yellowish brown commercial didymium oxide on the left, and the reddish brown mixed rare earth oxide on the right.

(b) Coding of the Catalyst Formulas

The catalyst formulas based on the light rare earth oxides, especially the four mentioned, have been coded with a designation of RE(a number). RE stands for a pure rare earth oxide formula, and the value of the number in parentheses following the RE is shown in Table III. In the case where the number in parentheses ends in 0, a pure rare earth oxide of the particular element, as shown in Table III, is being considered. If the number in parentheses is two digits, neither of which is 0, the formula contains the two rare earth oxides designated. RE(43) denotes the didymium oxide, whereby the majority oxide present is the neodymium. Formula RE(43)M denotes a commercial mixture of the didymium oxide which, beside neodymium and praseodymium, contains especially lanthanum and a number of other rare earth oxides, and only a trace of cerium oxide. The majority oxides in this case is lanthanum and neodymium. In Solar Formula No. 8, the cerium oxide is the majority. The formula RE(M) denotes a commercially available mixed rare earth oxide, wherein the majority component is cerium oxide, followed by those of lanthanum and neodymium. The Solar Formula No. 10 consists of a mixture of these mixed oxides with pure praseodymium oxide. Therefore, the number in parentheses is M3. The mixed oxides are the majority component in this particular formula. In the study reported here, we have

NOT REPRODUCIBLE

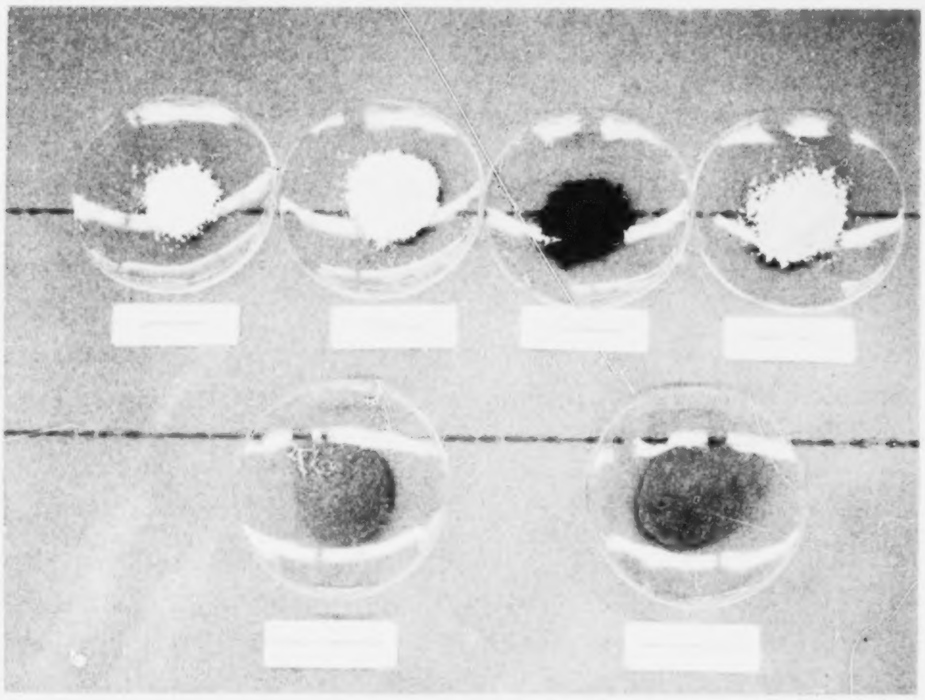

FIGURE 6. RARE EARTH OXIDES AS RAW MATERIAL FOR SOLAR CATALYST FORMULAS

TABLE III

CODING OF RARE EARTH OXIDE CATALYST FORMULAS

Formula	Component	
	Symbol	Name
RE(10)	La_2O_3	Lanthanum Oxide
RE(20)	CeO_2	Cerium Oxide
RE(30)	PrO_x	Praseodymium Oxide
RE(40)	Nd_2O_3	Neodymium Oxide
RE(43)	$Nd_2O_3 + PrO_x$ (D_2O_3)	Didymium Oxide, Pure
RE(43)M	D_2O_3	Didymium Oxide, Commercial
RE(23)75	$CeO_2 + PrO_x$	Solar Formula No. 8
RE(M)	REO	Mixed Rare-Earth Oxides
RE(M3)75	REO + PrO_x	Solar Formula No. 10

been concentrating on the pure and commercial didymium and on Solar Formula No. 8 and 10. The total catalyst producing effort, and its result, is shown in Figure 7 which encompasses all RE catalyst formulations prepared for this program.

(c) Elimination of Various Formulations and Selection of Catalysts to be Studied

Elimination of Pure Elemental Oxides. Formulas RE(20) and RE(30) each showed good catalytic testing and catalytic properties in early testing. However, their combination, RE(23), was superior in performance to that of each of their components and reduced the lower temperature threshold of catalytic activity by 100° F. Therefore, the pure elemental oxides, RE(20) and RE(30), were not considered for the program in their unmixed state.

Formula RE(10) by itself had not been tested; when added, however, to Formula RE(20), which resulted in the formulation called RE(21)75, it was found that the overall catalytic efficiency of RE(21) was lower than that of the pure oxide formula RE(20). Thus, RE(10) served merely to dilute the efficiency of the pure CeO_2, and on this ground the elemental oxide RE(10) was eliminated.

Elimination of Simple Oxide Mixtures. Didymium oxide, RE(43), comes in the form of a mixture of pure oxides, the latter of which contains a quantity of neodymium oxide. In Table III, our formula RE(43) denotes the pure didymium oxide, and RE(43)M, the commercial mixed oxides containin formulation. Both formulas were eliminated on the basis of the physical unstability due to hydration causing the pellets to disintegrate. Formula RE(M), the commercially available mixture of RE oxides consists principally of cerium oxide and lanthanum oxide, with smaller admixtures of the more abundant rare earth oxides and a low praseodymium oxide content. This essentially diluted the cerium oxide, and the conclusions reached for formula RE(21) are valid for RE(M) also, causing its elimination. An enrichment of RE(M) with RE(30) however, resulted in the effective and economical formulation of RE(M3), which remained in the program.

Finally, the low purity RE(23)75 catalyst as designated in Table III, Solar formula No. 8, was eliminated due to lack of sufficient spalling resistance, which shall be shown in Appendix C, and the presence of a low melting impurity in the formula, which interferred with its processing and its effective surface area.

RE Catalysts Evaluated for Their NO Reducing Efficiency. The catalyst formulas selected for further study are thus the following:

First, RE(23)75-P -- a high purity oxide mixture of cerium dioxide and praeseodymium oxide and second, RE(M3)75, a mixed oxide variation of the above mentioned formulation, which has better economic features.

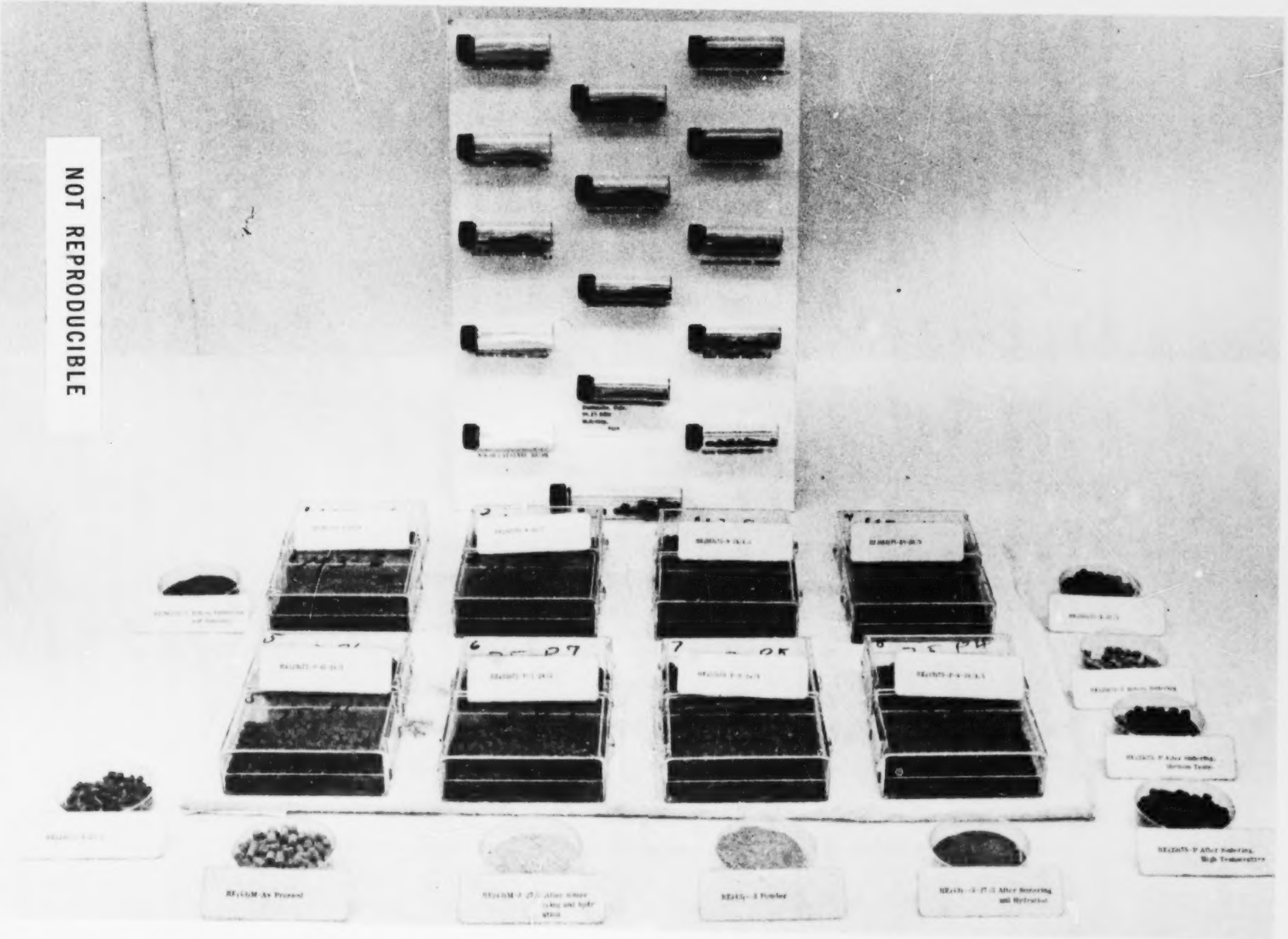

NOT REPRODUCIBLE

FIGURE 7. EXHIBIT OF SOLAR SPONSORED CATALYST DEVELOPMENT PROGRAM, COVERING FIVE FORMULATIONS, POISONING STUDIES, AND RAW MATERIALS UTILIZED

3.1.2 Catalyst Form

The selected catalyst formulations have been sintered into pellet form, a right circular cylinder, of radius of 0.1 inch and height of 0.2 inch.

Variations in the preparation of parameters of the catalyst pellets have been made with the object of increasing the surface area. The preparation parameters have been changed in various steps in order to obtain a surface area comparable with that of the copper dichromate. The parameters were changed for both rare earth catalyst formulas, the pure RE(23)75-P and the mixed RE(M3)75. Hence, four variations in the preparation parameters have been decided upon and executed for each of the two formulas being used. The result is a grouping of eight various catalysts. These have been pelletized and prepared for sintering, as shown in Figure 8.

The first row on top shows the grayish formula RE(23)75-P, and the second row the dark brown formula RE(M3)75. Each two boxes contain one-half pound of catalyst and these same pairs of boxes contain catalysts made under the same preparation conditions. The preparation parameters vary from one groupof two boxes to the next.

The catalyst pellets are shown as they appeared after completion of sintering in Figure 9. Formula RE(23)75-P has turned black, while RE(M3)75 is now reddish brown.

The results of the variation of the catalyst preparation parameters on the surface area indicated only a limited success within the parameter range selected. The two RE catalyst formulations showed a greater difference in surface area among themselves, than the variation in preparation parameters could achieve for either of them.

3.1.3 Rare Earth Oxide Catalyst Properties

(a) Surface Area

The catalyst surface area was measured by the BET method for both rare earth oxide formulations and the copper dichromate. Details are given in Appendix B. The results are that for catalyst RE(M3)75 the surface areas were found to be in the range from 0.1 to 0.2 m^2/gram, for catalyst RE(23)75-P in the range between 0.4 and 0.8 m^2/gram, and for $CuCr_2O_7$ at 11 m^2/gram. The range for the rare earth catalyst was obtained in part by the variation of the preparation parameters, mentioned in the prior subsections.

NOT REPRODUCIBLE

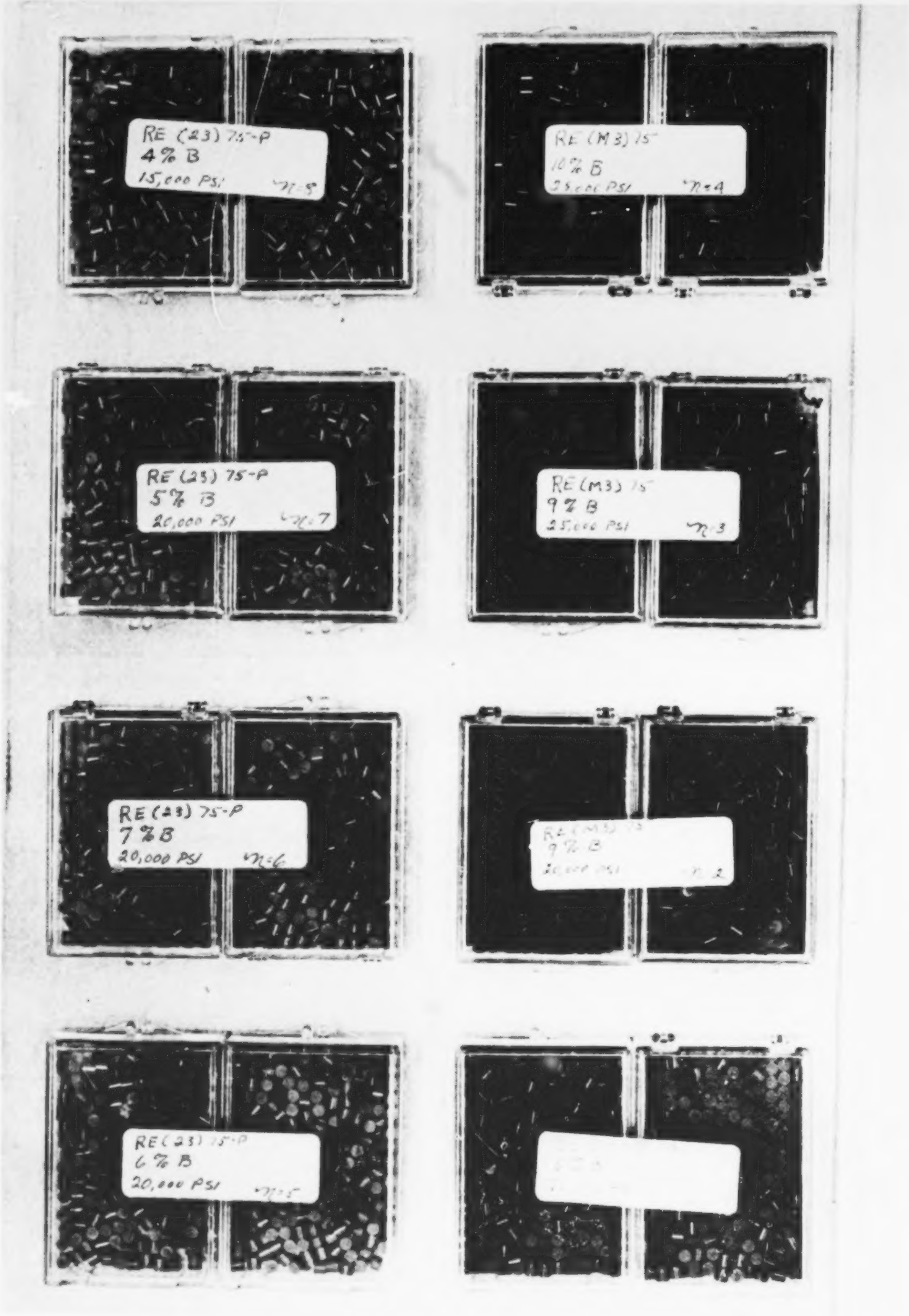
RE (23) 75-P
4% B
15,000 PSI
n=8
RE (M3) 75
10% B
25,000 PSI
n=4
RE (23) 75-P
5% B
20,000 PSI
n=7
RE (M3) 75
9% B
25,000 PSI
n=3
RE (23) 75-P
7% B
20,000 PSI
n=6
RE (M3) 75
9% B
20,000 PSI
n=2
RE (23) 75-P
6% B
20,000 PSI
n=5

FIGURE 8. VIEW OF NEWLY PELLETIZED REO CATALYSTS, SEGREGATED BY FORMULA AND PREPARATION PARAMETERS, PRIOR TO SINTERING

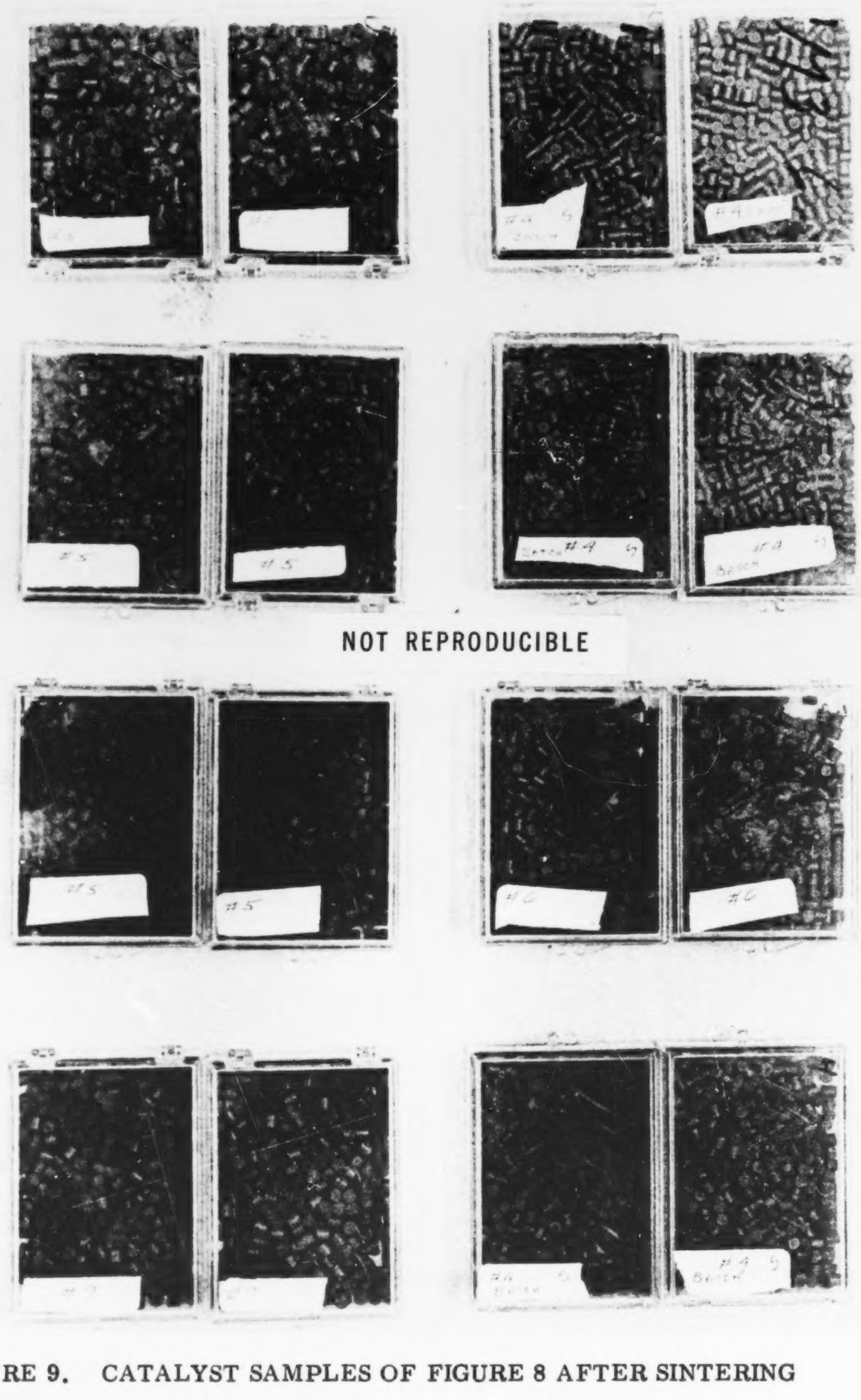
#5
#5
#5
#5
#5
#5
Batch #4
#4 Batch
#6
#6
#4 Batch
#4 Batch

NOT REPRODUCIBLE

FIGURE 9. CATALYST SAMPLES OF FIGURE 8 AFTER SINTERING

(b) Mechanical Properties - Spalling Resistance

Details of the measurement on spalling resistance are presented in Appendix C. Of the two rare earth oxide formulations of interest, RE(23)75-P showed the best resistance to cracking due to the influence of atmospheric water vapor.

(c) Chemical Properties - Lead Poisoning and Regeneration Study

A study of the mechanism of lead poisoning and preliminary catalyst regeneration was made on catalyst formula RE(23)75-P, and compared with the transition metal oxide combination $CuCr_2O_7$. The experimental procedures and results are given in Appendix D. The result indicates that rare earth oxide catalysts can be regenerated which is one of the reasons REO catalysts were considered for NO_x control in this program. The loss to catalyst RE(23)75-P was only 4 percent after one regeneration run.

(d) Economics of Rare Earth Oxide Catalysts

A study of the availability, cost, life cycle aspects, and comparative economics of the rare earth oxide catalysts is presented in Appendix E.

3.2 EXPERIMENTAL STUDY WITH OTHER CATALYSTS

The study of catalytic efficiency for the reduction of NO by CO, with the minimum quantity of NH_3 generation as a byproduct, was also extended to Monel 400, discussed by L. S. Bernstein et al, in Reference 4, and copper dichromate. The inclusion of these two catalysts allows a comparative analysis of the efficiency of the REO catalysts with the other ones, evaluated under identical conditions.

Data obtained with Monel 400 and $CuCr_2O_7$ will be presented in Chapter 4, and discussed along with the results of RE(23)75-P and RE(M3)75, in Chapter 5.

3.3 THE CATALYTIC GAS REACTION EXPERIMENT

This section describes the experimental apparatus, the synthetic exhaust gas mixture used for the experiment, the analytical apparatus used for the monitoring of the emissions for our catalytic gas reaction, the procedure for conducting the experiment, and the method of reducing the data.

3.3.1 Gas Flow Apparatus

The experimental apparatus used for the catalytical gas reaction $2NO + 2CO = N_2 + 2CO_2$ is shown in Figure 10. According to this figure, we can distinguish several main components of the apparatus:

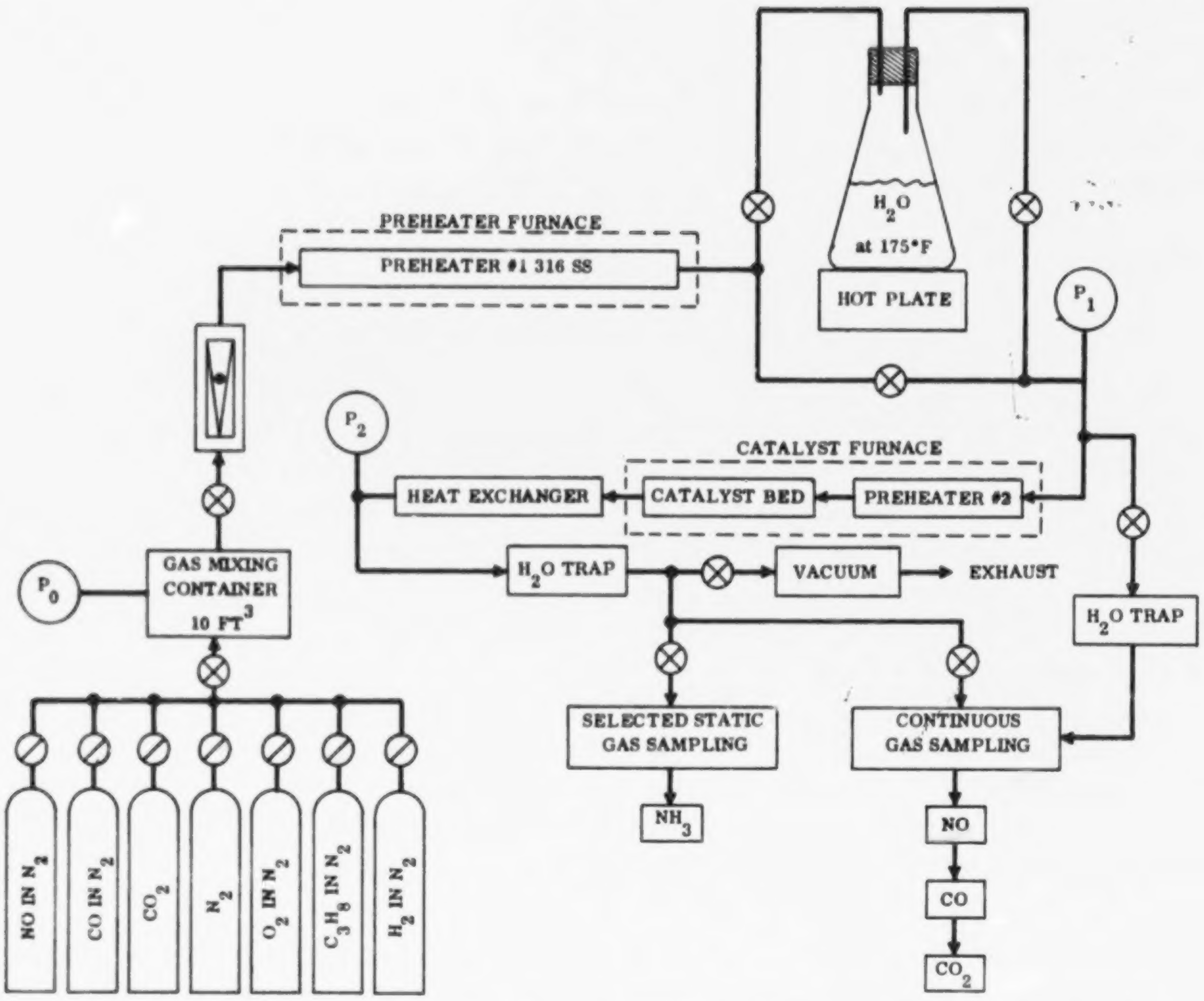
PREHEATER FURNACE
PREHEATER #1 316 SS
H_2O at 175°F
HOT PLATE
P_1
P_2
CATALYST FURNACE
HEAT EXCHANGER
CATALYST BED
PREHEATER #2
P_0
GAS MIXING CONTAINER 10 FT^3
H_2O TRAP
VACUUM
EXHAUST
H_2O TRAP
SELECTED STATIC GAS SAMPLING
CONTINUOUS GAS SAMPLING
NH_3
NO
CO
CO_2
NO IN N_2
CO IN N_2
CO_2
N_2
O_2 IN N_2
C_3H_8 IN N_2
H_2 IN N_2

FIGURE 10. SCHEMATIC OF CATALYTIC GAS REACTION APPARATUS FOR EXPERIMENTATION WITH SYNTHETIC EXHAUST GAS MIXTURES

1. On the bottom left of the schematic we have the manifold which is connecting the various gas tanks. The gas tanks involved are those containing NO, CO, O_2, C_3H_8 and H_2 in nitrogen, a CO_2 gas bottle and a nitrogen gas bottle.

2. The manifold leads the gases into the gas mixing container which has a volume of about 10 cubic feet at elevated pressure. This gas mixing container is an accumulator, that is a constant pressure vessel, containing a diaphragm which divides accumulator's interior into two parts. The gas is admitted into the accumulator by the method of partial pressures, read on the pressure gauge P_0. Once the full pressure, made up of the sum of partial pressure of all the gas components, is attained, one can, with the use of the diaphragm, keep the pressure in the accumulator constant by admitting nitrogen into the bottom part of the container (not shown in the sketch of the apparatus). In this manner,

the diaphragm will exert a constant pressure to the gas remaining in the accumulator; thus the flowrate will not decrease as a function of pressure in the mixing chamber. However, the maintenance of constant pressure is not necessary for the successful conduction of the experiment.

3. The flowrate entering the catalyst bed is determined by three flowmeters, which follow the accumulator. These three flowmeters, shown in the schematic as only one flowmeter, are placed in parallel. They consist of a large flowmeter which has a capability of flowrates up to 100, 000 cubic centimeters per minute, a medium flowmeter with a capability of flowrates up to 13, 600 cc/minute and a small flowmeter with a capability of up to 1, 400 cc/minute. The three flowmeters cover adequately the flow ranges considered in this experiment.

4. The gas enters a preheated furnace, which raises the temperature of the gas to about 630° F. The preheater is made from 316 stainless steel. Its length is approximately 40 feet. The purpose of this independent preheater furnace is to decompose any nitric dioxide formed in the accumulator into its components, nitric oxide and oxygen, so that a true measure of the catalytical activity on the nitric oxide can be obtained from our apparatus.

5. Leaving the preheater, the gas is passed into a water containing flask. This water is heated to a temperature of 175° F. According to literature, at this temperature the water-vapor will be 10 percent of the total gas leaving the flask through the exit tube, regardless of the actual flowrate (Ref. 11 and 12). There is a bypass valve, and additional inlet and outlet valves on the flask, allowing the synthetic exhaust gas to remain dry. In most instances of the experimentation however, the exhaust gas was properly moistened by this warm flask feature.

6. Following this step the reaction gases, the pressure of which is measured by the pressure gauge P_1, enter the catalyst furnace, which contains a small preheater No. 2 and the catalyst bed. There is a valve leading out of the gas line between the preheater furnace and the catalyst furnace, and which leads through a water vapor trap to our continuous gas sampling station. The purpose of this station is to obtain a composition of the gas regarding its NO, CO and CO_2 concentration, before the reaction. The gas which, through the preheater No. 2, passes into the catalyst bed, undergoes a catalytic reaction in the bed and leaves the furnace through a heat exchanger in order to cool it back down. The gas pressure beyond the catalyst bed is measured by the pressure gauge P_2. The gas then enters a water vapor trap and can be led either to the con-

tinuous gas sampling station for ob taining the data on NO, CO, and CO_2 after the reaction, or to a titration experiment to measure ammonia. The remainder of the gas is led through a vacuum pump into the exhaust.

(b) Catalyst Bed

The various components and features of the catalyst bed itself, which is placed inside the catalyst furnace, is shown in the next illustration.

In Figure 11 the catalyst bed, consisting of a small tubing with an I. D. of one inch, and length of 8 inches, which is placed in a larger tubing with a slide fit, is sketched in detail. A perforated ending is placed at the bottom of the smaller tubing and the catalyst put into this container. The gas coming from the preheater flows ; first into the larger tubing; and from there it continues into the smaller tubing, which is the only way toward the exit from the catalyst bed area. A flange is placed on the top of the larger tubing, which has been raised above the level of the furnace, so that the catalyst can be exchanged from time to time without the need of taking the entire apparatus apart.

The geometry of the catalyst bed and the method of monitoring its temperature profile are shown in Figure 12. The gas reaction chamber is 19 inches long, extruding on both sides of the 15 inch long furnace. The gas flow in the figure is from left to right, in the apparatus from top to bottom. The furnace itself has three resistance heaters, of dimensions as shown, with a 3 inch diameter. The location of the catalyst bed in the reaction chamber, with respect to the furnace heating elements, is given. It is 7.25 inches high with an I. D. of 1 inch and filled to a depth of 7 inches with the catalyst pellets. Starting at the bottom of the catalyst bed, at one inch intervals and with a clockwise rotation of 90 degrees each time, seven thermocouples are located such that the last thermocouple, No. 7, is placed one inch beneath the top surface of the catalyst.

Measuring the temperature profile of the catalyst bed, the variations from nominal are observed as plotted in Figure 12. A temperature close to the one indicated by thermocouple #3 has been selected as the nominal temperature. The indicated temperature gradient across the catalyst bed is the one as measured with the flowrate of 1000 cc/min.

(c) The Assembled Apparatus

A general view of the assembled apparatus is given in Figure 13. On the left is the gas manifold and the accumulator, placed underneath the table. The center background gives the flow section, preheater furnace and catalyst furnace, with the furnace controls on the right. The right foreground pictures a mass spectrograph

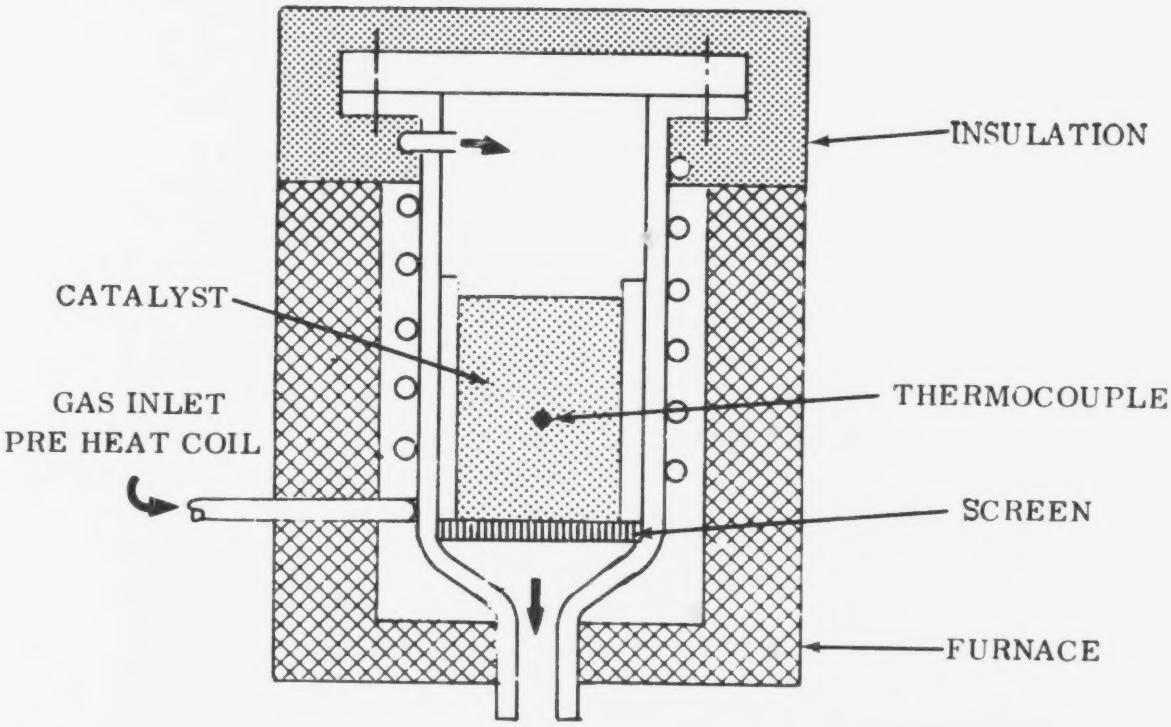
INSULATION
CATALYST
GAS INLET
PRE HEAT COIL
THERMOCOUPLE
SCREEN
FURNACE

FIGURE 11. DETAILED SKETCH OF CATALYST BED

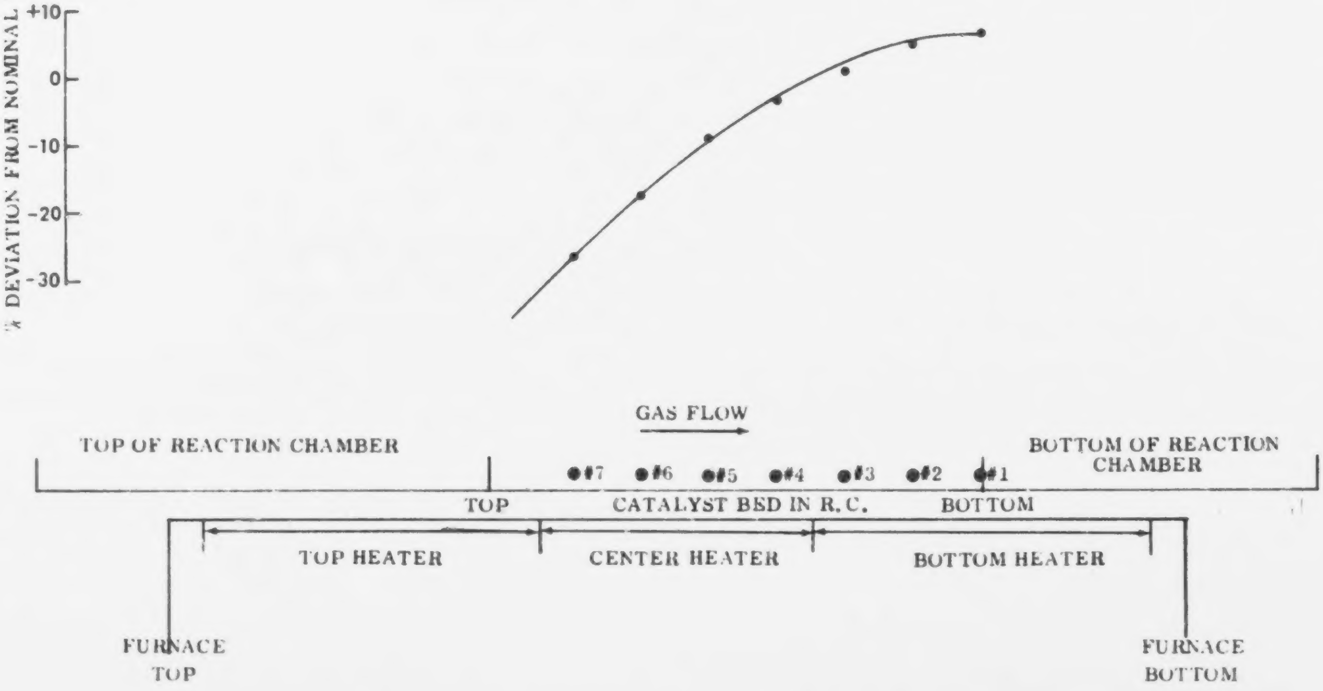

FIGURE 12. GAS TEMPERATURE PROFILE IN CATALYST BED

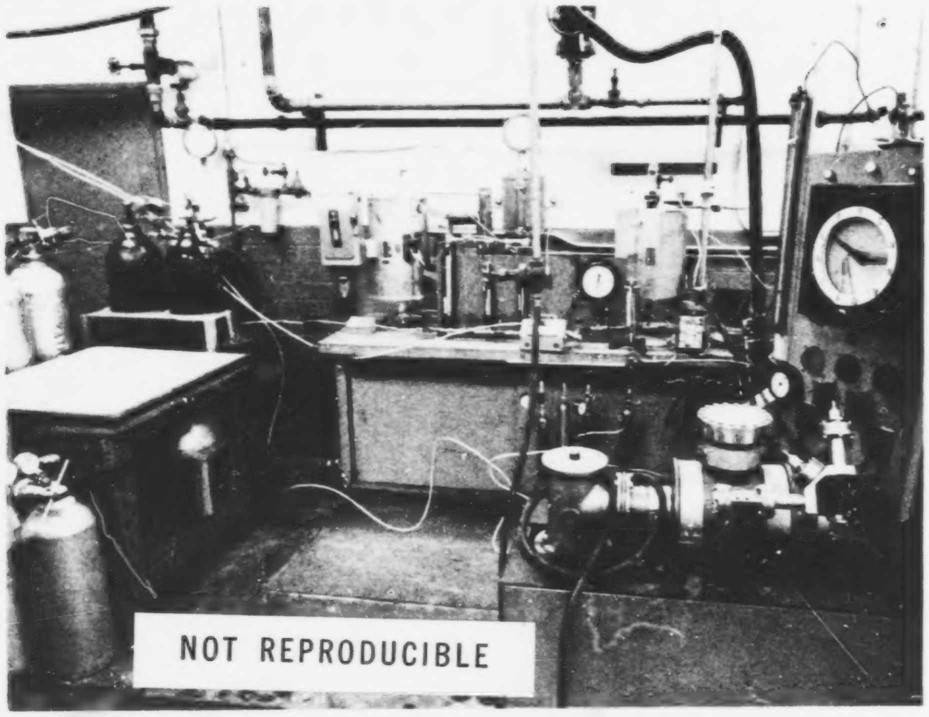

FIGURE 13. GENERAL VIEW OF CATALYTIC GAS REACTION APPARATUS IN FINAL VERSION

analyzer, which is on standby. A more detailed view of the manifold section of the catalytical gas reaction apparatus is shown in Figure 14. The gas bottles belonging to the equipment are clustered around the table, containing the gas accumulator, where the synthetic exhaust gas mixture is prepared. The gas bottles against the rear wall in this figure go with the Beckman NDIR Analyzer in the next room, which they serve to calibrate.

Figure 15, finally, gives a close-up of the gas flow measuring and catalyst bed sections of the apparatus. Also shown is the dynamic and static gas sampling stations. The white sampling lines lead from the apparatus to the Beckman NDIR Analyzer. The line on top leads to the station from which the gas composition before the catalytical reaction can be monitored; along with this dynamic outlet there is a manifold with three gas sampling bottles for gas chromatographic analysis. To the right of it is the station for gas analysis after the reaction. A water trap, standing on the floor, is hooked up into the sample line to the NDIR analyzer. A gas sample bottle for GC testing and/or ammonia analysis is connected to this same gas sampling station. Also visible in this figure is the heat exchanger and the temperature readout.

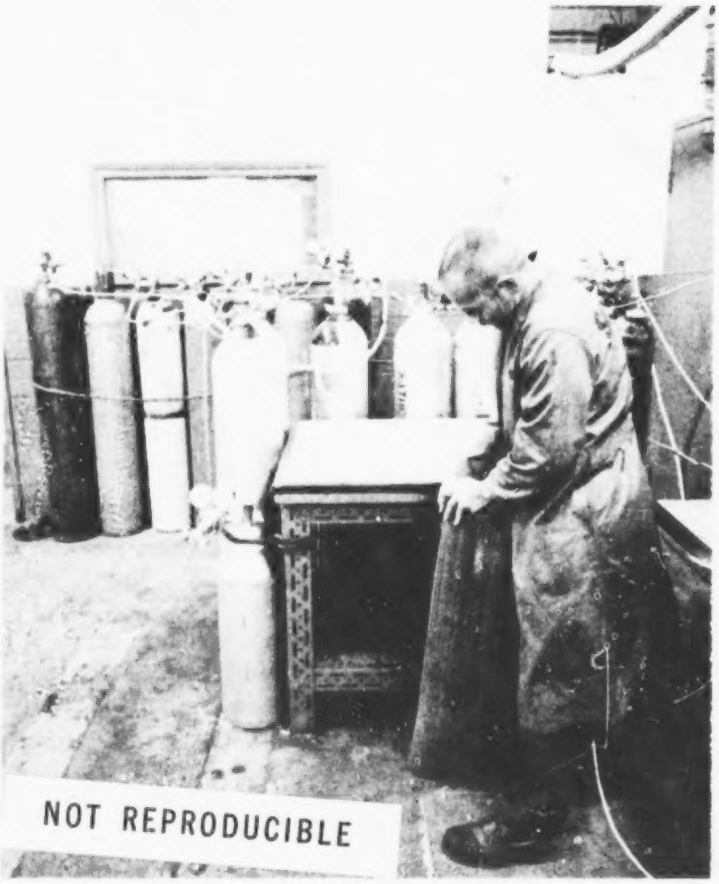

FIGURE 14.

RESEARCHER ROLLS SAFETY SCREEN IN FRONT OF GAS ACCUMULATOR UNDERNEATH GAS MANIFOLD SECTION OF CATALYTIC GAS REACTION APPARATUS

(d) Preliminary Experimentation for Qualification of Apparatus for Testing

After completion of the modifications in the experimental apparatus, preliminary test runs in the absence of catalyst were made to determine optimum operation parameters, especially regarding the optimum preheater temperature, the flowrate scans and temperature scans. The synthetic exhaust gas was mixed according to a formula, tabulated later on in this section. Table IV, below, gives the actual, certified gas mixtures obtained from Matheson and the deviations from the requested compositions.

The first task was to establish the best preheater temperature for the catalytical reaction study. The results, as functions of gas composition and flowrate, are given in the aforementioned Table V, below. At optimum preheater temperatures and constant catalyst furnace temperatures over the entire range, stable conditions prevailed in the absence of the catalyst.

3.3.2 The Synthetic Exhaust Gas Mixture

The synthetic exhaust gas mixture which is being used in this experiment, has been defined to approach the relative composition of automobile exhaust at an

NOT REPRODUCIBLE

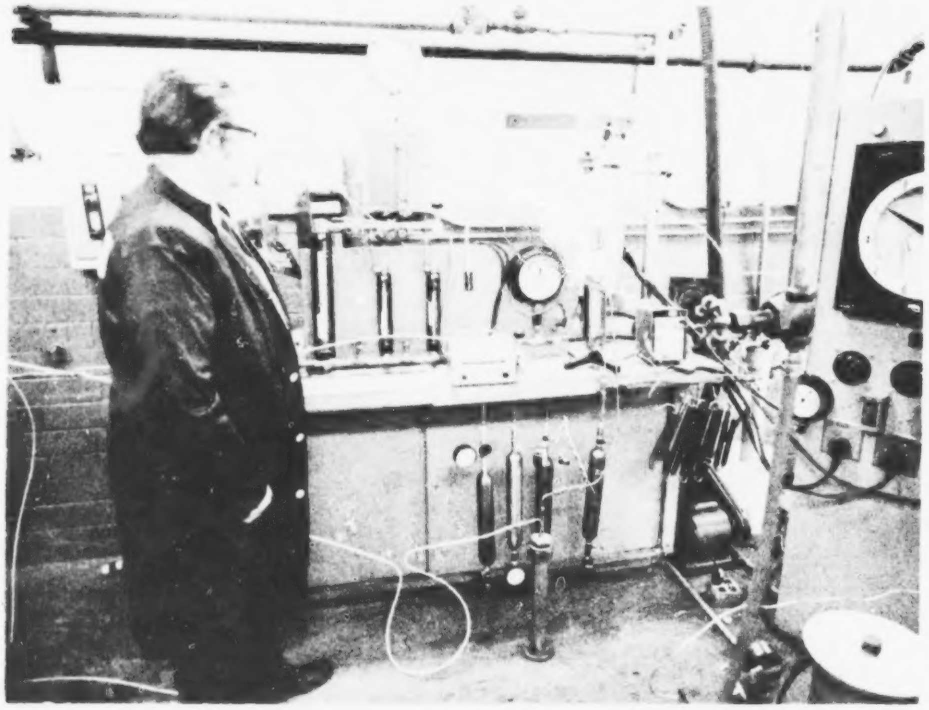

FIGURE 15. MAIN PART OF GAS REACTION APPARATUS WITH FLOW-MONITORING SECTION, CATALYST FURNACE, HEAT EXCHANGER, AND DYNAMIC AND STATIC GAS SAMPLING STATIONS LOCATED IN FRONT OF AND BEHIND THE CATALYST FURNACE

TABLE IV

CERTIFIED CONTENTS OF SYNTHETIC EXHAUST GAS COMPONENTS

Gas Component	Requested	Analysis	Deviation (%)
CO in N_2	8.8%	8.84%	+0.5
H_2 in N_2	2900 ppm	3130 ppm	+7.9
NO in N_2	6500 ppm	6650 ppm	+2.3
O_2 in N_2	1.75%	1.742%	-0.5
C_3H_8 in N_2	1800 ppm	1755 ppm	-2.5

TABLE V

PREHEATER TEMPERATURES USED IN RESTORING MIXTURE VALUES OF CO AND NO

Gas Composition	Flowrate cc/min.	Preheater Temperature
NO: 1080 or 540 ppm	18000	800° F ± 20° F
CO: 10500 or 5250 ppm	9000	700° F ± 20° F
O_2: 2900 ppm, H_2: 530 ppm	4000	630° F ± 20° F
C_3H_8: 300 ppm	1000	500° F ± 20° F
CO_2: 16%, H_2O: 10%		
N_2: 72.5%		
1000 ppm NO (Nominal) 1.0% CO (Nominal) 2000 ppm H_2 (Nominal) Balance N_2	9000	500° F ± 20° F
1000 ppm NO (Nominal) 2.4% CO (Nominal) 1.0% H_2 (Nominal) Balance N_2	9000	500° F ± 20° F

air/fuel ratio near to 14. The components of this exhaust gas mixture have been obtained from actual experimental data obtained by the IH Truck Division (Communication from Mr. Ed Fort), which are summarized in Figure 16, the exhaust gas composition of a typical Otto cycle engine, as a function of air/fuel ratio, and in Figure 17, which shows the NO concentration in exhaust gases as a function of speed, power, and A/F ratio.

The concentration of H_2 in the exhaust gas as a function of the A/F ratio was obtained from Reference 13, which, though dating from 1936, is, according to Mr. Fort, still considered as the best reference on the subject. Mr. Fort adds that recent unpublished work confirms D'Alleva's and Lozell's data on the H_2 concentration levels.

Based on the data of Figures 16 and 17, the gas components, and the synthetic exhaust gas mixture are shown in Tables VI and VII.

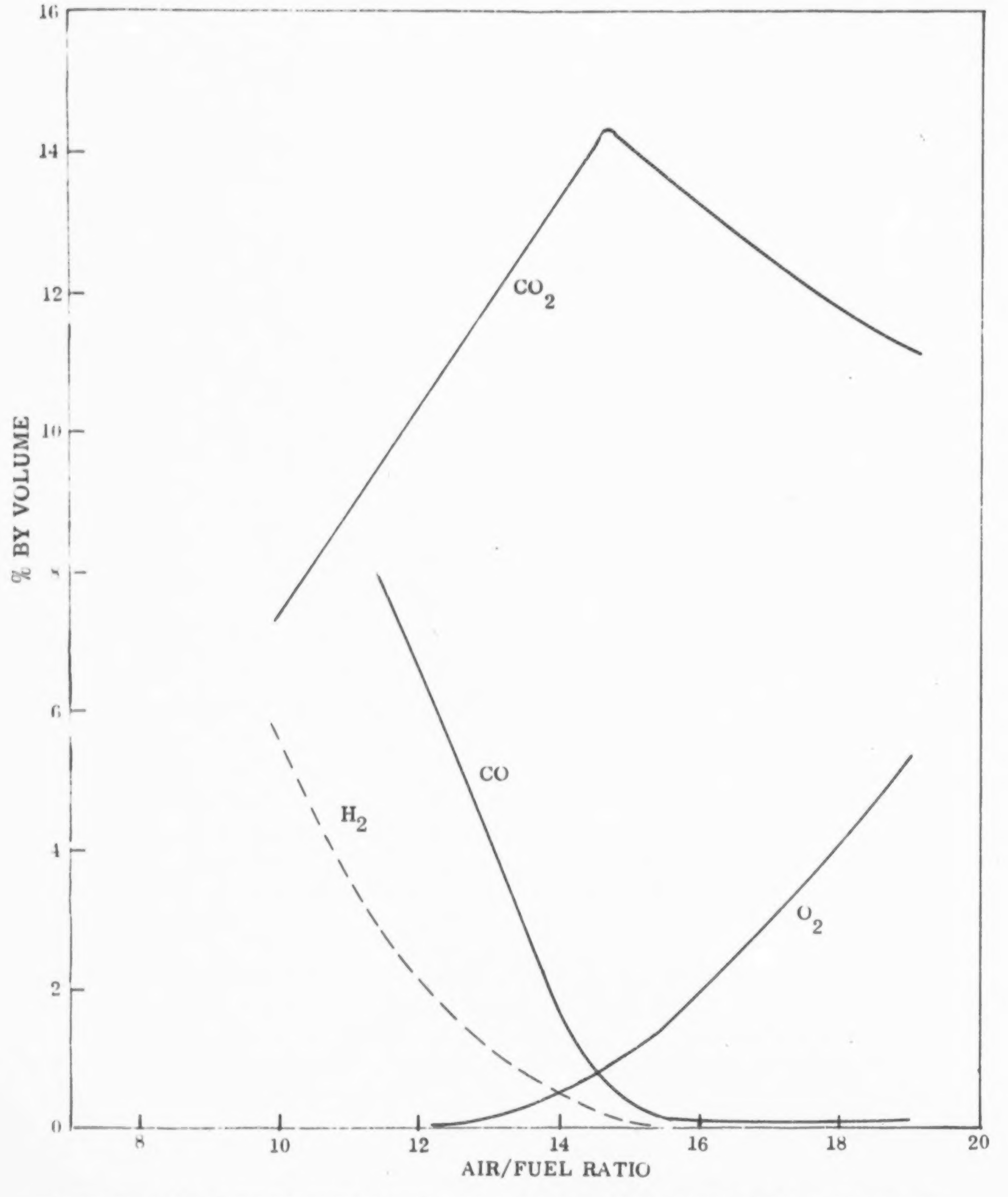

FIGURE 16. NO IN EXHAUST GAS. TYPICAL OF LOW-QUENCH S.I. ENGINES. FUEL H/C 1.9, RELATIVELY INDEPENDENT OF PPM PROVIDED IGNITION TIMING IS NEAR THAT FOR BEST TORQUE

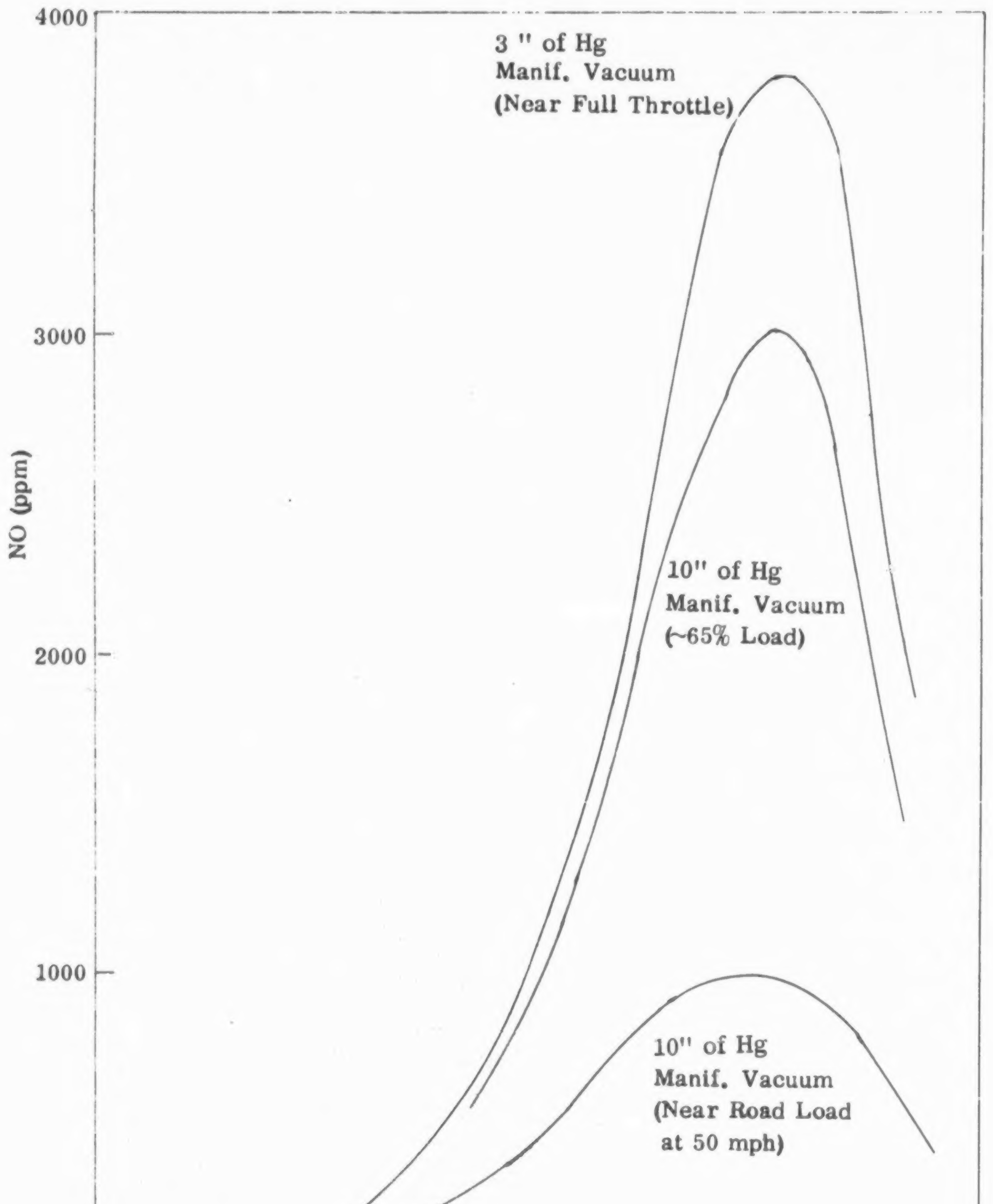

FIGURE 17. EXHAUST GAS COMPOSITION TYPICAL OF S.I. ENGINE USING FUEL WITH H/C: 1.9. SAMPLE DRIED TO SATURATED AT 32° F (ESSENTIALLY DRY SAMPLE)

TABLE VI

ACTUALLY USED SYNTHETIC EXHAUST GAS MIXTURES FOR CATALYST NO REDUCTION EFFICIENCY EXPERIMENTATION

Gas Mixture Code	Nominal NO ppm	CO/NO Ratio R	Nominal O_2 ppm
A	1080	10	2900
B	1080	5	2900
C	540	10	725
D	540	5	725

TABLE VII

DEFINITION OF GAS MIXTURE DENOTED "A"

Component	ppm	Percent	Range in Accuracy
NO	1,080	0.1	±10%
CO	10,500	1.0	±10%
CO_2	160,000	16.0	±8.5%
O_2	2,900	0.29	±10%
C_3H_8	300	trace	±10%
H_2	530	trace	±10%
H_2O	100,000	10.0	
N_2	724,690	72.5	±10%

3.3.3 Description of Analytical Apparatus for Emissions Monitoring

Dynamic Measuring Apparatus

Analytical equipment available at Solar for the evaluation of the catalytical efficiency in the gas reaction

$$2CO + 2NO \longrightarrow N_2 + CO_2$$

in the synthetic exhaust gas mixture is shown in Figures 18 and 19. This equipment consists essentially of the Beckman Gas Analyzer with its Non-Dispersive Infrared

NOT REPRODUCIBLE

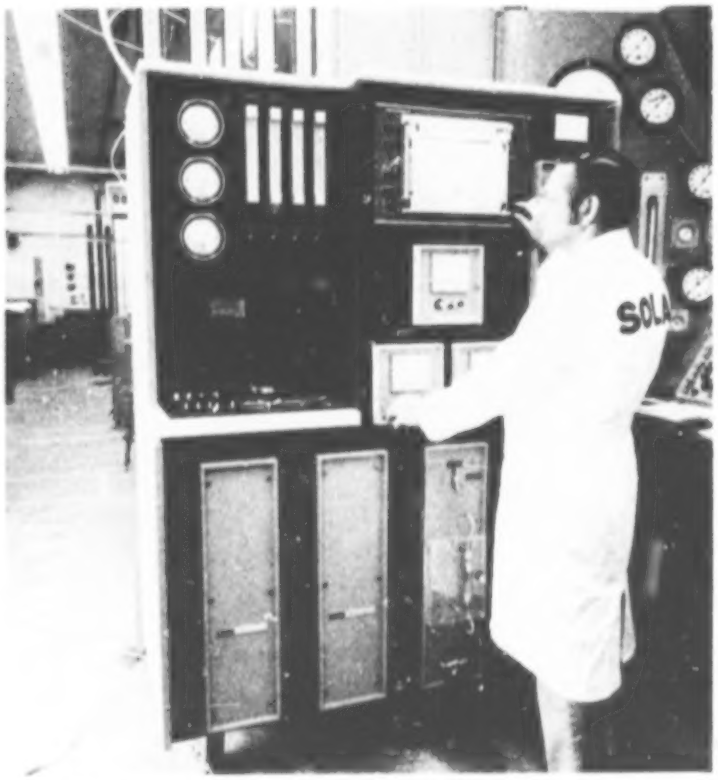

FIGURE 18A. THE NON-DISPERSIVE INFRARED RADIATION DETECTOR AND READOUT RECORDER OF THE BECKMAN GAS ANALYZER

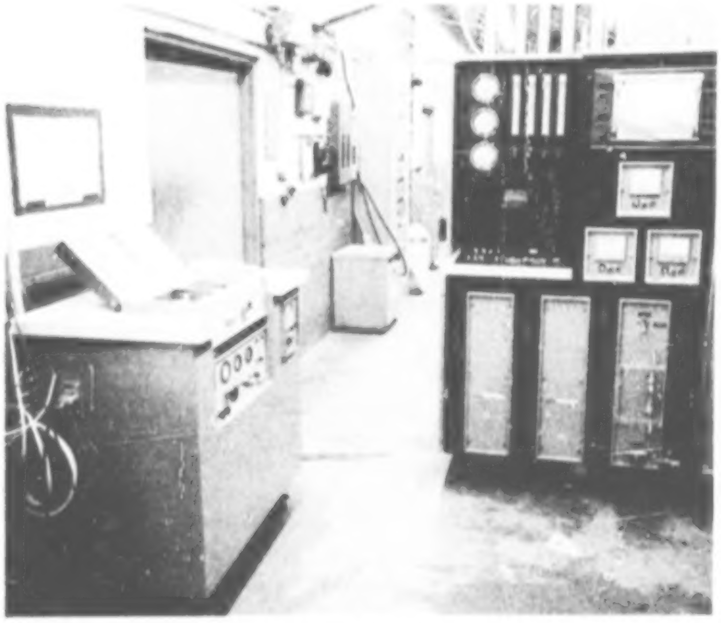

FIGURE 18B. TOTAL VIEW OF BECKMAN GAS ANALYZER INCLUDING THE FLAME IONIZATION DETECTOR FOR THE MEASUREMENT OF HC SHOWN AT LEFT

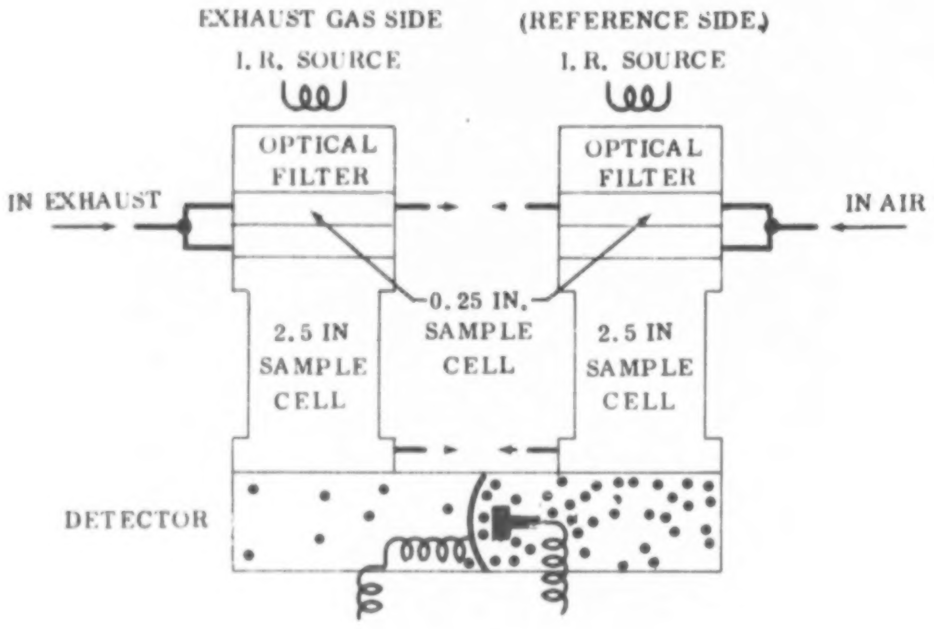
EXHAUST GAS SIDE
I. R. SOURCE
(REFERENCE SIDE)
I. R. SOURCE
OPTICAL FILTER
OPTICAL FILTER
IN EXHAUST
IN AIR
0.25 IN.
2.5 IN SAMPLE CELL
SAMPLE CELL
2.5 IN SAMPLE CELL
DETECTOR

FIGURE 19. PRINCIPLE OF OPERATION OF INFRARED ANALYZERS

Radiation detector, shown in Figure 18A, for the measurement of CO, CO_2, and NO, and its Flame Ionization Detector, shown on the left in Figure 18B for measuring the HC with the NDIR being pictured at right.

The principle of NDIR analysis is shown in Figure 19 taken from Reference 14. In the Beckman Instrument, the sample flows through the CO_2, CO and NO detecting chambers in series.

The flame ionization detector utilizes a hydrogen-air flame, which generates a minute current when a combustible material, such as hydrocarbons, in the carrier (nitrogen) enters the region of the flame. Sensitivities are extremely high, on a picogram full scale under ideal conditions for high response organic materials. The readout for the Beckman Flame Ionization Detector is located on the NDIR instrument panel, so that CH, NO, CO and CO_2 concentrations all can be read out together on one chart.

Static Measuring Apparatus

This apparatus used for this type of measurement is a Gas-Chromatograph with a sensitivity for CO and NO into the parts per billion range, shown in Figure 20. The Gas-Chromatograph has been used to spot-check and calibrate readings obtained from the two other pieces of analytical equipment available.

NOT REPRODUCIBLE

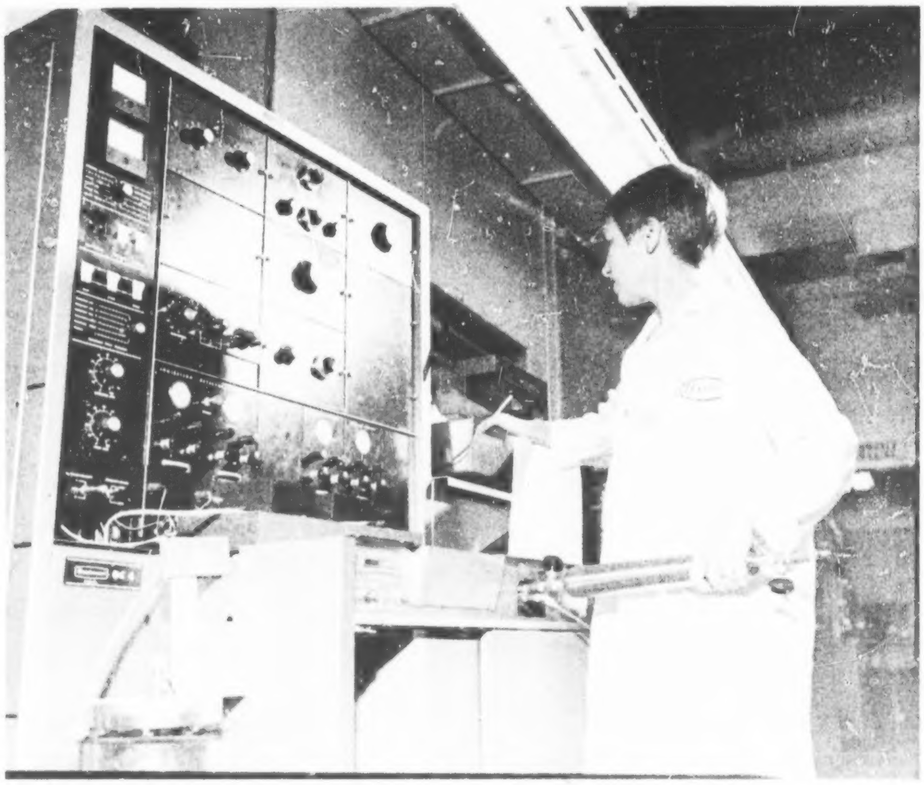

FIGURE 20. THE GAS CHROMATOGRAPH FOR STATIC MEASUREMENTS OF GAS EXHAUST COMPONENTS

Principles of Gas Chromatography

Gas chromatography is the physical separation of two or more molecular compounds based on their differential distribution between two phases, one of which is stationary, and the other gaseous. The compounds, after separation, may then be detected by various methods (see Ref. 15 and 16). The one used at Solar is the Helium Ionization Detection method.

This method permits analysis of inorganics and permanent gases in the fractional parts per million range. The helium ionization detector is nonradioactive, utilizing photoionization of the helium gas, and analyses with high sensitivity, one to two ppm full scale for most components.

Further details on gas chromatography are found in References 15 and 16.

3.3.4 Procedure for Conducting Experiment

The procedure which has been used for each sequential experimental step (determined by a given set of parameters for that step is as follows:

The accumulator is filled with the appropriate synthetic exhaust gas mixture to a pressure of 368 psig, the preheater and catalyst bed temperatures are set, a flowrate determined, and the gas, moistured by the vapor from the water in the heated flash, is allowed to pass through the catalyst bed and to the sampling stations. Two sample lines to the Beckman NDIR Analyzer are used, one to transport the gas before the reaction, the other one after the reaction. The gas is allowed to push its own way through the instrument cells, by means of a slightly higher pressure (~3 psig), in order to keep a good control on the flowrate. Data are taken on the NDIR instrument directly, or else gas is passed through an absorber for the titration method of NH_3 determination.

It was found that testing of the catalysts required various periods of running time for stabilization of catalyst effectivity. Stabilization times ranged from 10 minutes to almost an hour, depending on flowrate, temperature, and gas composition. Accordingly, all data points were accumulated at steady-state conditions and only when efficiency values were devoid of any drift in the NDIR Analyzer.

Evacuation of the system caused drastic variation from equilibrium efficiency states and, therefore, one atmosphere of pressure was maintained between runs. This method decreased the required stabilization time as long as pressure and the range of the gas compositions were maintained between runs. (System evacuation also had a transient effect on preheater gas conversion effectiveness.)

Rare earth catalyst test procedures included its exposure to a reducing atmosphere of 8.8 percent CO in N_2 for a period of 10 minutes at 1200° F. Such procedures have been used by other investigators (Ref. 5 and 7). After this the catalyst is not exposed to air. (This procedure was also observed to deviate the catalyst from its equilibrium efficiency.) It seems such a reducing condition is favorable to NO reduction and thus should give more optimal results than in motor vehicles.

Data points are accumulated by running synthetic gas through the entire system and sampling concentrations with the Beckman NDIR Analyzer until values of CO, NO and CO_2 are observed to be completely stable. At this point the gas sample pickup is switched instantaneously to catalyst bed inlet and allowed to remain there for the minimum time required for sampling equipment reading to stabilize. This procedure is normally repeated three times for each accumulator charge of 368 psig.

The NDIR equipment records the concentrations of NO, CO and CO_2 concurrently, using three pens with different colors of ink on the same strip chart. The analyzer is recalibrated before each set of experimental data by the use of the appropriate zero and span gases.

Chemical Procedure for Determination of Ammonia Formed in Synthetic Exhaust Gas

The general procedure for collection and determination of ammonia is as follows:

The sample is collected by allowing exhaust gas to bubble through 80.0 ml of an absorbing solution of boric acid, containing 20.0 grams of boric acid per liter, at a rate of 9.0 ± 0.5 ℓ/minute for a specified length of time, generally 10 minutes. The collection apparatus is similar to a standard gas washing bottle with a fritted gas dispersion tube. The diameter of the bottle is such that 80.0 ml yields a solution height of 3.5 inches above the fritted dispersion tube. The solution is maintained at low temperature in a dry ice water bath in order to ensure maximum absorbing efficiency during each experimental run.

After collection, the sample is titrated with 0.040 N hydrochloric acid to a Brom Cresol Green endpoint. One milliliter of 0.040 N hydrochloric acid is equivalent to 0.68 mg of ammonia. A blank titration is also performed, not only to determine the blank titration value, but also as an endpoint color standard. Parts per million ammonia ($\mu\ell/\ell$) is calculated from the following equation:

$$\text{ppm } NH_3 = N_{HCl} \times ml_{HCl} \times \frac{22{,}400 \text{ ml/mole}}{170 \text{ g/mole}} \times \frac{1}{\text{Litres of gas bubbled}}$$

The total percent error involved in this analytical determination is as follows:

$$\text{Total \% Error} = \left[\left(\frac{\Delta N}{N}\right)^2 + \left(\frac{\Delta mls}{mls}\right)^2 + \left(-\frac{\Delta L}{L}\right)^2\right]^{1/2} 100$$

where ΔN = ±0.002

Δml = ±0.02 mls

ΔL = ±5.0 liters (for ten minute runs)

L = flowrate x time

L = (9.0 ± 0.5 ℓ/min) x time

The maximum error attributable to the analytical technique used for the ammonia determination is calculated to be less than one percent. The largest factor contributing to the total error is the flowrate deviation. If the flowrate changes by 0.5 ℓ/min as a minimum deviation, this would result in a total flow error of 5.6 percent. Therefore, the error due to the analytical technique must be considered minimal when compared to the error introduced by the flowrate conditions.

3.3.5 Reduction of Data

The data measured are all in the form of gas constituent concentrations, by the NDIR method for NO, CO, CO_2 and by the titration method of Reference 17 for NH_3 concentrations. All the data obtained by various gas analysis methods, except for the titration, are dependent upon the calibration of the respective instruments with calibration gases, thus the accuracy of the data is a function of the calibration.

Since the NDIR method allows a dynamic monitoring of the gas component concentrations, the data can be obtained directly as a function of temperature and flowrate. The effects of initial NO concentration and NO/CO ratio has to be obtained only after a change in the corresponding parameters has been made.

As we have defined the NO reduction efficiency η of the catalyst to be

$$\eta = \frac{\text{Initial NO Concentration-Final CO Concentration}}{\text{Initial NO Concentration}} \times 100\%$$

we obtain the efficiency of the catalyst directly as a function of the temperature and flowrate, and as functions of CO/NO ratio and NO concentration after changing the appropriate parameters in the experimental sequence.

The results have been tabulated, plotted in graphs, and assembled in parametric form in the parametric design chart.

4

EXPERIMENTAL RESULTS

4.1 CATALYSTS AND CATALYTICAL REACTION PARAMETERS INVESTIGATED

The experimental program consisted of a parametric investigation of a number of catalysts, with emphasis on the rare earth oxide formulations. Additional catalysts were included after the shortcomings of the original rare earth formulations became apparent.

4.1.1 Catalysts Considered in the Program

The catalysts investigated in the course of this program were the following:

- Catalyst RE(23)75-P
- Catalyst RE(M3)75
- Monel 400
- Solar Monel 400 Mod.
- Solar Monel 400 Core
- Copper Dichromate, $CuCr_2O_7$
- Palladium Catalyst, 0.5% Pd on Al_2O_3 pellets
- Platinum Catalyst, 0.5% Pt on Al_2O_3 pellets

Also considered was the effect of the empty catalyst bed, consisting of stainless steel, with a catalytic action of its own.

4.1.2 Parameters Considered in the Program

The basic parameters are:

- Initial NO concentration
- CO/NO concentration ratio

- Catalyst temperature
- Flowrate of gas through the catalyst bed

The first two parameters can be combined into an entity defined as "gas mixture". With essentially two NO concentrations, 500 ppm and 1000 ppm nominal, and two CO/NO concentration ratios, four gas mixtures are needed, denoted A, B, C and D. Table VI in the previous chapter defines these gas mixtures in detail. Gas mixture A moreover, has been arrived at as the synthetic exhaust gas mixture for an A/F ratio near 14, and it is defined in Table VII, also in the prior chapter.

Catalyst temperatures have been selected in the range from 600° F to 1600° F in 200° F increments. The experimental flowrates, coded 1-5, are defined in Table VIII, below, both in terms of car flowrate in CFM, and experimental flowrates in cc/min.

TABLE VIII

FLOWRATE RANGE (REF. 18)

Flowrate Code	Car Mode	Car Flowrate CFM	Experimental Flowrate cc/min
1	Decelerating	5	460
2	Idling	10	1000
3	Partial Load, Cruising	45	4000
4	Full Load, Cruising	100	9000
5	Accelerating	200	18000

Though the concept of the space velocity combines both, catalyst bed temperature (assumed to be equal to gas temperature in the bed) and gas flowrate into one parameter, experimental data obtained have shown the NO-reducing efficiency of the catalyst to be more temperature dependent than flowrate dependent or space-velocity dependent.

4.1.3 Parametric Investigation of the NO-Reducing Efficiency of the Catalysts in This Program

Having reduced the parameters to three independent quantities, namely gas mixture, temperature, and flowrate, we may plot these on a three dimensional graph, using an "M" axis for the gas mixtures; a "T" axis for the temperature, and a "ϕ"

axis for the flowrates. The result is a three-dimensional grid, such as shown in Figures 21, 22, and 23. These figures give, at a glance, the parametric range of investigation of the NO-reducing efficiency η for each catalyst studied in the program.

Figure 21 shows the parameters along the M, T, and ϕ axes, varied for catalyst RE(23)75-P. The same parameters have also been used for the empty bed readings.

Figure 22 gives the parameters for the catalyst RE(M3)75. Here the lower temperature range has been omitted due to the relatively poor performance of this catalyst at the intermediate and higher temperatures.

Figure 23 gives the range of parameters used for all the remaining catalysts. As can be seen, the only parameter changed here was the temperature, thus all data points are on the "T" axis.

Each block in Figures 21 to 23 represents a data point. It is labelled with the values of the parameters at that particular location of the three dimensional parametric grid. The first number on the front-face of each block refers to the flowrate code, as

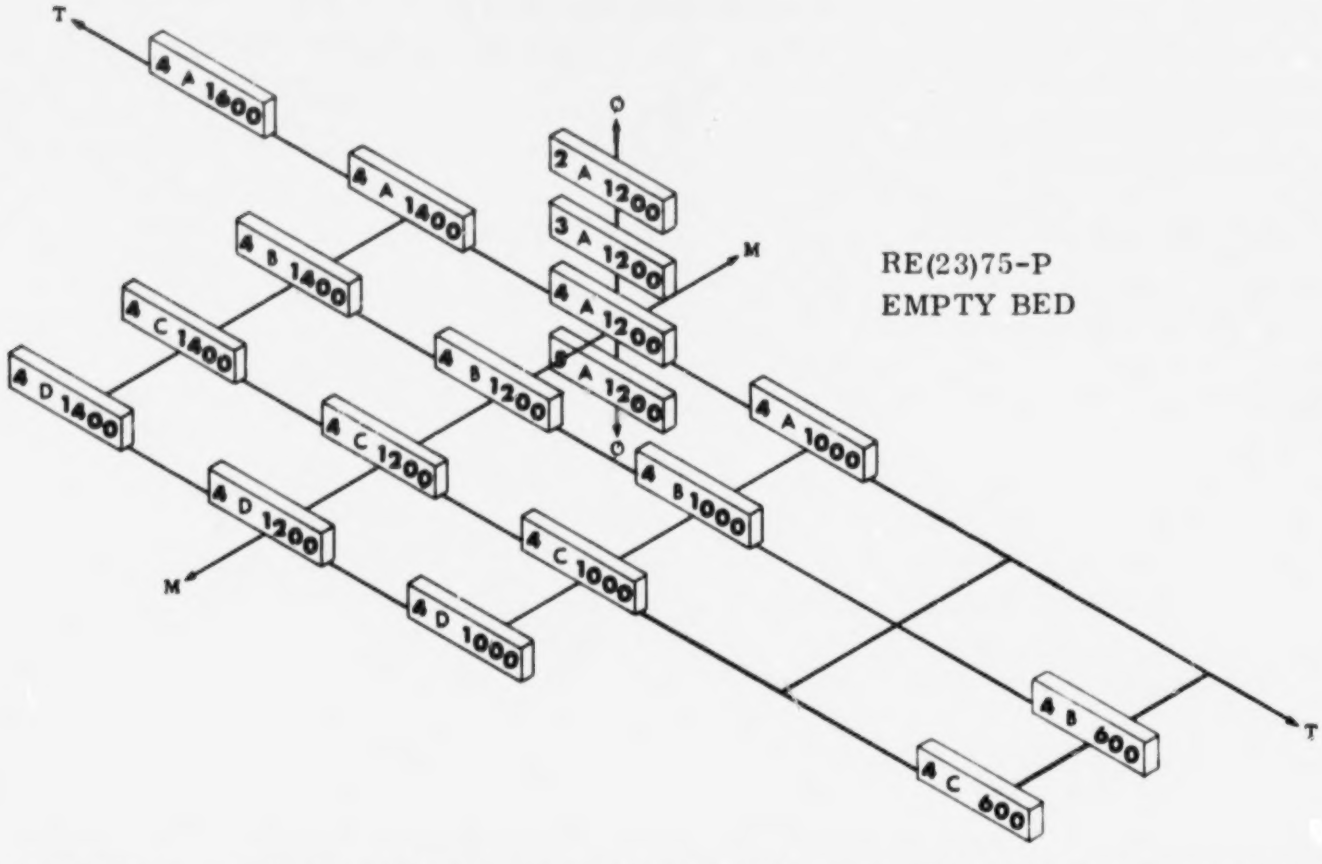
T
4 A 1600
4 A 1400
4 B 1400
4 C 1400
4 D 1400
ϕ
2 A 1200
3 A 1200
4 A 1200
5 A 1200
M
4 B 1200
4 C 1200
4 D 1200
ϕ
4 A 1000
4 B 1000
4 C 1000
4 D 1000
M
4 B 600
4 C 600
T

RE(23)75-P
EMPTY BED

FIGURE 21. THREE-DIMENSIONAL SCHEMATIC REPRESENTATION OF EXPERIMENTAL CONDITIONS FOR THE TESTING OF CATALYSTS NOTED

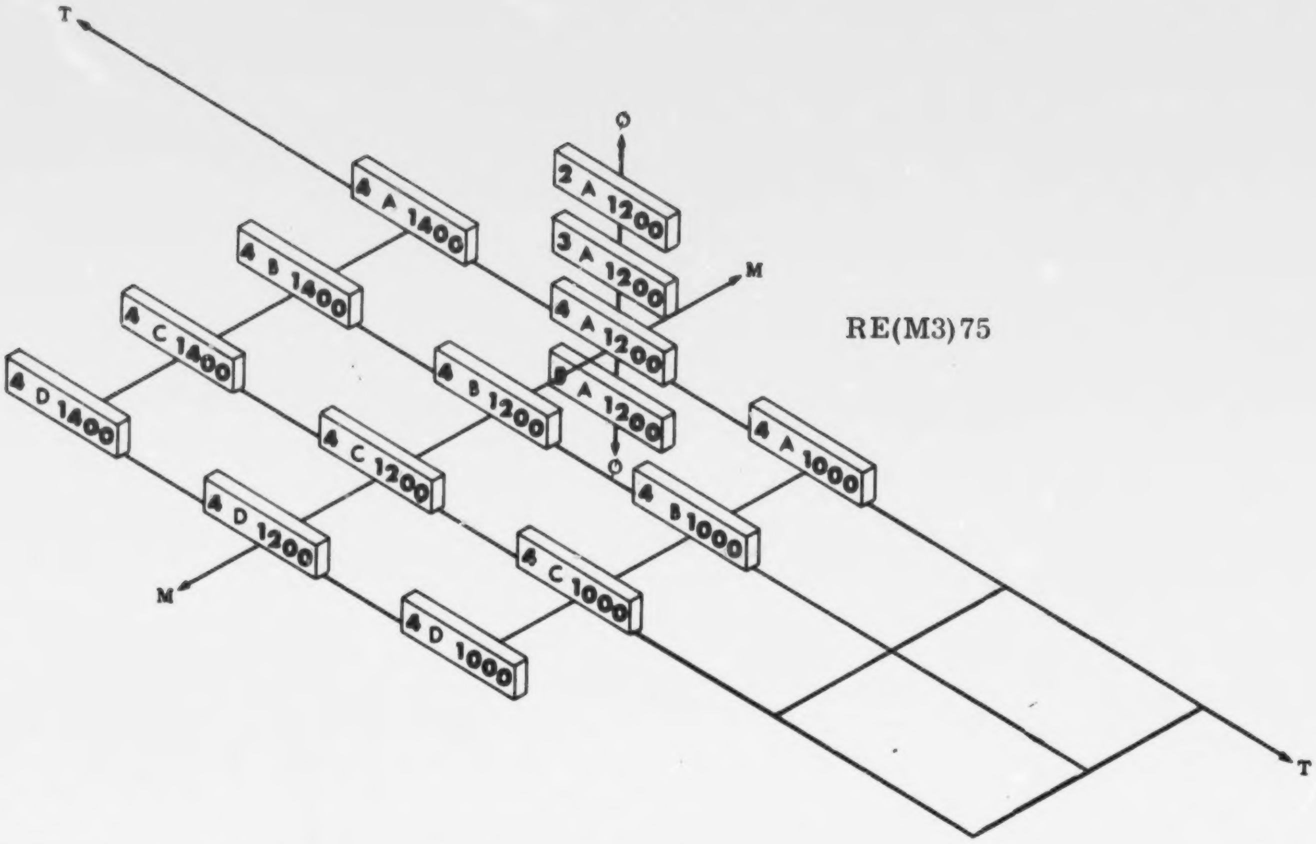
T
O
4 A 1400
2 A 1200
4 B 1400
3 A 1200
M
4 C 1400
4 A 1200
RE(M3)75
4 D 1400
4 B 1200
5 A 1200
4 C 1200
O
4 A 1000
4 D 1200
4 B 1000
M
4 C 1000
4 D 1000
T

FIGURE 22. THREE-DIMENSIONAL SCHEMATIC REPRESENTATION OF EXPERIMENTAL CONDITIONS FOR THE TESTING OF RARE EARTH CATALYST NOTED

defined in Table VIII. This is followed with the letter denoting the gas mixture code, as defined in Table VI. The number following the code letter, finally, gives the catalyst bed temperature in degrees F.

4.2 NO REDUCTION EFFICIENCY OF THE CATALYSTS TESTED

In this section, we shall first present, in tabular form, the experimental data for the rare earth oxide catalysts, i.e., RE(23)75-P, RE(M3)75, and the empty bed catalyst. Next follows the graphical presentation of these same data, and finally the NO reduction efficiency data of the other catalysts tested.

4.2.1 Experimental Data for Rare Earth Oxide Catalysts

A. Catalyst Formula RE(23)75-P

The data for the temperature, as well as gas mixture scan, is given in Table IX. These data correspond to the plane of data points given by the T-M axes in Figure 21, above. The table gives the quantities of the CO, NO, and CO_2 components

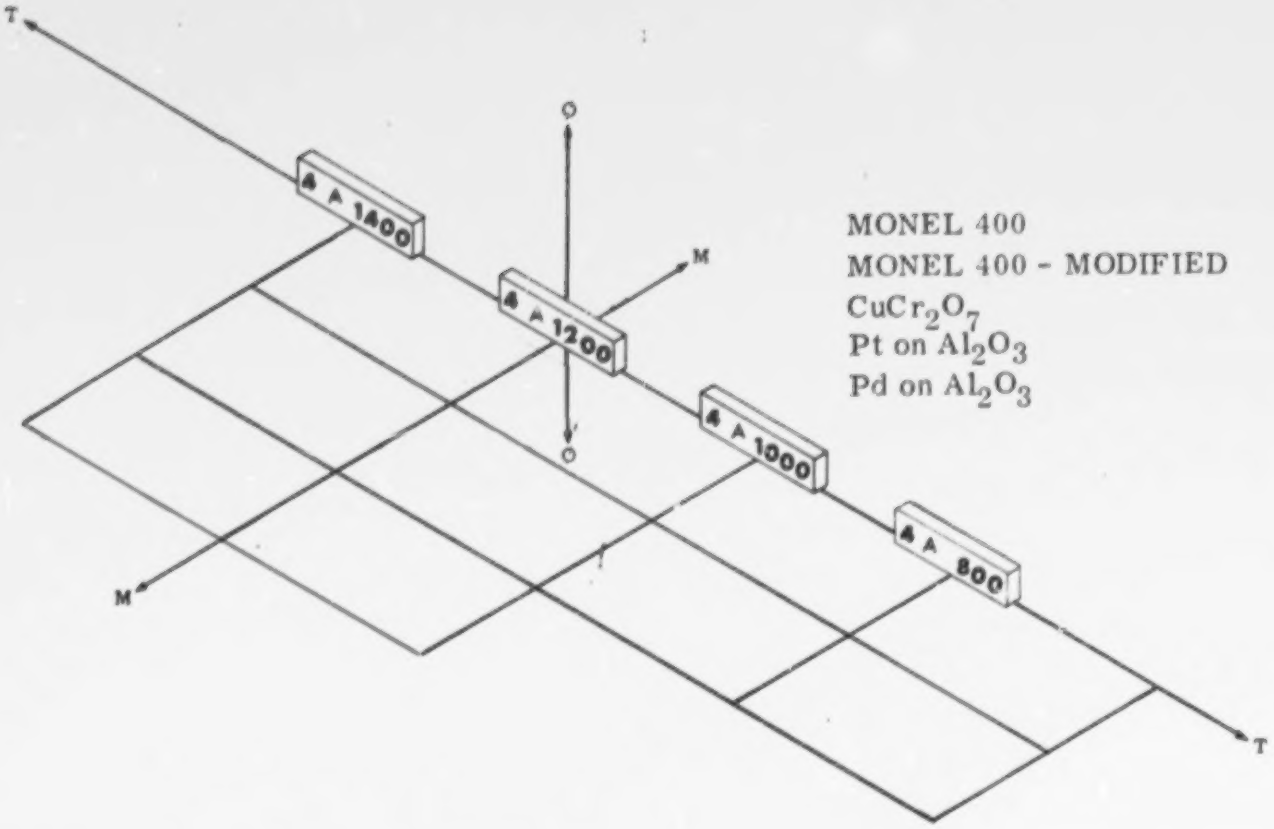

FIGURE 23. THREE-DIMENSIONAL SCHEMATIC REPRESENTATION OF EXPERIMENTAL CONDITIONS OF TRANSITION METAL AND NOBLE METAL CATALYSTS

of the synthetic exhaust gases, before and after the catalytic gas reactions, as measured by the Beckman NDIR apparatus. The loss percentages for the CO, and for the NO, the latter being equal to the NO-reducing efficiency η, are also shown in this table.

The flowrate scan data are given in Table X, below. These data correspond to the ϕ axis in Figure 21. Again, the quantities of CO, NO, CO_2, and the loss of CO and NO, the latter being again the NO-reducing efficiency η, are given in the table as a function of flowrate shown both in code number and actual dimensions of liters/minute.

B. Catalyst Formula RE(M3)75

The data for the temperature and gas mixture scans, at constant flowrate, are tabulated in Table XI. These data, corresponding to the data points shown on the T-M plane in Figure 22, above, are arranged in the same way as those in Table IX, for the catalyst formula RE(23)75-P. The table shows the catalytic efficiency, η, as a function of temperature, CO/NO concentration, and initial NO concentration.

TABLE IX

THE NO-REDUCING EFFICIENCY, AND PERCENT LOSS OF CO, FOR CATALYST RE(23)75-P AT A FLOWRATE OF 9000 cc/min

		CO (%)			NO (ppm)			CO_2(%)	
Composition	Temperature	Before	After	%Loss	Before	After	%Loss	Before	After
A	1600° F	1.20	0.72	39.2	1060	500	52.4	19.0	19.2
		1.17	0.72		1060	510		19.0	19.2
	1400° F	0.95	0.57	40	1120	587	47.6	15.8	16.0
		1.01	0.59	41.6	1060	565	46.7	15.8	16.0
	1200° F	1.02	0.635	37.7	1067	580	45.6	16.0	16.0
	1000° F	1.01	0.80	20.8	1200	660	45.0	15.2	15.2
		0.986	0.80	18.9	1120	740	33.9	15.2	15.2
		1.05	0.695	33.8	1090	830	23.8	15.6	15.6
B	1400° F	0.443	0.227	48.8	1120	630	43.8	15.33	15.4
	1200° F	0.50	0.250	50.0	1180	812	31.2	15.4	15.6
	1000° F	0.447	0.287	35.8	1203	1090	10.2	15.2	15.2
		0.49	0.24	51.0	1140	1080	5.3	15.2	15.2
	600° F	0.48	0.48	0	1040	1000	3.8	15.6	15.6
C	1400° F	0.587	0.365	37.8	645	300	53.5	14.83	14.8
	1200° F	0.60	0.443	26.2	617	317	48.6	15.07	15.2
	1000° F	0.57	0.515	9.6	735	485	34.0	15.3	15.6
	600° F	0.52	0.52	0	440	440	0	15.0	15.0
D	1400° F	0.277	0.16	42.2	688	358	48.0	15.0	14.8
	1200° F	0.345	0.225	34.8	643	353	45.1	14.8	14.8
	1000° F	0.25	0.19	24.0	645	560	13.2	15.0	15.0

TABLE X

NO REDUCING EFFICIENCY, AND PERCENT LOSS OF CO, AS A FUNCTION OF FLOWRATE FOR CATALYST RE(23)75-P, AT T = 1200° F, GAS MIXTURE A

Flowrate		CO(%)			NO (ppm)			CO_2(%)	
Code #	ℓ/min	Before	After	%Loss	Before	After	%Loss	Before	After
5	18	1.09	0.82	24.8	1155	700	39.4	15.3	15.5
4	9	1.02	0.635	37.7	1067	580	45.6	16.0	16.0
3	4	1.167	0.60	48.6	1115	427	61.7	15.5	15.8
2	1	0.91	0.37	59.3	955	80	91.6	16.25	16.4

The flowrate scan data, at constant gas mixture and temperature, corresponding to the ϕ axis in Figure 22, is given in Table XII, completing the parametric study of the NO reducing efficiency of catalyst RE(M3)75.

C. Data for the Empty Catalyst Bed

In order to determine what contribution, if any, the empty catalyst bed made to the NO-reducing efficiency of the two rare earth oxide catalysts, a temperature-gas mixture scan, corresponding to most of the data points in Figure 21 on the T-M plane, and a flowrate scan, corresponding to the ϕ axis of Figure 21 were made. These data are presented in Tables XIII and XIV, constructed along the same lines as the corresponding tables for catalysts RE(23)75-P and RE(M3)75. If the experimental parameters of some data points indicated that continued measurements would not yield measurable data, as it occurred at the lower catalyst bed temperatures, these data points were omitted.

D. American Oil Company Study

A supporting experiment for the measurement of the NO reducing efficiency of catalysts RE(23)75-P and RE(M3)75 was made by the American Oil Company Research Department. These data, obtained by the use of the pulse-flame apparatus, bear out the measurements obtained by Solar as to the relative efficiencies of the two rare earth oxide catalysts studied. These data, as well as data obtained by American Oil on the generation of ammonia by these two catalysts, are reproduced in Appendix F.

TABLE XI

THE NO REDUCING EFFICIENCY, AND PERCENT LOSS OF CO, FOR CATALYST RE(M3)75 AT A FLOWRATE OF 9000 cc/min

Gas Composition	Temperature (°F)	CO (%)			NO (ppm)			CO_2 (%)	
		Before	After	Average Conversion (%)	Before	After	Average Conversion (%)	Before	After
A	1400	1.03	0.83	18.2	1060	1000	5.6	16.0	16.0
		1.00	0.83		1080	1020		16.4	16.0
	1400	1.06	0.92	12.3	1090	1060	3.2	15.6	15.8
		1.04	0.93		1100	1065		15.8	15.8
		1.07	0.93		1110	1070		15.8	15.8
	1200	1.10	0.98	9.2	1060	1000	6.5	16.0	16.0
		1.08	1.00		1090	1010		16.4	16.3
	1000	1.09	1.03	5.6	1050	1020	2.8	16.2	16.6
		1.06	1.00		1050	1020		16.3	16.3
		1.06	1.00		1060	1030		16.6	16.6
B	1400	0.49	0.40	18.4	1060	1020	3.8	16.0	15.8
		0.49	0.40		1060	1020		15.8	15.8
		0.49	0.40		1080	1040		15.8	15.8
	1200	0.53	0.46	12.5	1060	1020	4.4	15.2	15.0
		0.53	0.46		1070	1020		15.2	15.2
		0.54	0.48		1080	1030		15.2	15.2
	1000	0.48	0.47	2.1	1055	1040	1.18	16.4	16.4
		0.48	0.47		1060	1050		16.4	16.4
C	1400	0.64	0.53	16.0	640	480	25.6	14.4	14.4
		0.64	0.55		650	480		14.4	14.4
		0.66	0.55		660	490		14.6	14.6
	1200	0.53	0.50	6.6	580	540	6.9	13.9	13.8
		0.53	0.49		580	540		14.0	13.9
	1000	0.54	0.53	1.85	610	580	4.5	14.6	14.4
		0.54	0.53		610	585		14.6	14.6
D	1400	0.30	0.25	14.8	620	600	4.3	14.0	13.6
		0.30	0.25		620	600		13.6	13.6
		0.28	0.25		640	600		13.6	13.6
	1200	0.31	0.28	9.6	560	520	7.4	15.8	15.8
		0.31	0.28		565	520		15.8	15.8
		0.32	0.29		570	530		16.0	15.8
	1000	0.34	0.33	2.9	610	590	2.9	15.8	15.8
		0.34	0.33		615	600		15.8	15.8

TABLE XII

NO REDUCING EFFICIENCY, AND PERCENT LOSS OF CO, AS A FUNCTION OF FLOWRATE, FOR CATALYST RE(M3)75, AT T = 1200° F, GAS MIXTURE A

Flowrate		CO (%)			NO (ppm)			CO_2(%)	
Code #	ℓ/min	Before	After	Average Conversion %	Before	After	Average Conversion %	Before	After
5	18	1.05	0.94	8.6	1100	1060	4.7	15.9	15.8
		1.05	0.94		1140	1090		15.6	15.6
		1.05	1.00		1170	1110		16.2	16.0
4	9	1.10	0.98	9.2	1060	1000	6.5	16.0	16.0
		1.08	1.00		1090	1010		16.4	16.3
3	4	1.15	0.96	18.4	1210	1140	6.3	15.0	15.0
		1.17	0.92		1230	1140		15.0	15.0
		1.15	0.95		1220	1150		15.0	15.0
2	1	1.00	0.42	55.4	1180	140	88.0	15.0	15.2
		1.02	0.48		1200	145		14.9	15.1

4.2.2 Experimental Data for Transition Metal and Noble Metal Catalysts

The program was extended to cover additional catalysts after it became apparent that the rare earth oxide catalysts do not meet expectations regarding both NO reducing efficiency and ammonia generation factor, to be discussed below. Three transition metal catalysts were investigated, namely Monel 400, Solar Monel 400-Mod., which contains a minor additive in order to modify the oxidation resistance of Monel 400, and Copper Dichromate. The first two were non-oxidized metal sheets, bent into the form of burl saddles, as described in Reference 4. The last consisted of pressed oxide pellets, of 0.18 inch in height and diameter.

The two noble metal catalysts contained 0.5 percent of Palladium or Platinum, respectively, mixed into aluminum trioxide pellets of 0.15 inch height and 0.125 inch diameter.

The data obtained in the temperature scan, at constant gas mixture and flowrate, as shown in Figure 23, is tabulated in Table XV, for all five catalysts. The data are averaged again in the same fashion as those for the temperature scans of the rare earth oxide catalysts and the empty catalyst bed. The evaluation and discussion of these data will follow in Chapter 5.

TABLE XIII

PERCENT LOSS OF NO AND CO, VERSUS GAS MIXTURE AND TEMPERATURE, FOR EMPTY CATALYST BED, AT A GAS FLOWRATE OF 9000 cc/min

		CO (%)			NO(ppm)			CO_2(%)	
Composition	Temperature	Before	After	%Loss	Before	After	%Loss	Before	After
A	1400° F	0.97	0.90	7.2	1133	1098	3.1	16.6	16.63
		1.07	1.00	6.5	1118	1083	3.1	16.1	16.7
	1200° F	1.15	1.13	1.7	1120	1100	1.8	16.0	16.0
	1000° F	*	*	*	*	*	*	*	*
B	1400° F	0.487	0.433	11.1	1203	1193	0.8	15.8	15.8
	1200° F	0.49	0.466	4.9	1080	1080	0	16.0	16.0
	1000° F	*	*	*	*	*	*	*	*
	600° F	*	*	*	*	*	*	*	*
C	1400° F	0.673	0.62	7.9	713	567	20.5	15.87	15.87
		0.65	0.63	3.1	660	573	13.2	15.7	15.63
	1200° F	0.57	0.55	3.5	650	640	1.5	15.0	15.6
	1000° F	*	*	*	*	*	*	*	*
	600° F	*	*	*	*	*	*	*	*
D	1400° F	0.32	0.30	6.3	743	713	4.0	14.53	14.53
	1200° F	0.253	0.243	4.0	630	617	2.0	15.33	15.33
	1000° F	*	*	*	*	*	*	*	*

* Not Measured Due to Lack of Effect.

TABLE XIV

PERCENT LOSS OF NO AND CO, AS A FUNCTION OF FLOWRATE, FOR EMPTY CATALYST BED AT T = 1200° F, GAS MIXTURE A

Flowrate		CO (%)			NO (ppm)			CO_2(%)	
Code #	ℓ/min	Before	After	%Loss	Before	After	%Loss	Before	After
5	18	0.925	0.885	4.3	1065	1045	1.9	17.13	17.03
4	9	1.15	1.13	1.7	1120	1100	1.8	16.0	16.0
3	4	0.98	0.857	12.6	1083	957	11.6	15.93	16.0
2	1	1.047	0.66	36.9	1080	286.6	73.5	15.8	16.0

An additional catalyst, denoted Solar Monel 400-Core,* was also tested. It was placed into a tube 4 inches long, with a diameter of slightly over one inch. Its volume was thus 61.5 cc, its weight was 110 grams. Four experimental runs at constant temperature were made with this new catalyst bed. The results are shown in Table XVI, which also lists the space velocity involved for each run.

The data indicate a slight space velocity dependence of the efficiency η, but in general the percentage of NO reduced is the same as that obtained with the burl saddles of Monel.

4.3 THE AMMONIA GENERATING FACTOR FOR ALL CATALYSTS TESTED

The study of the catalytic reduction of NO by CO in exhaust gases showed both in the literature (Ref. 4 and 5) and at Solar, that ammonia is formed as a byproduct. Since, with a two-stage catalyst bed, all ammonia is reconverted into NO at the oxidizing stage, ammonia generation will effectively limit the NO reduction efficiency of the catalyst. Experiments have therefore been run, measuring the quantity of NH_3 generated for each of the catalysts tested.

The method of analysis has been discussed already in Chapter 3. The data obtained, along with the experimental conditions, are given in Table XVII. The evaluation of the catalysts, along with the calibration of their ammonia-producing factors, will follow in Chapter 5.

---

* Solar Monel 400-Core is a design consisting of extended surfaces of Monel interleaved between stainless steel sheet collected in a right cylinder configuration.

TABLE XV

NO REDUCING EFFICIENCY OF SELECTED TRANSITION METAL AND NOBLE METAL CATALYSTS, VERSUS TEMPERATURE, IN SYNTHETIC EXHAUST GAS APPARATUS

(Gas Composition A and Flowrate of 9000 cc/min Apply to All Tests, Except Where Otherwise Noted)

Catalyst	Temperature	CO (%)			NO (ppm)			CO_2(%)	
	°F	Before	After	%Loss	Before	After	%Loss	Before	After
Type 400 Monel	1400	1.23	0.14	88.6	1070	55	94.9	17.2	18.0
	1200	1.22	0.19	84.4	1100	65	94.1	17.2	18.0
	1000	1.22	0.07	94.3	1100	65	94.1	17.2	18.0
	800	1.21	0.10	91.7	940	70	92.6	17.0	18.0
Type 400 Monel-Modified	1400	1.28	0.10	92.2	1170	80	93.2	17.4	18.2
		1.28	0.10		1170	80		17.4	18.2
		1.30	0.10		1190	80		17.6	18.3
	1400	1.23	0.11	91.1	1230	85	93.1	17.4	18.2
	1200	1.18	0.10	91.5	1170	85	92.7	17.2	18.0
	1200	1.175	0.07	94.0	1210	80	93.4	17.0	18.0
	1000	1.27	0.18	85.8	1170	80	93.2	17.4	18.0
		1.27	0.18		1190	80		17.2	18.0
	1000	1.15	0.11	90.4	1210	80	93.4	17.0	18.0
	800	1.17	0.22	81.2	1210	100	91.7	17.8	18.0
Copper Dichromate $CuCr_2O_7$	1400	1.35	0.15	88.9	1140	230	79.8	17.8	18.6
	1200	1.26	0.15	88.1	1160	220	81.0	17.6	18.4
	1000	1.13	0.13	88.5	1130	220	80.5	16.9	17.7
	800	1.26	0.15	88.1	1160	220	81.0	17.6	18.4
Palladium (0.5% in Al_2O_3)	1400	1.16	0.69	41	1150	280	75.6	16.9	17.2
		1.16	0.68		1150	280	75.6	16.8	17.2
	1000	1.20	0.88	28	1080	460	57.4	16.0	16.5
		1.22	0.88		1090	450	58.7	16.5	16.5
Platinum (0.5% in Al_2O_3)	1400	1.20	0.65	46	1160	320	72.4	16.8	17.0
		1.20	0.63	48	1170	320	72.6	17.0	17.2
		1.22	0.65	47	1190	320	73.1	17.0	17.2
	1200	1.18	0.52	56	1200	320	73.3	17.0	17.4
		1.17	0.52	56	1200	325	72.9	17.1	17.4
		1.19	0.53	55	1220	325	73.4	17.2	17.4
	1000	1.16	0.33	72	1000	240	76.0	15.9	16.8
		1.13	0.34	70	1030	250	75.7	13.9	16.8
		1.11	0.33	70	1030	250	75.7	16.1	16.9
	800	1.17	0.375	68	1190	325	72.7	16.8	17.2
		1.16	0.36	69	1190	330	72.2	16.8	17.2
		1.15	0.35	70	1200	330	72.5	16.8	17.2
	800 No Water	1.25	0.73	42	1260	240	80.9	17.0	17.2
		1.25	0.75	40	1270	250	80.3	17.0	17.2
		1.25	0.73	42	1280	260	79.7	17.0	17.2

TABLE XVI

NO REDUCING EFFICIENCY OF MONEL 400 CATALYST IN DIFFERENT STRUCTURAL CONFIGURATION

(Solar Monel 400-Core)

Log Book Ref. 148/9; Gas Mixture A, NO = 1160, R 10,
V_{cat} = 61.5 cc, T = 1400° F

ω cc/min	ν hr^{-1}	CO (%)		NO (ppm)		η (%)	η average (%)	CO_2 (%)	
		Before	After	Before	After			Before	After
4000	12874	1.00	0.375	1160	55	95.26		18.1	18.7
4000	12874	1.00	0.375	1160	55	95.26	95.26	18.2	18.7
9000	28967	1.17	0.50	1180	90	92.37		18.2	18.5
9000	28967	1.20	0.48	1200	75	93.75	93.06	18.2	18.7

Note: The runs with the gas composition other than gas mixture A, using the catalyst Monel 400, were made to duplicate and verify the data reported in Reference 4. With the use of these special gas mixtures the results reported in the literature cited were verified, which at the same time, therefore, confirms the validity of the data obtained with Solar's experimental apparatus utilizing gas mixture A (1000 ppm NO, CO/NO = 10).

TABLE XVII

AMMONIA FORMATION FOR ALL CATALYSTS STUDIED IN THIS PROGRAM AT T = 1400° F (EXCEPT WHERE NOTED OTHERWISE), AND GAS FLOWRATE OF 9.0 ℓ/min

Catalyst	Gas Composition	Run No.	Titration Period	Ammonia (ppm)	Average For Set of Runs (ppm)
RE(23)75-P	A	I 1	10 min	196	174
		2	"	146	
		3	"	157	
		4	"	197	
RE(M3)75	A	VI 1	"	25.0	31.6
		2	"	49.2	
		3	"	43.0	
		4	"	30.0	
		5	"	11.0	
None Bed Empty	A	II 1	"	7.4	5.0
		2	"	5.3	
		3	"	3.7	
		4	"	3.7	
Monel 400	A	III 1	"	16.3	12.6
		2	"	16.4	
		3	"	9.3	
		4	"	8.4	
Monel 400	NO: 870 ppm; CO: 1.15% H_2: 2000 ppm; N_2: Bal.	IV 1	7.5 min	19.4	26.2
		2	10 min	21.3	
		3	8 min	21.3	
		4	8 min	42.6	
Monel 400	NO: 820 ppm; CO: 2.4%; H_2: 1.0%; N_2: Bal.	V 1	10 min	83	108
		2	6 min	72	
		3	6 min	128	
		4	10 min	103	
		5	10 min	156	
Solar Monel 400 Modified	A	XI 1	10 min	14.0	10.8
		2	"	11.5	
		3	"	7.0	
$CuCr_2O_7$	A	XII 1	"	11.5	9.1
		2	"	8.2	
		3	"	7.7	
Pd on Al_2O_3	A	XIV 1	"	220	218
		2	"	216	
Pt on Al_2O_3	A	VIII 1	"	462	454
		2	"	491	
		3	"	408	
Pt on Al_2O_3	A 800° F	IX 1	"	663	467
		2	"	354	
		3	"	385	
Pt on Al_2O_3	A, No Water 800° F	X 1	"	776	534
		2	"	423	
		3	"	404	

5

EVALUATION OF DATA AND DISCUSSION

This chapter has been divided into two sections, the first one of which will give a graphical presentation of all the experimental data obtained in measuring the parameters for the catalytical NO reduction efficiency, and then evaluate the NH_3 generation data; the second section will summarize the data into a parametric design chart and discuss its limitations.

5.1 EVALUATION OF EXPERIMENTAL DATA

5.1.1 Graphical Presentation of Catalytical Efficiency Parameters

In presenting the data in graph form, we shall proceed in the same order as in the previous chapter, namely, first show the data for catalysts RE(23)75-P, RE(M3)75, and the empty bed, and then those for the other catalysts in the program.

A. Data for Catalyst RE(23)75-P and Relative Empty Bed Effect

The experimental data for the high purity rare earth oxide catalyst, RE(23)75-P, are presented in the next four figures. The first one, Figure 24, gives the flowrate dependence of the catalytical efficiency. Since the data obtained with the "empty bed" showed a large contribution of this factor for low flowrates, the "empty bed" efficiency versus flowrate has also been entered into Figure 24. Thus, the only problem was to find a proper method of evaluating the actual catalyst efficiency, in the face of the significant empty bed contribution at the two lower flowrates. (This effect was the reason why no measurements at the flowrate of 460 cc/min, code #1, have been made.)

Let us denote the efficiency of the bed-catalyst system η_c, and of the empty bed η_o. A direct subtraction, in order to obtain the catalyst efficiency η, of the form

$$\eta = \eta_c - \eta_o \tag{17}$$

would yield an anomalous result for the η vs. φ graph, namely the catalyst efficiency would vanish as the gas residence time increases. Since a result like that does not

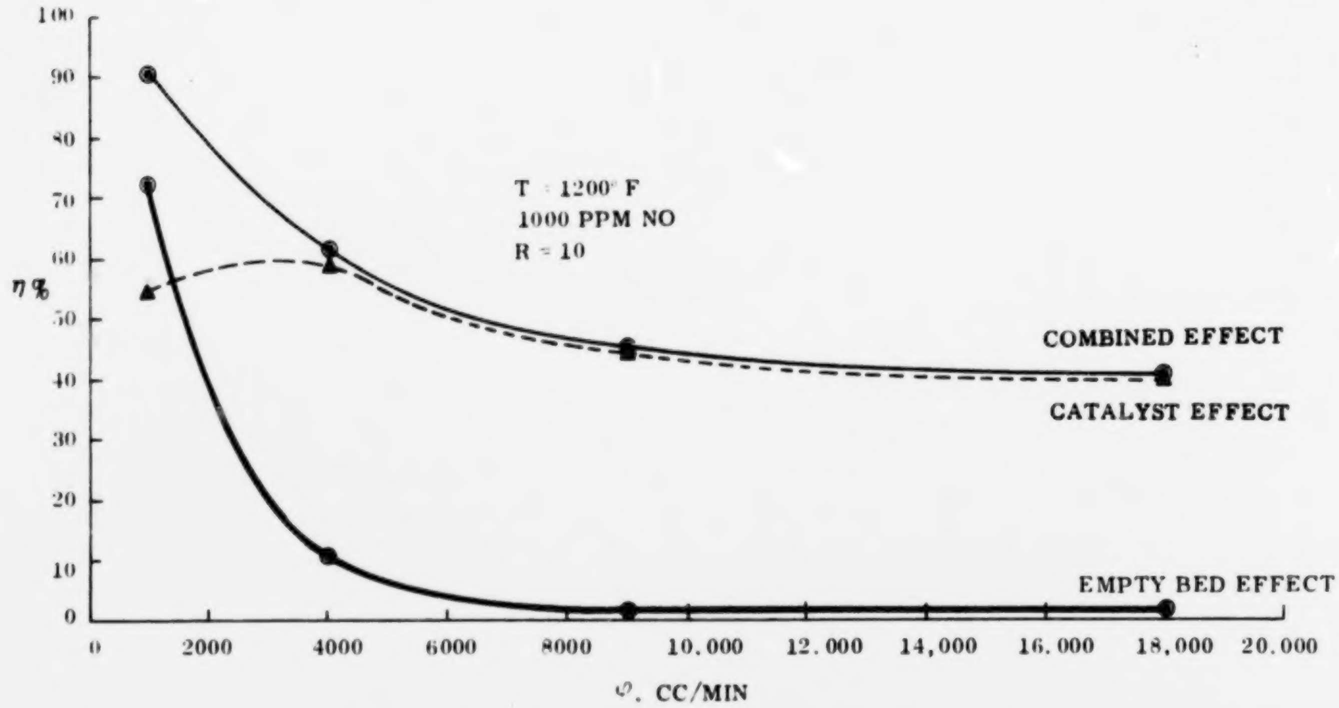

FIGURE 24. NO REDUCING EFFICIENCY η VERSUS FLOWRATE φ FOR RE(23)75-P. (DATA FOR COMBINED EFFECT, EMPTY CATALYST BED, AND DERIVED VALUES FOR THE CATALYST)

appear reasonable, it was rather assumed that the bed and the catalyst caused the combined efficiency effect in a rather non-linear fashion. Thus, the approach was chosen to obtain the effective catalyst efficiency parameter by the relation

$$\eta = \sqrt{\eta_c^2 - \eta_o^2} \qquad (18)$$

The result is shown in Figure 24. For the high flowrates, relation (18) gives a difference between η_c and η in the third decimal, while (17) would give one in the second. This is shown, in exaggerated fashion in Figure 24, by the placement of the dashed η curve underneath the solid combined curve, though at that scale the two would coincide until close to $\varphi = 4000$ cc/min. Here the difference between η according to relation (17) and relation (18) becomes significant. The η curve is drawn according to relation (18) until $\varphi = 1000$ cc/min.

However, let us consider also another approach. Due to the large contribution of the "empty bed", the catalyst does not see a 1000 ppm NO concentration, but only a 286 ppm one. Thus, the initial test conditions are here no longer valid. Hence, if one considers that only 286 ppm NO reach the catalyst here, which is the quantity left after the "empty bed" was through with it, and the catalyst reduces that to the 91 ppm level, the efficiency is 63 percent, or about equal to that at the 4000 cc/min flowrate, which appears to be the most reasonable result. Thus, this figure shows that the flowrate dependence of the NO reducing efficiency of RE(23)75-P is only very slightly temperature dependent.

Figure 25 gives the temperature dependence of η for RE(23)75-P at $\varphi = 9000$ cc/min. This figure gives the mean of η as measured for all four gas compositions tested, so that the general trend is visible. With increase in temperature, η first grows slowly, then faster between 1000 and 1200° F, only to slow down again above 1200° F.

The actually measured values of η as a function of temperature for both initial NO concentrations and both CO/NO ratios is shown in Figure 26. Here it is interesting to note that while the ratio effect behaved as generally expected, even though not so pronounced, the catalyst appeared to be slightly more efficient for the smaller initial NO concentration than for the larger one. According to theory there should have been no effect due to initial concentration changes. The average values of η, shown in Figure 25, are designed by the triangular points and the full curve in Figure 26.

Figure 27 represents a map of the catalyst efficiency in NO reduction versus the space velocity ν, within a given region of temperatures and flowrates. The space velocity is defined as

$$\nu = \frac{60\varphi P_o T_1}{V P_1 T_o} \left[\mathrm{hr}^{-1}\right] \tag{19}$$

where 60φ is the flowrate in cc/hr (60 min/hr and φ in cc/min), V is the volume of the catalyst in cc, P_o and T_o are the standard temperature and pressure, in absolute units, and P_1 and T_1 are the gas pressure and temperature, respectively, also in absolute units. For a given catalyst of volume V and entering gas pressure P_1, the space velocity can be expressed as

$$\nu = A \varphi T \tag{20}$$

where

$$A = \frac{60\, P_o}{V P_1 T_o} \tag{21}$$

Thus, ν can be plotted out on the φ, T scale as a family of parabolas, determined by A. This was done in Figure 27, for the range of T between 1460 and 1860° R. or 1000 and 1400° F, and flowrates between 0 and 23,000 cc/min. The abscissa itself is the

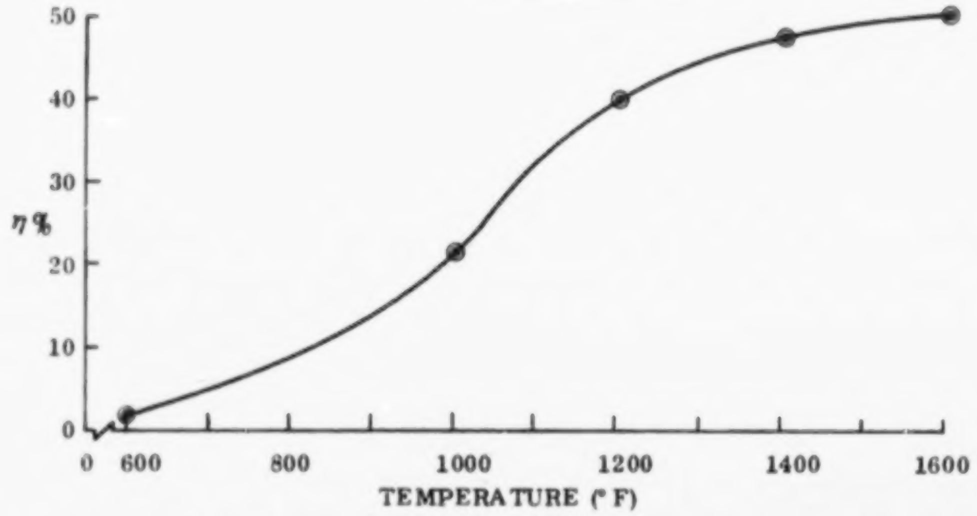

FIGURE 25. NO REDUCING EFFICIENCY η OF CATALYST RE(23)75-P VERSUS TEMPERATURE T, AVERAGED OVER FOUR GAS COMPOSITIONS TESTED

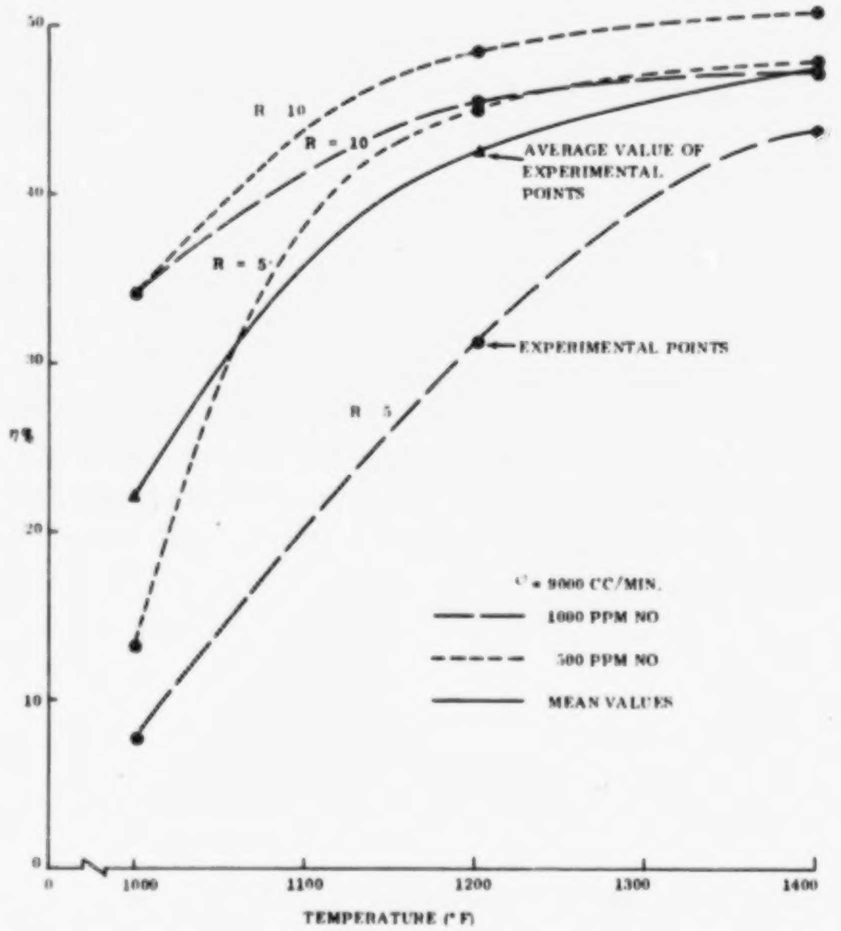

FIGURE 26. NO REDUCING EFFICIENCY η OF CATALYST RE(23)75-P VERSUS TEMPERATURE T, FOR VARIOUS NO CONCENTRATION AND CO/NO RATIOS R

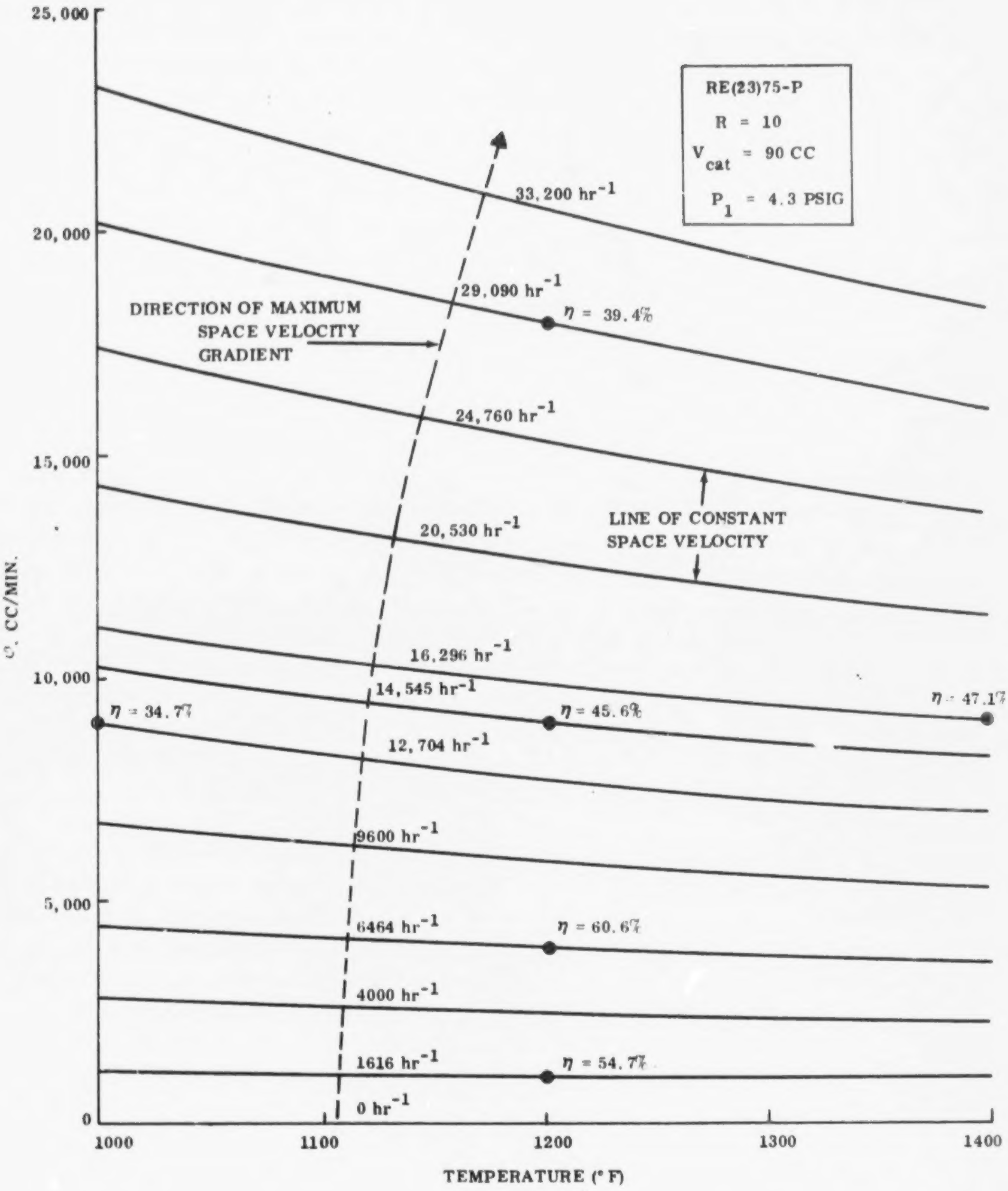

FIGURE 27. MAPPING OF CATALYST EFFICIENCY η VERSUS SPACE VELOCITY ν WITHIN A GIVEN TEMPERATURE AND FLOWRATE REGION. INITIAL NO CONCENTRATION IS 1000 PPM NOMINAL

parabolic curve for $\nu = 0\ \mathrm{hr}^{-1}$, and selected segments of the family of parabolas for various values between $1616\ \mathrm{hr}^{-1}$ and $33,200\ \mathrm{hr}^{-1}$ are given. The dashed curve denotes the direction for steepest gradient of increase in ν. It shows the magnitude of the relative contributions of the temperature and flowrate on spece velocity, by its degree of inclination. This is also seen from the experimental points: ν changes from $12,704\ \mathrm{hr}^{-1}$ to $16,296\ \mathrm{hr}^{-1}$ at $\varphi = 9000$ cc/min between 1000 and 1400° F, while at constant T, ν changes from $1600\ \mathrm{hr}^{-1}$ to $2900\ \mathrm{hr}^{-1}$ with increase in φ.

The values of η themselves show that it is more temperature dependent than space velocity dependent in the range of consideration. Thus, this figure gives a pretty good idea of the interaction of temperature, flowrate, and space velocity with the NO reducing efficiency. It also shows that the majority of testing was done in the neighborhood of $\nu = 15,000\ \mathrm{hr}^{-1}$, which is the same value of νas that reported for most catalysts in the literature (Ref. 4-7).

The value of η for the low flowrate of $\varphi = 1000$ cc/min was obtained by the method of equation (18). If one uses instead the reduction of the remnant NO by the catalyst, as we have done earlier in this section, η would be 63 percent instead of the value of 54.7 percent, as shown in Figure 27.

B. Data for Catalyst RE(M3)75 and Relative Empty Bed Effect

The next two figures, Figure 28 and 29, give the flowrate and temperature/gas mixture dependence of the efficiency of catalyst RE(M3)75, while Figure 30 gives the temperature/gas mixture dependence of the efficiency of the "empty catalyst bed". It shows that this catalyst has insignificant NO reducing efficiency.

First, Figure 28 gives the flowrate dependence of the NO reducing efficiency for RE(M3)75 and for the empty bed. The graph is based on the four experimental data points obtained at $\varphi = 1000$ cc/min, 4000 cc/min, 9000 cc/min and 18,000 cc/min. While on three of these four points the efficiency of RE(M3)75 is slightly above that of the empty bed (being of stainless steel it is a catalyst in its own right) at the point of $\varphi = 4000$ cc/min it is even below that for the empty bed. The meaning of this particular result is not clear, however, the data taken as a whole clearly indicate that the NO reducing efficiency of RE(M3)75 differs little from that of its stainless steel housing.

Figure 29 shows the dependence of η for RE(M3)75 on the parameters T, R, and initial NO concentration. The figures shows that η is essentially independent of temperature, in the case of this catalyst, and the lower NO concentration resulted in slightly higher efficiencies. The curve for R = 10, NO initial = 1000 ppm appears anomalous, compared to the other three curves, showing a high temperature dependence and much higher values for η. Therefore, the corresponding data for the empty bed

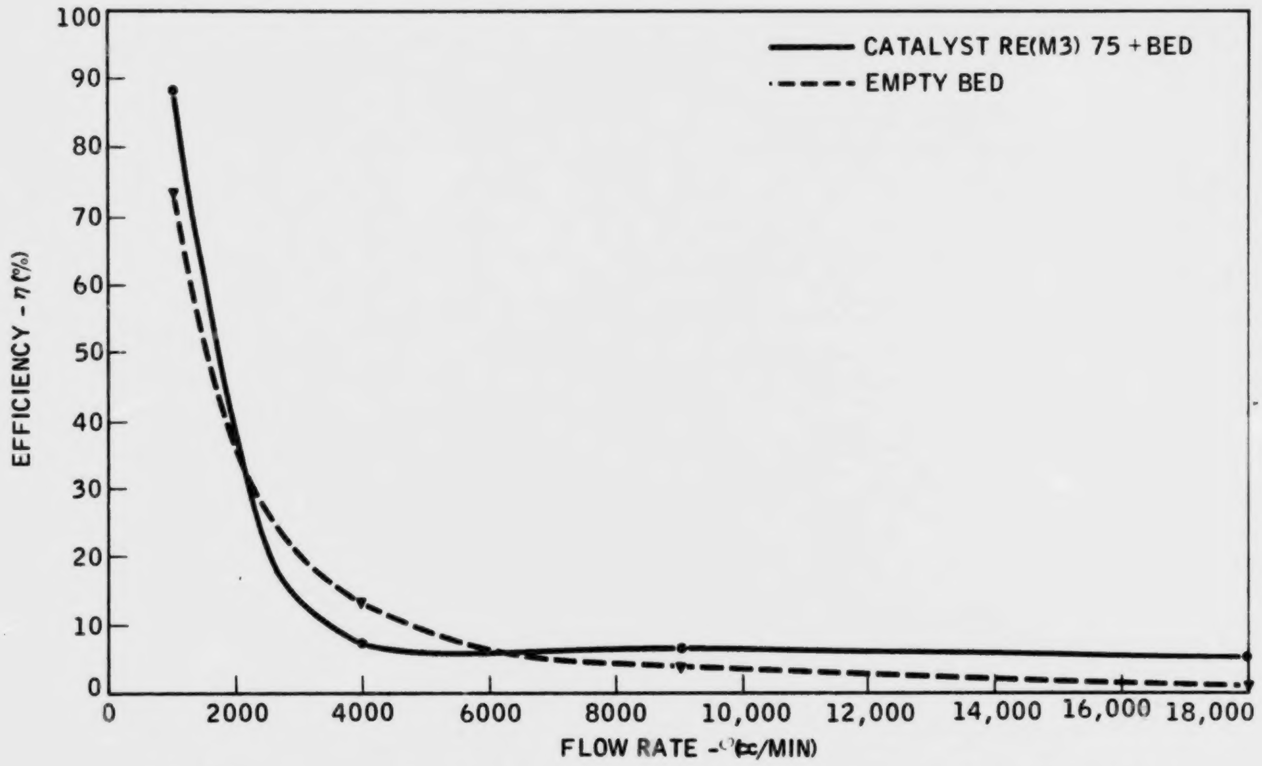

FIGURE 28. NO-REDUCING EFFICIENCY η VERSUS FLOWRATE φ

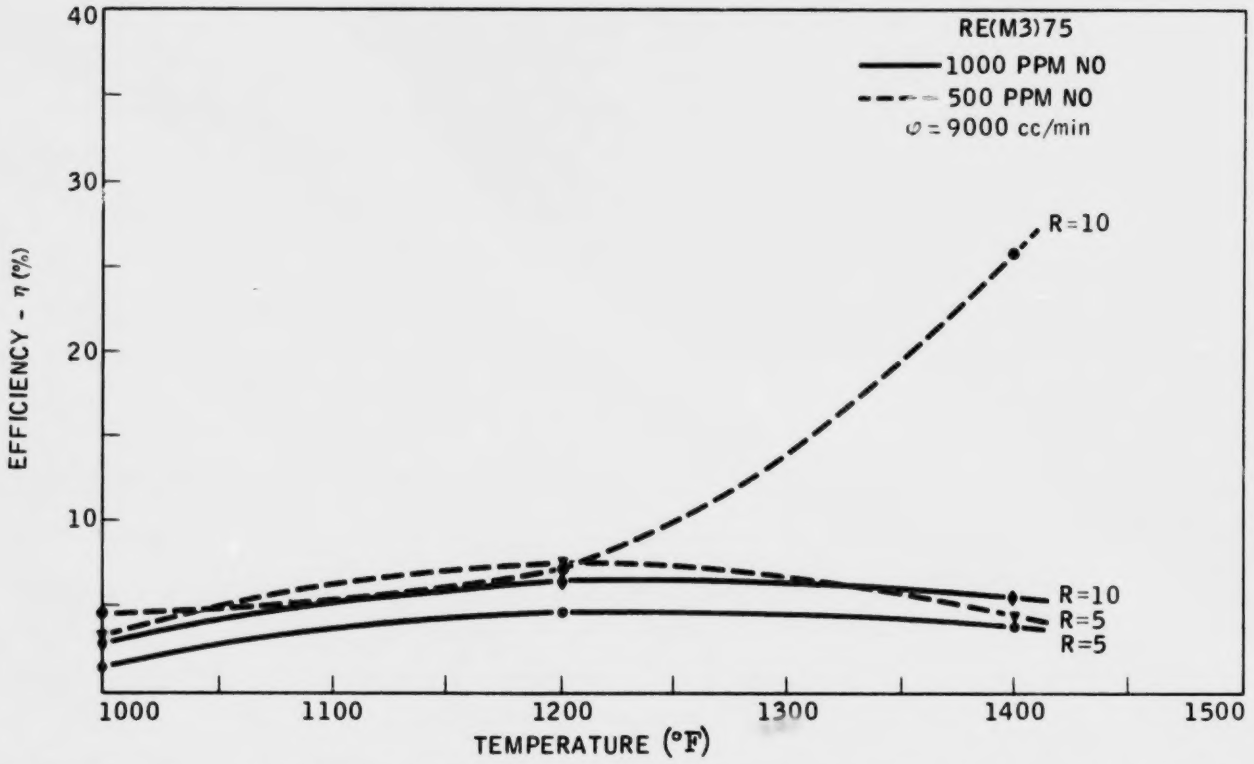

FIGURE 29. NO-REDUCING EFFICIENCY η VERSUS TEMPERATURE T, FOR VARIOUS NO CONCENTRATIONS AND CO/NO RATIOS R

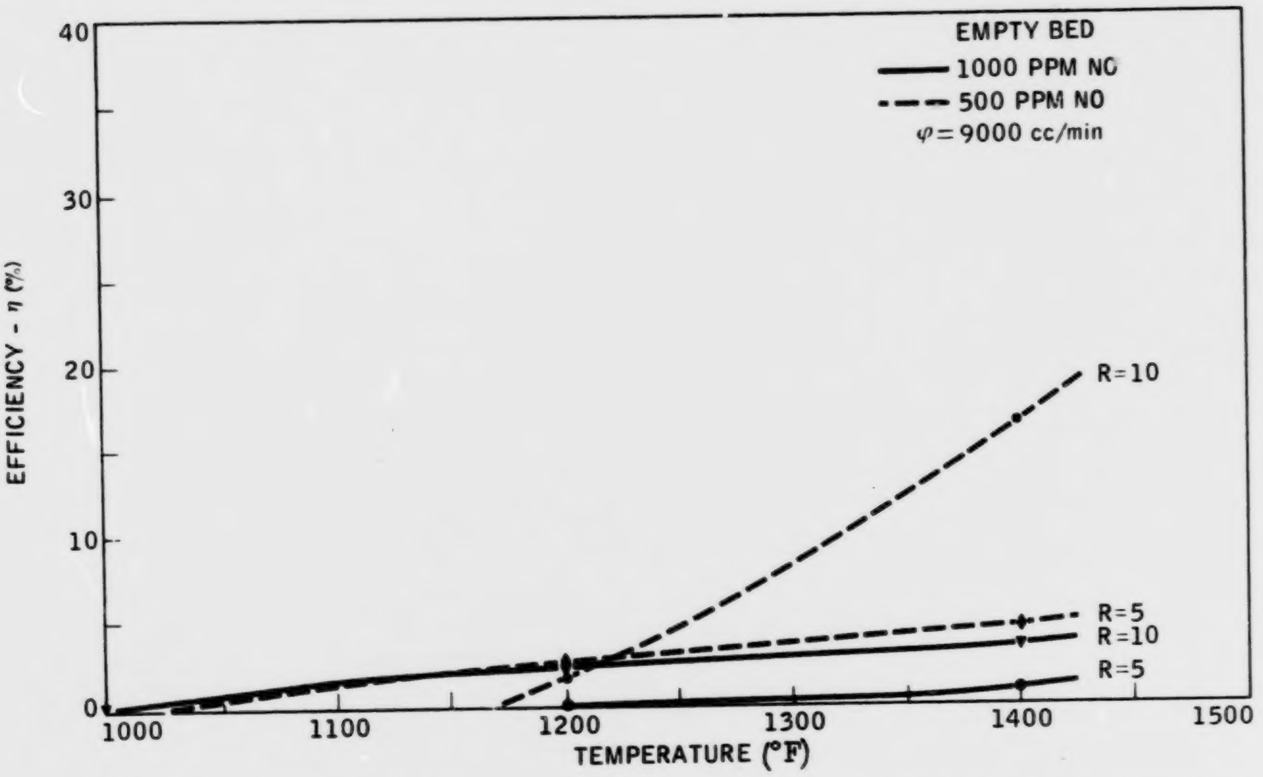

FIGURE 30. NO REDUCING EFFICIENCY η FOR THE EMPTY BED VERSUS TEMPERATURE T, FOR VARIOUS NO CONCENTRATIONS AND CO/NO RATIOS R, IN THE CATALYST BED IN ABSENCE OF CATALYST

Figure 30, were also plotted. This figure shows, too, essentially no temperature dependence of η, with the exception of R = 10, NO initial = 1000 ppm. The anomalous behavior of that curve in Figure 29 thus finds its explanation.

Comparing Figures 29 and 30, one sees that η for RE(M3)75 is only by a factor of two greater than that of the empty stainless steel bed. This catalyst, therefore, showed no behavior different from that of the empty bed, and has to be adjudged as not suited for catalytic reactions of the type studied in this program.

C. Comparison of η Versus T for Transition Metal Catalysts and Noble Metal Catalysts With the Rare Earth Oxide Catalysts

The data of Table XV, regarding the NO reducing efficiency of the five non-rare earth oxide catalysts, have been plotted out in Figure 31, with the data for the two REO catalysts and the empty bed, all taken under the same experimental conditions, being added. In this way, Figure 31 becomes a comparison criterion for all eight catalyst configurations considered. One data point for Solar catalyst Monel 400-Core, taken at 1400° F under the same gas mixture and flow conditions, has been added, for purposes of comparison. However, due to its smaller volume, this catalyst is being

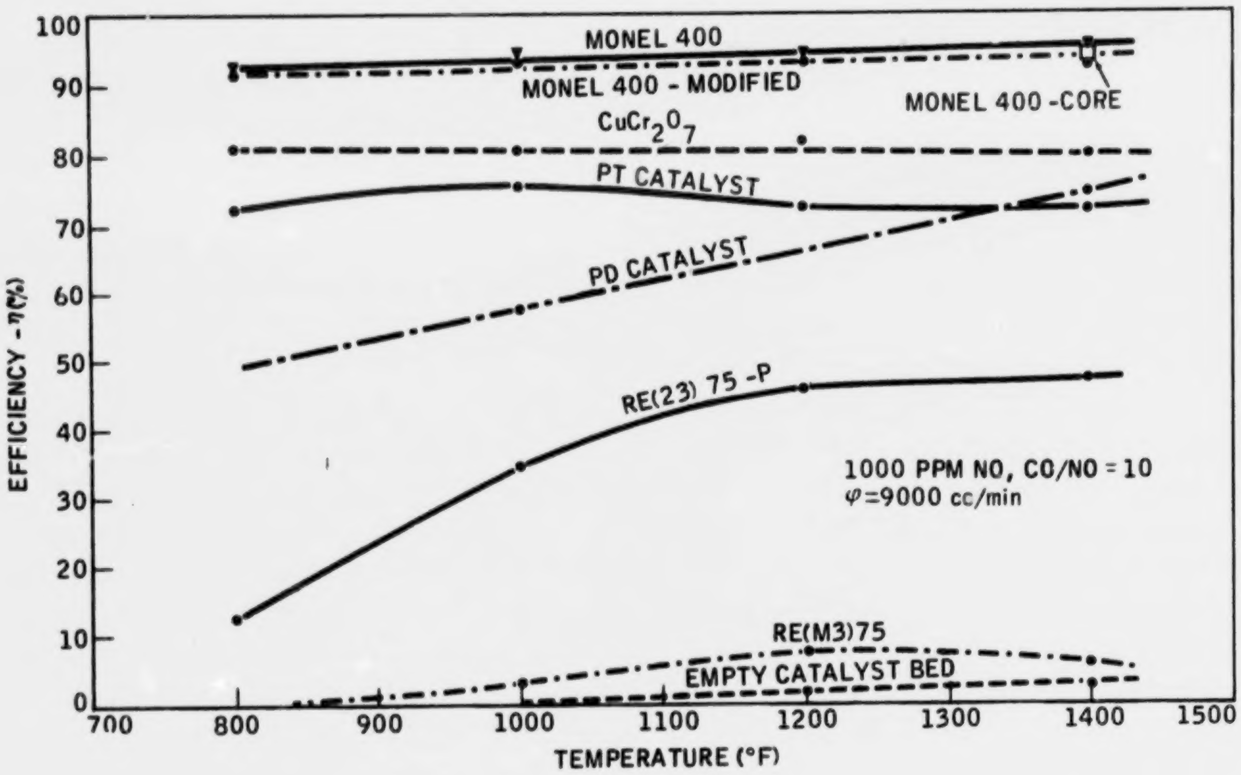

FIGURE 31. COMPARISON OF THE NO REDUCING EFFICIENCY η AS A FUNCTION OF T FOR THE VARIOUS CATALYSTS TESTED

measured at a larger space velocity than all the others. The conditions of flowrate, CO/NO ratio, NO concentration, and temperature range, are all noted in that figure.

Monel catalyst had the highest effectivity at NO reduction plus NH_3 generation. Although it is well known Monel 400 cannot meet the goal -- long term catalyst stability, Solar Modified Monel had essentially the same effectivity however, and is expected to show substantially increased stability. The data point for Solar Monel 400-Core falls between those of the two other Monel catalysts.

Next comes $CuCr_2O_7$, in the 80 percent efficiency range. Its efficiency decreases with rising catalyst temperatures, indicating its maximum efficiency temperature to be below 800° F. Next follows the platinum catalyst over the temperature range up to 1300° F. It shows an increase in η between 800 and 1000° F, but falls off thereafter. The palladium catalyst, starting out in the 50 percent range, appears to have a strong temperature dependence, and it overtakes the faltering platinum catalyst above 1300° F. However, only two data points have been obtained with the Pd catalyst, thus its curve is only an indication of its behavior.

Further down, rising from 10 to about 47 percent efficiency, we find the catalyst RE(23)75-P. It shows the strongest temperature dependence of all in the lower temperature region, flattening out somewhat, but still rising, in the higher regions of temperature. Last, just slightly above the empty bed levels, is RE(M3)75.

The conclusion to be drawn from Figure 31 is that while the pure REO have a vastly better NO-reducing efficiency than the mixed REO, which contain also other impurities, even the pure rare earth oxide catalysts trail far behind those consisting of the transition metals and precious metals, at least in their present formulation. Monel appears to be the best NO reducing catalyst of all.

Figure 31 shows, essentially, that the REO catalysts are not suited for the reduction of NO by CO in an exhaust gas environment, containing O_2, H_2O, hydrogen and other components. However, of the other catalysts tested, both the Pd and Pt catalysts were also disappointing. The Pd catalyst appears to be regarded as the leader in some circles. However, it is possible that its performance improves with an increase of the precious metal content. That approach, however, would destroy the economic feature of these catalysts, as compared with the others in this program. In addition, Table XV shows that the Pt catalyst, which is essentially an oxidation catalyst, did not do too well with the oxidation of CO, either. The Pt catalyst does not exceed a 70 percent CO oxidation efficiency, and the Pd catalyst is at most 41 percent effective here. This shows that for the Pt catalyst oxygen is needed to remove CO from the exhaust, while the Monel catalysts, and also $CuCr_2O_7$, are highly effective on the CO front as well.

5.1.2 Comparison of Ammonia-Generating Factor E for All Catalysts Tested

In completing the evaluation of the five catalysts studied in this program, their ammonia generating factors would also have to be compared. This ammonia-generating factor, denoted here E, is defined as the fraction of the ammonia generated in ppm, divided by the nitric oxide reduced. It is based on the assumption that all NH_3 generated derives from the original NO concentration, and none from the free nitrogen molecules in the gas mixture. To be expressed in percent E, is given by the expression

$$E = \frac{c}{X_{NO}^{\circ}\,\eta} \quad \times 100\%$$

where c is the concentration of NH_3 generated, X_{NO}° is the initial NO concentration, and η, as before, the NO reducing efficiency; however, it is now expressed as a number between 0 and 1, and not in percent:

$$0 \leq \eta \leq 1$$

This factor E has been tabulated in Table XVIII where the catalysts are arranged according to their values of η, in descending order. The mean of the concentrations of NH_3, plus the percent error due to the maximum deviations in c are noted in the table, resulting in a mean value of E, as well as in the tabulation of the total range in E for each catalyst, due to the error in c. The data for c have been obtained from Table XVII in Chapter 4. The experimental conditions are denoted beneath the title of Table XVIII.

TABLE XVIII

COMPARISON OF AMMONIA GENERATION FACTOR E (IN % OF NO REDUCED) FOR THE VARIOUS CATALYSTS TESTED AND WITH PREHEATER PLUS EMPTY BED ONLY

NO = 1000 ppm Nominal Initially, CO/NO = 10
T = 1400° F, $\varphi = 9$ ℓ/min, in Basic Exhaust Gas Mixture A

Catalyst	Overall NO Reducing Eff. η	Ave. NH_3 Generated ppm	Maximum Deviation in NH_3 Generated ppm	% Error in NH_3 Generated (from max.dev.)	Mean Value of E %	Total Range in E (based on max.dev. in NH_3) %
Monel 400	0.95	12.6	± 4.2	± 33	1.21	0.81 - 1.61
Monel 400-Mod.	0.93	10.8	± 3.8	± 35	1.06	0.69 - 1.41
$CuCr_2O_7$	0.80	9.1	± 2.4	± 26	1.03	0.76 - 1.30
Pd on $A\ell_2O_3$	0.76	218	± 2	± 0.92	26.23	25.97 - 26.49
Pt on $A\ell_2O_3$	0.73	454	± 46	± 10.13	56.75	51.00 - 62.50
RE(23) 75-P	0.47	174	± 28	± 16	33.65	28.27 - 39.03
RE(M3) 75	0.06	31.6	± 20.6	± 65	47.88	16.76 - 79.00
Empty Bed	0.03	5.0	± 2.4	± 48	15.15	7.88 - 22.42

As a result of the data of Table XVIII, the two Monel catalysts and $CuCr_2O_7$ appear all to be in the same leading class, generating the least percentage of ammonia. Solar's Monel 400-Mod. seems here to lead the ordinary Monel formulation, pointing to the conclusion that modifications of Monel's oxidation resistance also have an influence on the ammonia generation factor.

Next follows the empty bed, outclassing not only the rare earth oxide catalysts, but also the two noble metal catalysts as well.

Next in line follows the palladium catalyst, which gave the most consistent readings on ammonia generation and the least scattering of data. As a result, its ammonia generation factor is most precisely defined, from among all the catalysts tested.

The next higher class in ammonia formation is represented by the two rare earth oxide catalysts. Formula RE(23)75-P generates about twice as much ammonia than does the "empty catalyst bed". Formula RE(M3)75 appears to have a slightly higher value of E than its pure oxides sister formulation, however, due to the large scatter in the data on its NH_3 generation, the range in E is so large that nothing definite can be said about it on the basis of these results. If one takes into consideration, however, the data obtained by the American Oil Company, as listed in Table III of Appendix F, one sees that the true value of E for RE(M3)75 falls into the low part of the range as shown in Table XVIII, and this catalyst generates less ammonia than RE(23)75-P and even the palladium catalyst; as a matter of fact, RE(M3)75 falls into the same class as the "empty bed".

The catalyst with the highest ammonia formation factor is the platinum one, which turns over one half of the NO reduced into NH_3. This suggests that the Pt catalyst is not suited as a catalytic agent for the reduction of NO. The catalyst was included in this study for comparative purposes.

A new theory of the generation of ammonia in automobile exhaust gases, indicating the complexity of the catalytical reactions in these gas mixtures, has been proposed by Richard L. Klimisch and Gerald J. Barnes of GM (Ref. 20). They believe that the carbon monoxide is not necessarily the prime reducing agent for the nitric oxide in automobile exhaust gases. Instead the carbon monoxide reacts with water to yield carbon dioxide and hydrogen; the hydrogen then reduces the nitric oxide, producing ammonia in the process. As exhaust temperature increases, less ammonia is generated because it becomes unstable and decomposes into nitrogen and hydrogen. From this theory there follows that a catalyst generates less ammonia if it can bring preferentially CO and NO together, instead of H_2 and NO.

Both of the above theories, namely that NH_3 is a byproduct of the NO-CO reaction, or NH_3 is an intermediate step, assume essentially that all NH_3 generated derives from the original NO concentration. However, there is another school of thought which states that at sufficiently high temperatures in exhaust gases ammonia is generated from nitrogen itself by reactions with hydroxide radicals and hydrogen atoms, yielding both ammonia and nitric oxide (Ref. 21). Under such conditions our ammonia generating factor E would lose all significance. However, in the exhaust gases the temperature is too small for free hydroxide radicals to exist, and, following Klimisch's reasoning, any ammonia generated at the combustion temperatures will automatically decompose into its elements, before getting into the exhaust stream.

5.2 PARAMETRIC DESIGN CHARTS FOR CATALYST FORMULA RE(23)75-P

The experimental data for catalyst RE(23)75-P have been summarized in a nomograph type chart and a standard version parametric design chart has been constructed. Both these figures shall be discussed in detail below.

No charts have been made for RE(M3)75, since its efficiency is insignificant. The other catalysts considered in this program are well known in the literature. Solar's catalyst Monel 400-Mod. behaves essentially in the same manner as the standard Monel 400.

Figure 32 presents a summary of all experimental data for the catalyst RE(23)75-P in the form of a nomograph, with an extension to the CO/NO ratio of 15.

The variables have been combined into two groups: the CO/NO ratio and the initial NO concentration being the first variable, and the catalyst temperature and exhaust gas flowrate being the second variable. By connecting a point starting with the selected CO/NO ratio and the NO concentration, to a point showing the correct catalyst bed temperature and gas flowrate, and extending this line to the efficiency scale, the efficiency of the catalyst RE(23)75-P is obtained. The data points for the CO/NO ratio of 5 and 10 for all the temperature-flowrate combinations listed in the figure have actually been measured. The higher CO/NO ratio of 15 is the only extension of the experimental data in this figure.

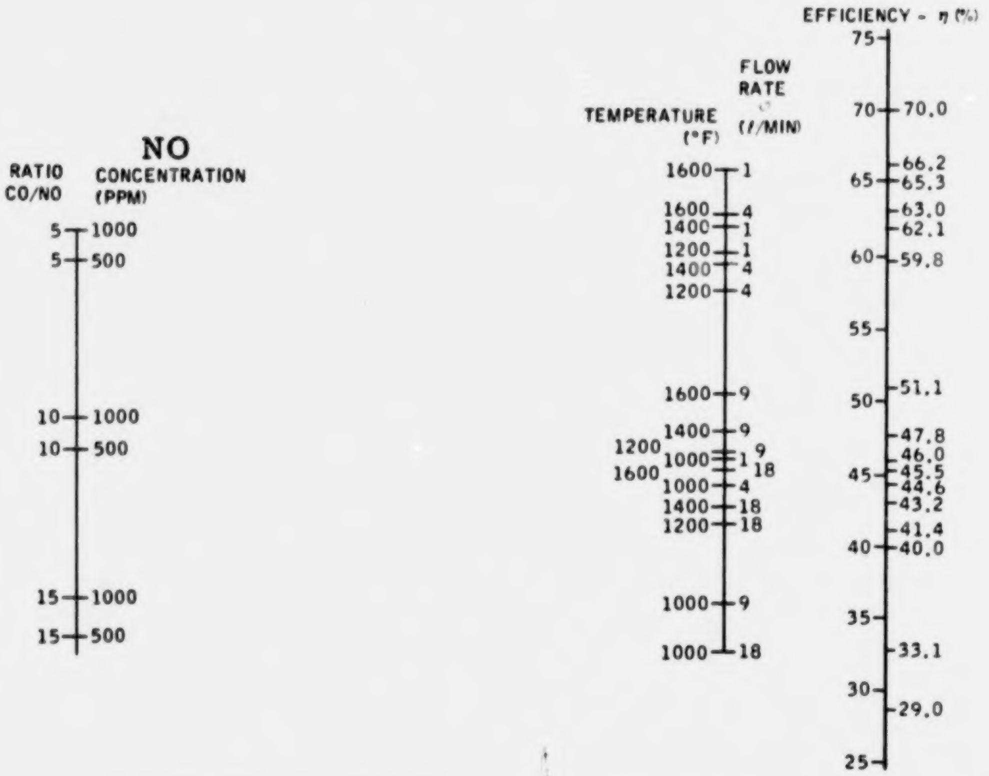

FIGURE 32. VERSION OF PARAMETRIC DESIGN CHART FOR RE(23)75-P IN NOMOGRAPH FORM

A conventional Parametric Design Chart is given in Figure 33. The curves for the initial NO concentration had, however, to be reversed from the originally planned design, in order to better approximate the effect of the parameter of the catalyst. This Parametric Design Chart is only an approximation of the actual function of the several parameters of the NO reducing efficiency of the catalyst RE(23)75-P, because it had been found during experimentation that the parameters were not independent of each other, as had been predicted by the theoretical analysis of the CO-NO reaction as presented in Chapter 2. The reason for this might be due to the fact that the catalytical reaction in the presence of oxygen, hydrogen, water vapor and hydrocarbons proceeds according to the theory of Klimisch, via the production of ammonia and other intermediaries, rather than the straight CO + NO equals N_2 + CO_2 reaction. However, for the data points, around which this Parametric Design Chart was constructed, the resulting curves are correct. These data points are indicated by the dashed line in Figure 33. In addition, for each independent quadrant of this figure the parameter curves are also correct. It is only due to the fact that the various parameters can clearly be seen. The efficiency increases both with flowrate and temperature though not uniformly. For instance, for an efficiency of 80 percent at the flowrate

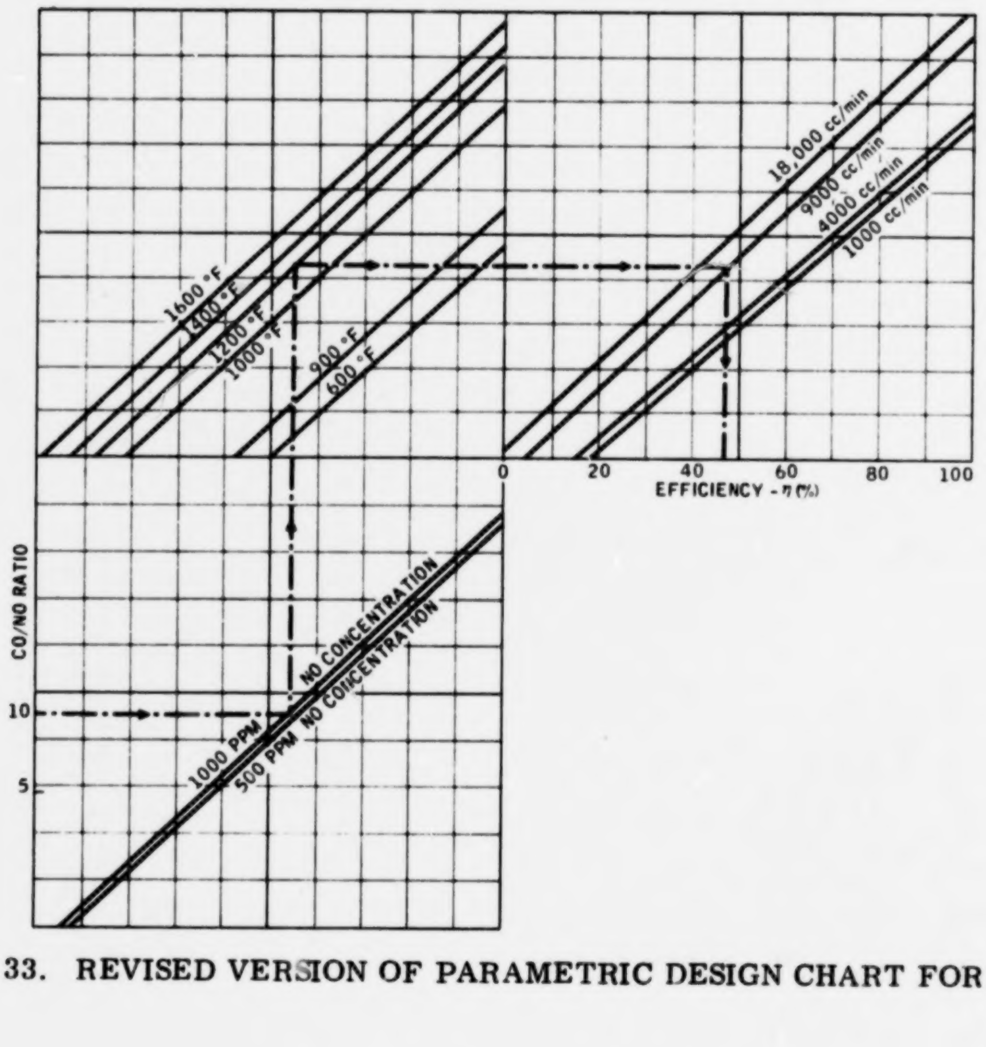

FIGURE 33. REVISED VERSION OF PARAMETRIC DESIGN CHART FOR RE(23)75-P

of 9000 cc/min we see that for a 1000 ppm NO concentration and the 900° F catalyst bed temperature, the CO/NO ratio has to be near 10. As the temperature increases to, for instance, 1200° F, the CO/NO ratio can be much less than 5.

Theory does not predict any effect of the initial NO concentration on the final catalyst efficiency. The difference obtained in our experimental data may be due, again, to the secondary reactions, such as described by Klimisch, for instance. The chart does follow the experimental results, however, and indicates a slightly higher efficiency for the 500 ppm initial concentration.

6

SUMMARY AND CONCLUSIONS

In this program, two rare earth oxide catalysts,

- Catalyst RE(23)75-P
- Catalyst RE(M3)75;

four transition metal catalysts, namely

- Monel 400
- Solar Monel 400-Mod
- Solar Monel 400-Core
- Copper Dichromate;

and two noble metal catalysts, i.e.,

- Palladium impregnated on alumina pellets
- Platinum impregnated on alumina pellets,

were investigated as to their respective nitric oxide reducing efficiency and their ammonia generating factors. These catalytic reactions were taking place in a synthetic automobile gas exhaust mixture, prepared to specifications approximating an air/fuel ratio of 14.

These results would indicate that in order to obtain an efficient rare earth oxide catalyst, the economy feature would be lost, due to the fact that the impurities, contained in the mixed oxide form, tend to inhibit the catalyst reaction. This seems to be valid on both counts -- the direct NO reduction and the indirect ammonia formation. Hence, the RE(M3)75 formulation showed a superior characteristic with respect to the ammonia formation than did the high purity formulation. However, both rare earth oxide catalysts, as presently formulated, show an insufficient catalytic nitric oxide reducing efficiency, and an unacceptable high rate of ammonia formation. Thus, this program, which started out to demonstrate the capabilities of rare earth oxide catalyst, which had appeared rather promising on the basis of earlier experi-

Preceding page blank

mentation in the absence of secondary reactions, proved to be insufficient for the purpose intended; namely, the control of NO emissions from mobile sources.

However, it might be pointed out here that additional experimentation with the catalyst RE(23)75-P showed a NO reducing efficiency of over 90 percent in the absence of H_2O in the synthetic exhaust gases. All the other competing gas components were present for those tests, except the water vapor.

On the other hand, Monel 400 was confirmed to be the best NO reducing catalyst on the basis of our data. These data show that Monel outranked even the precious metal catalysts such as Platinum and Palladium. These results confirm the data in the literature regarding Monel 400, but the noble metal catalysts did not turn out too well. In addition, the ammonia generating factors of the noble metal catalysts are also unacceptable.

A comparison of various catalysts, reported in the literature (Ref. 4, 5, 6, 7, and 22) has been made, to which have been added the data on catalyst RE(23)75 -P, obtained in the program. This data is tabulated in Table XIX. All important physical and chemical features of the catalysts have been placed into the table, as far as they have been reported. The data verified that the space velocity used for the rare earth oxide catalyst corresponds to that which has been applied on most of the other catalysts studied in the literature. Again, it is apparent from Table XIX that Monel catalyst is the leader, both in terms of efficiency and space velocity. In terms of ammonia formation, Monel again is the leader with the least quantity generated while the rare earth oxide catalyst occupies a middle position. Thus, the data agree generally with those in the literature.

The secondary parameter of the surface area has been shown to be rather insignificant with the Monel catalyst, a fact which also has been verified by our own testing. It is probable that UOP's noble metal catalyst makes up on surface area what it lacks on catalytic activity, and thus remains competitive. However, the data published on it (Ref. 22) are meager.

In conclusion, the following observations can be stated:

The rare earth oxide catalysts by themselves do not appear to be suited for the function of controlling the NO_x emissions of exhaust gases.

Furthermore, it appears that more knowledge of the intermediate and side reactions in the exhaust system for the CO/NO reaction is needed for the design of an optimum catalyst.

TABLE XIX

STATE OF ART IN NO REDUCING CATALYSTS

Producer	Esso	American Oil and Ford		UOP	Solar	Chemetron	Girdler	Harshaw Chemical	Linde(UC)	Cobalt, Vanadium, Alumina
Catalyst	Monel	Copper Based	Iron Oxide Stainless Steel	Mixed Oxide(Pt) on Alumina	REO(RE(23)75-P)	← Non-noble Transition Metals →		Cu-1808T		
Surface Area	Less than 0.01 m^2/g	390 to 57 m^2/g		400 m^2/g	0.2 till 10m^2/g				Not Measured	
Space Velocity	100,000 $hr.^{-1}$	15000-50000 $hr.^{-1}$	15000-50000 $hr.^{-1}$		15,000 $hr.^{-1}$	15,000 $hr.^{-1}$	15,000 $hr.^{-1}$	15,000 hr^{-1}	15,000 $hr.^{-1}$	15,000 $hr.^{-1}$
Durability	31,000 mi.	10,000 mi.	Insufficient	Probably some	Poor, so far					
Activation	None	Useful	High temp. active + CO		Yes	Yes	Yes	Yes, 3 hrs. 550°C 3% Co in N_2	Yes	Yes
Deactivation	None	Yes, after 2+ hours			Yes					
Temperature	1300°F up	660-800-1000°F	1600-1900°F		Around 1200°F	1000°F		1000°F 170°F pretreated	1000°F	1000°F
Ammonia Formation	10% of NO Reduced	50% of NO Reduced	40% to 50% of NO Reduced		33.3% Reduced					
Gas Composition	Net Reduction	Net Reduction	Net Reduction	Net Reduction	Net Reduction	Net Reduction	Net Reduction	Net Reduction	Net Reduction	Net Reduction
Catalyst Volume	1 liter (1000 cc)				90cc	25cc	25cc	25cc	25cc	25cc
Vehicle Tests	Yes	Yes	Yes	Not Yet	None	None	None	None	None	None
Back Pressure	2X Standard & Up				Moderate, φ Dependent					
Heating	3 Min.	Problematical, but solved			Not Investigated					
Meets Target	Yes on NO	Yes	Yes		Not Yet					
Poisoning	Below 1500°F	Yes	Yes		No	Yes	Yes	Yes	Yes	Yes
Efficiency	95%	80%	Less than Cu based	90% of all 3 at one A/F	47%	90%	90%	Supported-90% at RT if pre-treated	90%	90%
Economy	Good	Good	Good	High	Good	← Poor for bulk catalysts →				

Support Surface Areas - 10, 20, 25, 50-70, 186, 200, 227, 390 m^2/g
Study on supported catalysts including FeO_2, CuO, CrO_3, Co, Vanadium
R = 10, 1.5% CO, 1500 ppm NO

Stanford Studies with lead, 80% 18,000 mi.
Space velocity 10,000 $hr.^{-1}$

Copper Chromite - poor attrition resistance — 12 to 25 lbs. per unit, \$1.-2.50/lb.
$CuCr_2O_4$

Space Velocities at 1400°F, near 1 atm.

The program resulted in the design and putting in operation of an experimental approach capable of accurately measuring catalyst performance under synthetic exhaust gas conditions for an air-fuel ratio near 14.

It appears from this program that the best future approach in the development of an appropriate catalyst for the CO/NO reaction lies in increasing the life of the catalyst material -- Monel 400 (Solar Monel 400-Mod series).

REFERENCES

1. Anon, "Air Quality Criteria for: Carbon Monoxide, Nitrogen Oxide From Mobile Sources, Hydrocarbons", U.S. Dept. of Health, Education and Welfare, Public Health Service, National Air Pollution Control Administration, Washington, D. C. (March 1970).

2. Lewis, James, "Peroxyacyl Nitrates", Task Force 7, Section 4, Project Clean Air, University of California Task Force Assessments (9/1/70).

3. Shelf, M., "Catalytic Reduction of Nitric Oxide", First National Symposium on Heterogeneous Catalysts for Control of Air Pollution, Franklin Institute, Philadelphia, Pa., published by Scientific Research Staff, Ford Motor Company (November 21-22, 1969).

4. Bernstein, L. S., et al., "Application of Catalysts to Automotive NO_x Emissions Control", Esso Research and Engineering Co., Standard Oil Co. (N) SAE Paper #710014 (January 1971).

5. Meguerian, G. H. (American Oil Company), Lang, C. R. (Ford Motor Co.), "NO_x Reduction Catalysts for Vehicle Emission Control", SAE Paper #710291 (January 1971).

6. Yolles, R. S., Wise, H., and Berriman, L. P., "Study of Catalytic Control of Exhaust Emissions for Otto Cycle Engines", SRI Project PSU-8028, Standford Research Institute (April 1970).

7. Balgard, W. D., "Novel Catalysts and Catalyst Supports for Control of NO_x in Automobile Exhaust", presented at the Second International Clean Air Congress, Washington, D.C. (Dec. 6-11, 1970).

8. Penner, S. S., Thermodynamics, Vol. 7, Reading, Mass.: Addison-Wesley Publishing Co., Inc. (1968).

9. (a) Progress in Technology, Vol. 6, "Vehicle Emissions - A Selection of SAE Technical Papers on the Definition, Measurement, and Control of Emissions from Motor Vehicles to the Atmosphere", covers period 1955-1963. Includes bibliography with abstracts of SAE material.

9 (b) Progress in Technology, Vol. 12, "Vehicle Emissions - Part 2". Thirty-six technical presentations dating from 1963 to 1969 form the second volume of a comprehensive, evaluated technical work in the emissions field. Major sections include Fundamentals, Control, Measurement, Diesel, and Evaporation Loss.

10. Bevan, D. J. M., Hyde, B. G., and Eyring, LeRoy, "Phase Relationships in the PrO_x System", Third Rare Earth Conference, Session III, pg. 72 (1963).

11. Kuo, J. C. (Mobile R&D Corp.), Lassen, H. G. (Ford Motor Co.), and Morgan, C. R. (Mobile R&D Corp.), "Mathematical Modeling of Catalytic Converter System", presented at the Automotive Engineering Congress, Detroit, Mich., SAE paper #710289, Appendix D (Jan. 11-15, 1971).

12. Jagel, K. I., and Dwyer, F. G., "HC/CO Oxidation Catalysts for Vehicle Exhaust Emission Control", presented at the Automotive Engineering Congress, Detroit, Michigan, SAE paper #710290 (January 11-15, 1971).

13. D'Alleva, B. A. and Lozell, W. G., SAE Journal, Vol. 38, No. 3 (March 1936).

14. Wolf, P. C., "Carbon Monoxide Measurement and Monitoring in Urban Air", Environmental Science and Technology, pg. 214 (1971).

15. General Course in Gas Chromatography, Hewlett Packard Publication.

16. Jones, Theron, "Beckman Gas Chromatography Applications Manual", Beckman Bulletin 756-A.

17. Westwood, L. C., "A Chemical Method for the Determination of Ammonia in Automotive Exhaust", Technical Memorandum SRM 70-25, EPA-Technical Services and Administration Dept. (9/22/70).

18. Obert, Edward F., Internal Combustion Engines - Analysis and Practice, 2nd ed., 4th printing, Chapter 11 - Carburation, pp. 327 ff, especially Figures 11-3 and 11-13, Scranton, Penna.: International Textbook Company, (June 1952).

19. Eyring, LeRoy, Ed., Progress in Science and Technology of the Rare-Earths, New York: The McMillan Co. (1964).

20. Environmental Science and Technology, Vol. 5, No. 7, pg. 579 (July 1971).

21. Bowman, C. T., "Investigation of Nitric Oxide Formation Kinetics in Combustion Processes: The Hydrogen-Oxygen-Nitrogen Reaction", United Aircraft Research Laboratories paper, submitted for publication to Combustion Science and Technology.

22. Zmuda, J. P., "New: A Catalytic Converter that Really Cleans up Auto Exhaust", Popular Science Monthly, pg. 47 (Dec. 1970).

23. Gschneidner, Karl A., Jr., "Rare Earths, The Fraternal Fifteen", U.S. Atomic Energy Publication.

24. Anon, "Present and Potential Sources of Rare-Earth Minerals", Industrial Minerals, London, England (Nov. 1968).

25. Private communication with J. G. Cannon, Manager, Rare-Earth Development, Molybdenum Corp. of America, New York, New York.

26. "Problems and Issues of a National Materials Policy," compiled by Science Policy Research Division, Legislative Reference Service, Library of Congress, for Committee on Public Works., U. S. Senate, requested by Hon. J. Caleb Boggs (December 1970).

APPENDIX A

Preceding page blank

BLANK PAGE

APPENDIX A

CALCULATED ISO-OCTANE/AIR EQUILIBRIUM EXHAUST COMPOSITION USING THE "DYNAMIC SCIENCE" GENERALIZED KINETICS PROGRAM

Tables A-I through A-VI show the calculated equilibrium exhaust composition at O/F ratios from 10-15 when octane and air are burned. For each O/F, compositions are presented at temperatures from 2300-1000° F. These are read columnwise and the major species concentrations presented directly below. It is interesting to note that no NO exists at these temperatures at equilibrium. NO is a product that is formed at high temperature and "freezes" during temperature decreases. It also can be shown that CO concentrations measured in engine exhaust can be an order of magnitude different from that at equilibrium.

A scattering of runs designed to look at the range of exhaust conditions were made with the Generalized Kinetics Program. Measured emission values coupled with equilibrium values of the major species (CO_2, H_2O, N_2) were used as exhaust composition. Major species were selected from Tables A-I through A-VI at conditions representative of the particular engine operating mode being examined. Runs were made with and without the addition of trace (2000 ppm) O_2.

The results of these data are summarized in Section 2.2.

Preceding page blank

TABLE A-I

ISO-OCTANE/AIR EQUILIBRIUM EXHAUST COMPOSITION

O/F = 10

CASE NO. 1

Chemical Formula

Fuel	C	8.00000	H	18.00000
Oxidant	O	2.00000		
Oxidant	N	2.00000		

O/F = 1.0000 + 01, Percent Fuel = 0.0909 + 00, Equivalence Ratio = 1.4371 + 00

THERMODYNAMIC PROPERTIES

P, psi	14.70	14.70	14.70	14.70	14.70	14.70
T, °R	2300	2000	2000	1500	1250	1000
H, BTU/lb	-595.8	-700.9	-771.2	-894.2	-1064.0	-1170.2
S, BTU/(lb)(R)	2.2408	2.1918	2.1548	2.0794	1.9559	1.8620
M, MOL wt.	26.266	26.267	26.268	26.503	27.817	28.426
(DLV/DLP)T	-1.00000	-1.00001	-1.00010	-1.01184	-1.01079	-1.00185
(DLV/DLP)P	1.0000	1.0001	1.0014	1.2017	1.1920	1.0361
CP, BTU/(lb)(R)	.3509	.3505	.3530	.6095	.5585	.3331
Gamma (S)	1.2749	1.2753	1.2736	1.1988	1.2062	1.2878
Son Vel. ft/sec	2355.9	2.197.3	2083.0	1836.6	1641.6	1500.8

MOLE FRACTIONS

CH_4	.000000	.000001	.000021	.004469	.029484	.041087
CO	.085861	.075740	.066736	.043207	.006440	.000171
CO_2	.081367	.091489	.100480	.121055	.141178	.139721
H_2	.073081	.083194	.092113	.099209	.043838	.007419
H_2O	.115048	.104929	.095967	.081595	.096318	.113932
NH_3	.000002	.000006	.000013	.000055	.000076	.000050
N_2	.644640	.644642	.644669	.650410	.682665	.697620

TABLE A-II

ISO-OCTANE/AIR EQUILIBRIUM EXHAUST COMPOSITIONS

O/F = 11

CASE NO. 1

Chemical Formula

Fuel	C	8.00000	H	18.00000
Oxidant	O	2.00000		
Oxidant	N	2.00000		

O/F = 1.1000 + 01, Percent Fuel = 8.3333 + 00, Equivalence Ratio = 1.3064 + 00

THERMODYNAMIC PROPERTIES

P, psi	14.70	14.70	14.70	14.70	14.70	14.70
T, °R	2300	2000	1800	1500	1250	1000
H, BTU/lb	-652.3	-755.3	-823.8	-931.5	-1070.0	-1172.3
S, BTU/(lb)(R)	2.1985	2.1506	2.1145	2.0488	1.9476	1.8571
M, MOL wt.	26.919	26.919	26.919	26.995	27.903	28.461
(DLV/DLP)T	-1.00000	-1.00000	-1.00003	-1.00462	-1.00955	-1.00175
(DLV/DLP)P	1.0000	1.0000	1.0004	1.0773	1.1679	1.0341
CP, BTU/(lb) (R)	.3442	.3424	.3425	.4355	.5193	.3278
Gamma (S)	1.2731	1.2749	1.2750	1.2369	1.2158	1.2920
Son Vel. ft/sec	2325.5	2170.1	2058.8	1.848.6	1645.6	1502.3

MOLE FRACTIONS

CH_4	.000000	.000000	.000005	.001384	.018247	.028619
CO	.063708	.055002	.047309	.030662	.005395	.000149
CO_2	.093393	.102099	.109790	.125496	.139203	.137333
H_2	.051448	.060149	.067817	.079222	.040880	.007059
H_2O	.125289	.116584	.108902	.095184	.105722	.122496
NH_3	.000001	.000004	.000008	.000040	.000069	.000047
N_2	.666161	.666162	.666169	.668011	.690483	.704298

TABLE A-III

ISO-OCTANE/AIR EQUILIBRIUM EXHAUST COMPOSITIONS

O/F = 12

CASE NO. 1

Chemical Formula

Fuel	C	8.00000	H	18.00000
Oxidant	O	2.00000		
Oxidant	N	2.00000		

O/F = 1.2000 + 01, Percent Fuel = 7.6923 + 00, Equivalence Ratio = 1.1976 + 00

THERMODYNAMIC PROPERTIES

P, psia	14.70	14.70	14.70	14.70	14.70	14.70
T, °R	2300	2000	1800	1500	1250	1000
H, BTU/lb	-700.6	-801.4	-868.0	-968.0	-1076.9	-1174.2
S, BTU/(Lb)(R)	2.1614	2.1145	2.0794	2.0186	1.9387	1.8525
M, MOL wt.	27.497	27.497	27.497	27.512	28.010	28.494
(DLV/DLP)T	-1.00000	-1.00000	-1.00001	-1.00103	-1.00768	-1.00161
(DLV/DLP)P	1.0000	1.0000	1.0001	1.0168	1.1337	1.0312
CP, BTU/(lb)(R)	.3374	.3340	.3322	.3469	.4687	.3216
Gamma (S)	1.2725	1.2761	1.2781	1.2726	1.2298	1.2970
Son Vel. ft/sec	2300.5	2148.2	2039.6	1857.3	1651.8	1504.3

MOLE FRACTIONS

CH_4	.000000	.000000	.000001	.000266	.009309	.018111
CO	.043238	.036561	.030685	.919241	.004327	.000127
CO_2	.104892	.111570	.117445	.128705	.137260	.135264
H_2	.033131	.039807	.044675	.056071	.036146	.006508
H_2O	.133514	.126837	.120964	.110100	.114908	.129898
NH_3	.000001	.000002	.000005	.000024	.000058	.000042
N_2	.685224	.685224	.685226	.685593	.697992	.710051

TABLE A-IV

ISO-OCTANE/AIR EQUILIBRIUM EXHAUST COMPOSITIONS

O/F = 13

CASE NO. 1

Chemical Formula

Fuel	C	8.00000	H	18.00000
Oxidant	O	2.00000		
Oxidant	N	2.00000		

O/F = 1.3000 + 01, Percent Fuel = 7.1429 + 00, Equivalence Ratio = 1.1055 + 00

THERMODYNAMIC PROPERTIES

P, psia	14.70	14.70	14.70	14.70	14.70	14.70
T, °R	2300	2000	1800	1500	1250	1000
H, BTU/lb	1742.4	-840.9	-905.6	-1001.0	-1086.3	-1176.2
S, BTU/(lb)(R)	2.1281	2.0822	2.0482	1.9902	1.9277	1.8479
M, MOL wt.	28.013	28.013	28.013	28.014	28.168	28.528
(DLV/DLP)T	-1.00000	-1.00000	-1.00000	-1.00010	-1.00446	-1.00137
(DLV/DLP)P	1.0000	1.0000	1.0000	1.0015	1.0768	1.0267
CP, BTU/(lb)(R)	.3307	.3254	.3216	.3149	.3908	.3135
Gamma (S)	1.2731	1.2788	1.2830	1.2917	1.2576	1.3035
Son Vel. ft/sec	2279.7	2130.6	2024.5	1854.3	1665.8	1507.2

MOLE FRACTIONS

CH_4	.000000	.000000	.000000	.000022	.002752	.009185
CO	.024186	.020045	.016411	.009730	.003023	.000104
CO_2	.115943	.120084	.123717	.130384	.135130	.133419
H_2	.017587	.021728	.025359	.031943	.027913	.005648
H_2O	.140057	.135916	.132283	.125651	.125041	.136477
NH_3	.000000	.000001	.000002	.000010	.000040	.000034
N_2	.702227	.702227	.702227	.702259	.706100	.715133

TABLE A-V

ISO-OCTANE/AIR EQUILIBRIUM EXHAUST COMPOSITIONS

O/F = 14

CASE NO. 1

Chemical Formula

Fuel	C	8.00000	H	18.00000
Oxidant	O	2.00000		
Oxidant	N	2.00000		

O/F = 1.4000 + 01, Percent Fuel = 6.6667 + 00, Equivalence Ratio = 1.0265 + 00

THERMODYNAMIC PROPERTIES

P, psia	14.70	14.70	14.70	14.70	14.70	14.70
T, °R	2300	2000	1800	1500	1250	1000
H, BTU/lb	-779.0	-875.1	-937.9	-1029.6	-1103.4	-1178.6
S, BTU/(lb)(R)	2.0971	2.0523	2.0192	1.9635	1.9098	1.8426
M, MOL wt	28.475	28.475	38.475	38.475	28.477	38.573
(DLV/DLP)T	-1.00000	-1.00000	-1.00000	-1.00000	-1.00013	-1.00085
(DLV/DLP)P	1.0000	1.0000	1.0000	1.0000	1.0021	1.0164
CP, BTU/(lb)(R)	.3241	.3166	.3109	.3001	.2912	.2977
Gamma (S)	1.2744	1.2828	1.2894	1.3030	1.3167	1.3167
Son Vel, ft/sec	2262.3	2116.5	2013.1	1847.3	1695.2	1513.6

MOLE FRACTIONS

CH_4	.000000	.000000	.000000	.000000	.000031	.001714
CO	.006344	.005157	.004118	.002291	.000915	.000066
CO_2	.126603	.127790	.128829	.130656	.132010	.131626
H_2	.004379	.005566	.006604	.008430	.009672	.003810
H_2O	.145186	.144000	.142961	.141134	.139829	.142814
NH_3	.000000	.000000	.000000	.000001	.000008	.000019
N_2	.717487	.717488	.717488	.717488	.717534	.719951

TABLE A-VI

ISO-OCTANE/AIR EQUILIBRIUM EXHAUST COMPOSITION

O/F = 15

CASE NO. 1

Chemical Formula

Fuel	C	8.00000	H	18.00000
Oxidant	O	2.00000		
Oxidant	N	2.00000		

O/F = 1.5000 + 01, Percent Fuel = 6.2500 + 00, Equivalence Ratio = 9.5806 - 01

THERMODYNAMIC PROPERTIES

P, psia	14.70	14.70	14.70	14.70	14.70	14.70
T, °R	2300	2000	1800	1500	1250	1000
H, BTU/lb	-742.0	-836.9	-898.7	-988.8	-1061.0	-1130.7
S, BTU/(lb)(R)	2.0853	2.0411	2.0086	1.9539	1.9012	1.8391
M, MOL wt	28.645	28.645	28.645	28.645	28.645	28.645
(DLV/DLP)T	-1.00000	-1.00000	-1.00000	-1.00000	-1.00000	-1.00000
(DLV/DLP)P	1.0000	1.0000	1.0000	1.0000	1.0000	1.0000
CP, BTU/(lb)(R)	.3206	.3120	.3057	.2943	.2838	.2733
Gamma (S)	1.2761	1.2859	1.2936	1.3084	1.3235	1.3401
Son Vel, ft/sec	2257.1	2112.7	2010.3	1845.6	1694.5	1525.1

MOLE FRACTIONS

CO_2	.125381	.125381	.125381	.125381	.125381	.125381
H_2O	.141052	.141054	.141054	.141054	.141054	.141054
NO	.000072	.000020	.000007	.000001	.000000	.000000
N_2	.724952	.724979	.724986	.724989	.724989	.724989
OH	.000004	.000000	.000000	.000000	.000000	.000000
O_2	.008538	.008566	.008572	.008575	.008576	.008576

APPENDIX B

Preceding page blank

APPENDIX B

CATALYST SURFACE AREA MEASUREMENTS BY THE BET METHOD

CATALYST SURFACE AREA DETERMINATION USING THE BET EQUATION

The surface area of porous and non-porous solids may be estimated from measurements of the adsorption of gases. The starting point is the experimental determination of the adsorption isotherm, and then calculating from it, using the BET (Brunauer, Emmett and Teller) equation, the monolayer capacity of the adsorbent solid. The monolayer capacity is defined as the amount of adsorbed gas required to form a completely filled, single layer of molecules on the surface of the solid. The surface area, per unit mass of solid, can be calculated from the monolayer capacity if the area occupied by a single molecule of adsorbed gas in the completed monolayer is known.

The adsorption isotherm is a plot of the amount adsorbed, per gram of solid, as a function of the equilibrium pressure, for a given gas adsorbed on a given solid at a constant temperature. A general expression for the adsorption isotherm is of the form

$$X = f(P/P_o)_{T,\ \text{gas. solid}} \qquad (1)$$

where X is the amount of gas adsorbed per gram of adsorbent, P is the equilibrium pressure, P_o is the saturation vapor pressure of the gas, and T is the temperature. For this analysis X will be expressed as a volume reduced to (N.T.P.) standard temperature and pressure (0° C, 760 Torr), i.e., the volume the adsorbed gas would occupy at normal temperature and pressure.

The BET Equation and Surface Area

Braunauer, Emmett, and Teller developed a mathematical expression for the adsorption isotherm from a simple kinetic model. This expression, the "BET equation", has proved remarkably successful in the calculation of surface areas and net heats of adsorption from adsorption isotherms.

Preceding page blank

The form of the BET equation most often used in interpreting experimental data is

$$\frac{P}{X(P_o - P)} = \frac{1}{X_m C} + \frac{C - 1}{X_m C} \left(\frac{P}{P_o}\right) \tag{2}$$

where X is the amount adsorbed (cm^3 at N.P.T.) per gram of adsorbent at pressure P, X_m is the amount adsorbed when the monolayer is completed, P_o is the saturation vapor pressure of the adsorbed gas, and C is a constant related to the latent heat of condensation and the net heat of adsorption. According to Equation (2), when the experimentally determined adsorption isotherm data (X vs. P) is plotted in the form

$$\frac{P}{X(P_o - P)} \text{ vs. } \frac{P}{P_o} ,$$

a straight line should result with slope

$$S = (C - 1)/X_m C \tag{3a}$$

and intercept

$$I = 1/X_m C \cdot \tag{3b}$$

Solution of these two simultaneous equations immediately yields X_m and C, viz.,

$$X_m = 1/(S + I) \tag{4a}$$

$$C = (S + I)/I . \tag{4b}$$

The surface area A_s(m^2/gm) is related to the monolayer capacity X_m by the equation

$$A_s = \frac{X_m N A_m x\, 10^{-20}}{22414} ,$$

where N is Avogadro's number and A_m is the molecular cross sectional area of the adsorbed gas in square Angstroms. The cross sectional area A_m is usually calculated from the density of the gas in the ordinary liquid form, i.e., it is assumed that the arrangement of the molecules on the surface is the same as it is within the bulk liquid. For nitrogen at -195° C, $A_m = 16.2$ Å^2.

Measurement of Adsorption Isotherms

A number of different experimental methods have been successfully used for the determination of adsorption isotherms. The most common is the volumetric method which consists essentially in admitting to the adsorbent successive charges of gas from some sort of volumetric measuring device; when equilibrium is reached the pressure of the gas in the dead space is measured, and the quantity of gas remaining unadsorbed is then calculated with the aid of the gas laws. Knowing the dead space volume, and by subtracting the amount remaining unadsorbed from the total amount which has been admitted, the quantity which has been adsorbed can be calculated.

Figure B-1 shows a schematic of the volumetric adsorption apparatus used for determining the adsorption isotherm of N_2 at -195° C on a number of perspective catalyst materials. The catalyst sample is contained in a small glass bulb which is immersed in a liquid nitrogen bath. Gas pressures are measured by the manometer. The reference volume is used for calibrating the various parts of the dead space and must be of accurately known volume. The volume of the line a should be either small compared to the reference volume or measured and included in the reference volume.

The total dead space volume of the system is defined as the sum of:

1. The volume of lines b and c.
2. The space above and surrounding the catalyst particles.
3. The pore volume of the particles.

This means that the amount adsorbed is equal to the amount of gas admitted (by valve 1 from the reference volume) minus the amount of gas present in the dead space, or, mathematically,

$$X = V_a - V_d ,$$

where X is the volume of gas adsorbed, V_a is the amount admitted, and V_d is the amount in the dead space. The dead space volume is determined using a charge of helium in the reference volume since it will act to fill the dead spaces but not be adsorbed.

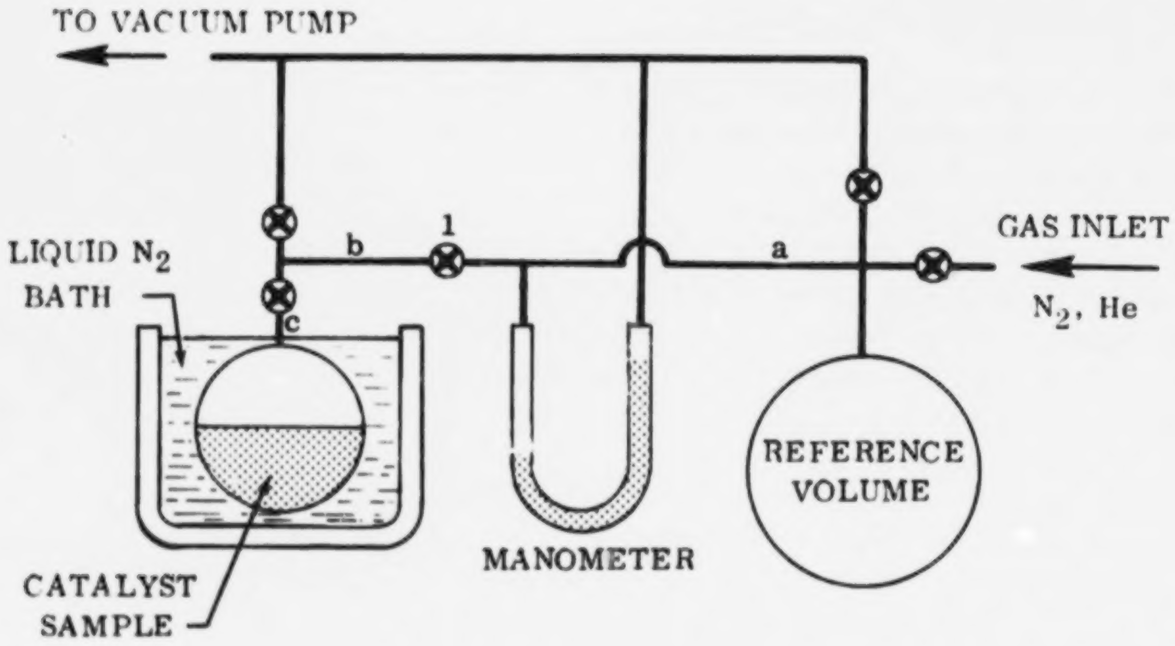

FIGURE B-1. SCHEMATIC DIAGRAM OF THE APPARATUS USED FOR THE DETERMINATION OF ADSORPTION ISOTHERMS

The BET Surface Measurement of the Catalyst

A BET surface measurement apparatus has been constructed and the surface area of a charge of the catalysts has been measured. The procedure used is as follows.

After the determination of the dead space, which has been discussed in the above subsection, and which for the copper dichromate catalyst came out to be 28.9 cm^3, the nitrogen adsorption isotherm measurements were made. For this, various amounts of volumes of nitrogen gas were allowed into the system and the gas pressure before and after adsorption onto the catalyst was measured. Several points have been obtained, whereby the highest nitrogen gas pressure has to be kept below 1/2 atm. The volume measured for each absorption consists of the total volume admitted minus the volume in the dead space and the volume left in the reference vessel. This volume is plotted versus a function P_f/P_s, where P_f is the gas pressure remaining after adsorption and P_s is the saturation vapor pressure of nitrogen at the catalyst temperature of 74° K, that is the boiling point of liquid nitrogen which is equal to 1 atm. Using the BET equation, the data are then replotted in the form of P_f divided by $V(P_s - P_f)$ versus the ratio P_f/P_s and the best straight line through the data points is drawn. For copper dichromate, this is shown in Figure B-2. The slope S and the intercept I is measured and the

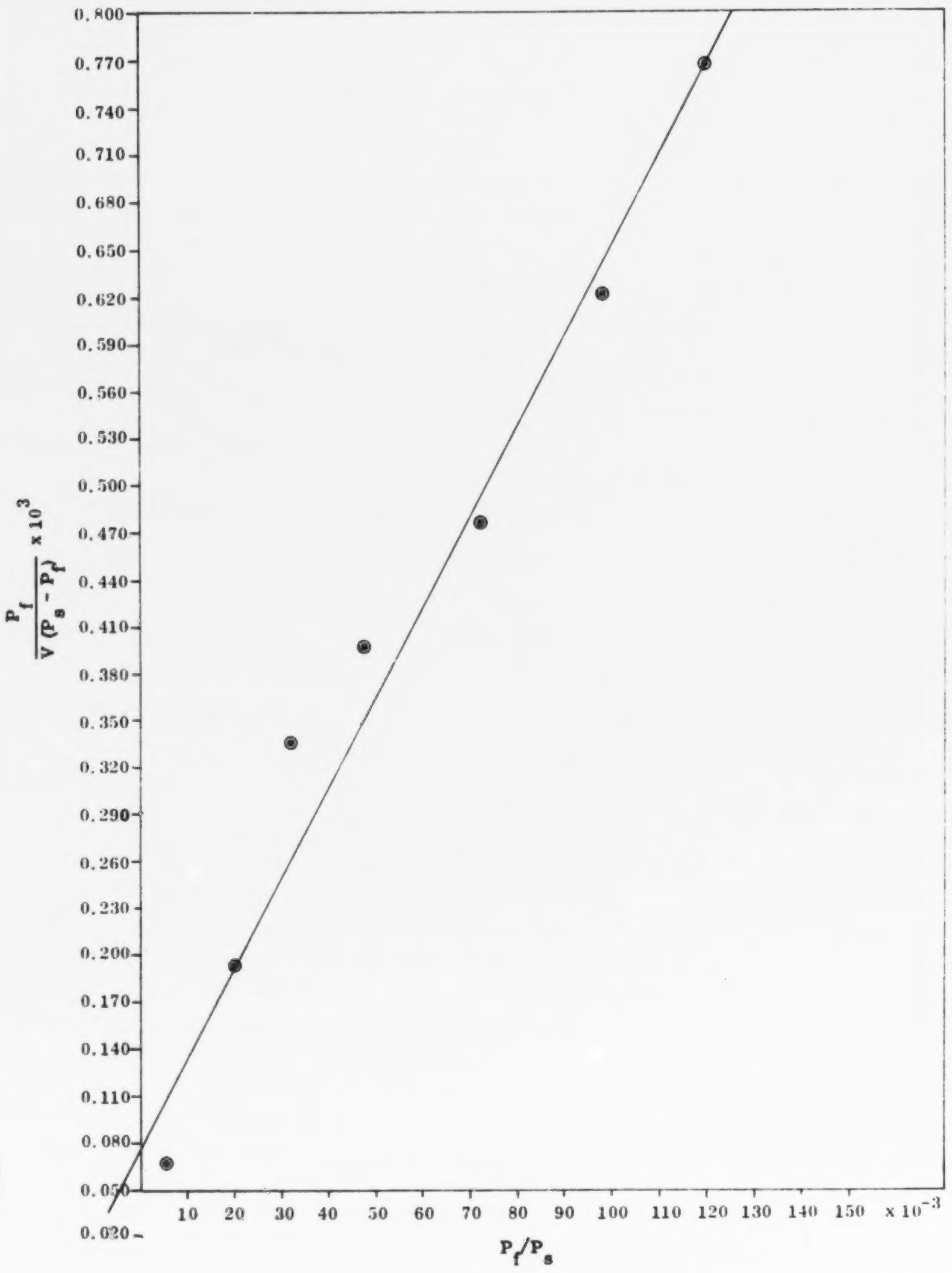

FIGURE B-2. ADSORPTION ISOTHERM FOR BET SURFACE AREA MEASUREMENT OF $CuCr_2O_7$ CATALYST volume absorbed by the monolayer of nitrogen is given by the equation

$$V_M{}^* = \frac{1}{S + I} \quad (\text{cm}^3 \text{ at STP})$$

The volume V_M per unit mass is obtained by dividing $V_M{}^*$ by the mass M, which is the weight of the catalyst charge. The catalyst surface then is given by the expression

$$A_S = \frac{V_M N A_M \times 10^{-20}}{22414}$$

where $N = 6.0226 \times 10^{23}$ molecules/mole

$A_M = 16.2$ Å^2/molecule for nitrogen

Thus, the expression for A_S, using the constants defined, becomes

$$A_S = 4.3529 \times V_M \text{ in m}^2/\text{gram}$$

For our charge of $CuCr_2O_7$, the value of the surface area is

$$A_S = 6.5 \text{ m}^2/\text{gram.}^{**}$$

This is, according to Reference 6, a very small surface area. A good catalyst should have an area of the order of 70 m^2/gtam. Therefore, if it takes 12 pounds of $CuCr_2O_7$ at 6.5 m^2/gram to achieve a given catalytic conversion efficiency for the reduction of NO, the same job can be completed by 1.2 pounds of a catalyst with a 65 m^2/gram surface area. Our experimentation has shown that such surface areas cannot be obtained with our present pelletized catalysts, but would require supported ones.

The equipment for the BET apparatus is shown in Figure B-3. The reference volume of 500 ml is clearly visible, while the volume with the catalyst bed has been placed into the bath of liquid nitrogen in the vessel covered by black tape. The mercury manometer, with which the pressure difference is measured, is also seen. The system is evaluated by the vacuum pump system underneath the

---

** Later measurements, with better degassed $CuCr_2O_7$ pellets, yielded surface areas of 10.3 and 11.0 m^2/gram (see Table B-1).

NOT REPRODUCIBLE

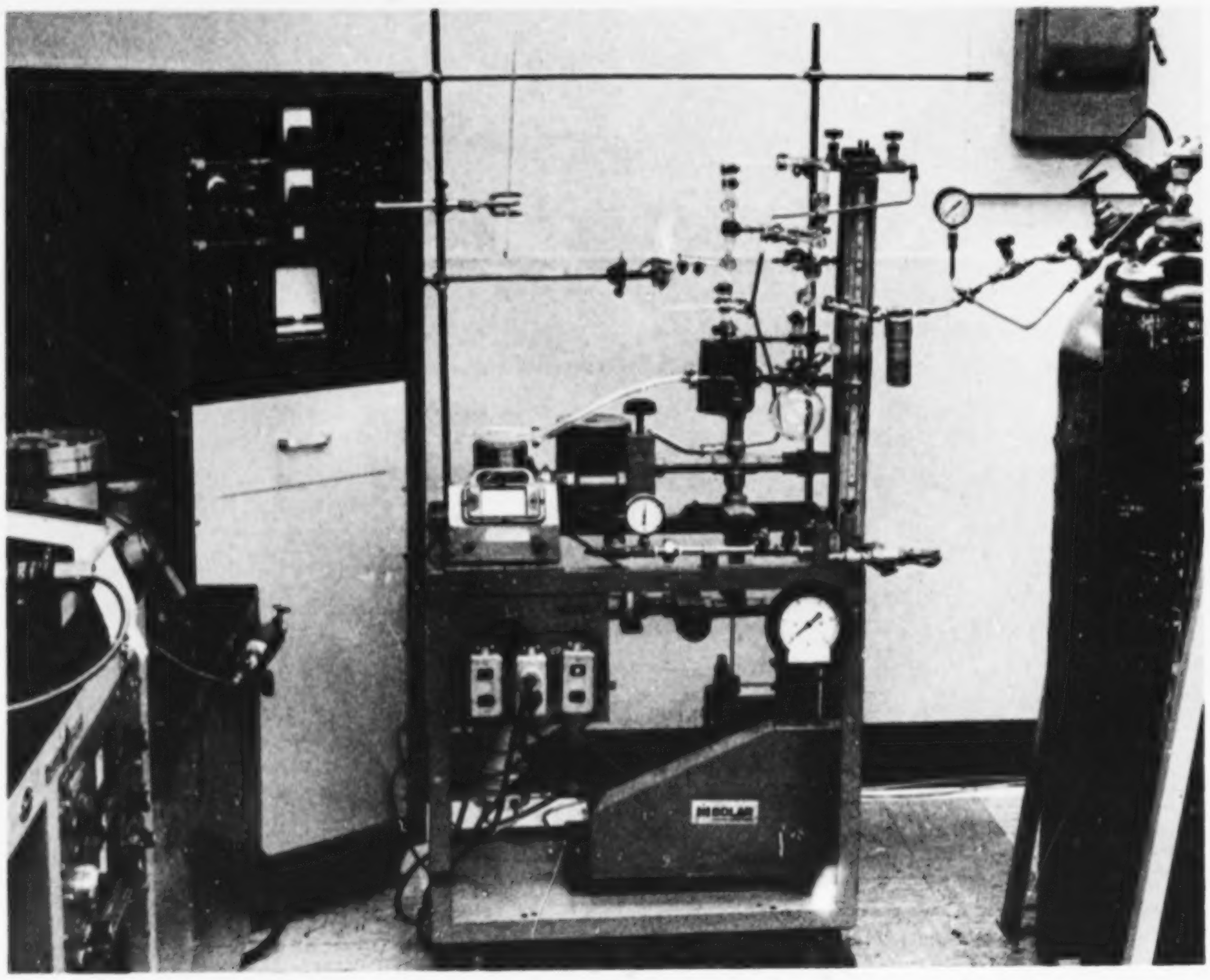

FIGURE B-3. VIEW OF BET SURFACE AREA MEASUREMENT APPARATUS

assembly, and the helium and nitrogen gas tanks used for measuring the dead space and the absorbed volumes, respectively, is seen on the right hand side of the figure. The results of the surface area measurements by the BET method are shown in Table B-I.

In the BET data obtained, the material factor as well as preparation parameters were shown to play an important role. The high purity oxide pellets had a larger surface area per unit mass than the mixed oxide pellets; the latter had initially a much greater hardness as well. However, after a storage of a few months, many of the RE(M3)75 pellets showed signs of lamination cracking, while the RE(23)75-P pellets proved to be much more stable.

Preparation parameters showing some influence on the pellet surface area were temperature and pressure, with preparation temperature to be the one with greater effectiveness.

TABLE B-I

RESULTS OF BETA SURFACE AREA MEASUREMENTS OF CATALYSTS

Catalyst Sample (Pellet Form)	Weight After Degassing g	Total Surface m^2	Specific Surface Area m^2/g
$CuCr_2O_7$ *	19, 9887	60.0	10. 3
$CuCr_2O_7$	19, 9887	64.1	11. 0
RE(M3)75	22, 3959	0. 8	0. 109
RE(M3)75**	20, 6360	1. 4	0. 24
RE(23)75-P	20, 9296	5. 0	0. 81

* Incompletely outgassed

** Catalyst Pellets with moderate lamination cracking.

APPENDIX C

BLANK PAGE

APPENDIX C

RARE EARTH OXIDE CATALYST MECHANICAL PROPERTIES - SPALLING RESISTANCE

The spalling resistance was measured for four catalyst formulations, namely the copper dichromate catalyst, formula RE(23)75 of lower purity, formula RE(23)75-P of highest purity, and formula RE(M3)75.

Figure C-1 shows the four catalyst formulas selected for the spalling test as they appear originally. These four catalyst formulas were then placed for five days in a closed chamber, as shown in Figure C-2. Inside the chamber a sieve-like container was put, and the four formulas were placed inside this container. The container, divided into four chambers, one for each formula, was then put into the humidity chamber, which at its bottom had about one inch high of pure, distilled water. The arrangement is shown in Figure C-3. After five days, during which the average temperature was 74° F and the relative humidity in the chamber 100 percent, which results in a water vapor content of 0.03 moles, the catalyst formulas were removed from the chamber and each catalyst, after being weighed, was placed separately into the catalyst bed of the flow apparatus and heated to about 200° F in the first hour and to about 860° F in the second hour, under a constant flow of high purity helium of 7600 cc per minute. After completion of the testing, the various catalysts were removed from the catalyst bed, weighed and photographed.

Table C-I shows the weight of the catalyst before, during and after the spalling test, whereby the weight during the test is the one obtained after the catalyst was removed from the humidity chamber and before it was exposed to heat and flow in the catalyst bed. As can be seen all catalysts gained slightly in weight due to the adsorption of moisture on the catalyst surface, whereby the copper dichromate catalyst gained most moisture, and after the spalling test was completed all catalysts lost weight to even below their original value, indicating that some moisture was adsorbed to them even before the beginning of the test.

Preceding page blank

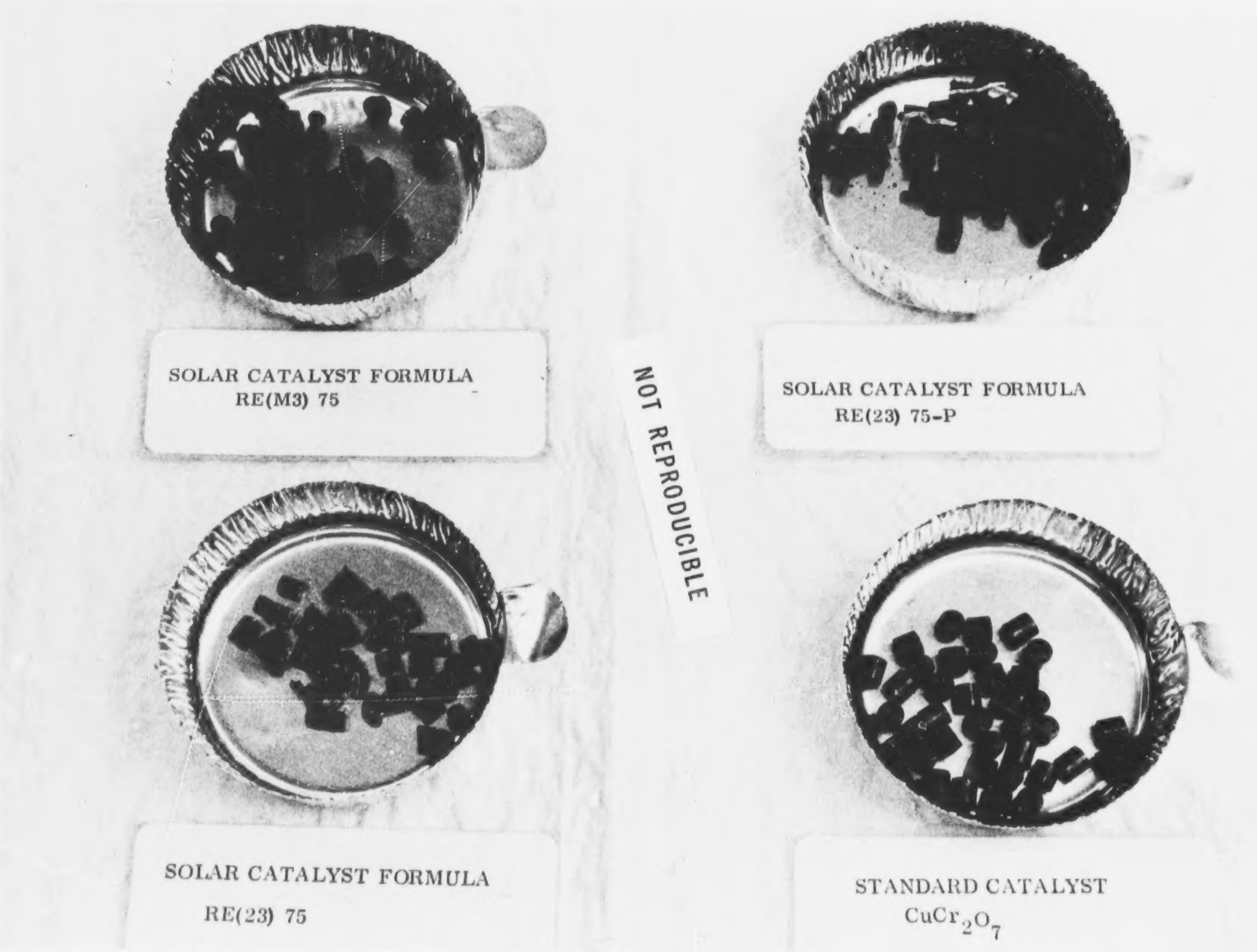
SOLAR CATALYST FORMULA
RE(M3) 75
SOLAR CATALYST FORMULA
RE(23) 75-P
SOLAR CATALYST FORMULA
RE(23) 75
STANDARD CATALYST
$CuCr_2O_7$

NOT REPRODUCIBLE

FIGURE C-1. SOLAR CATALYST FORMULAS AS THEY APPEARED BEFORE SPALLING TEST

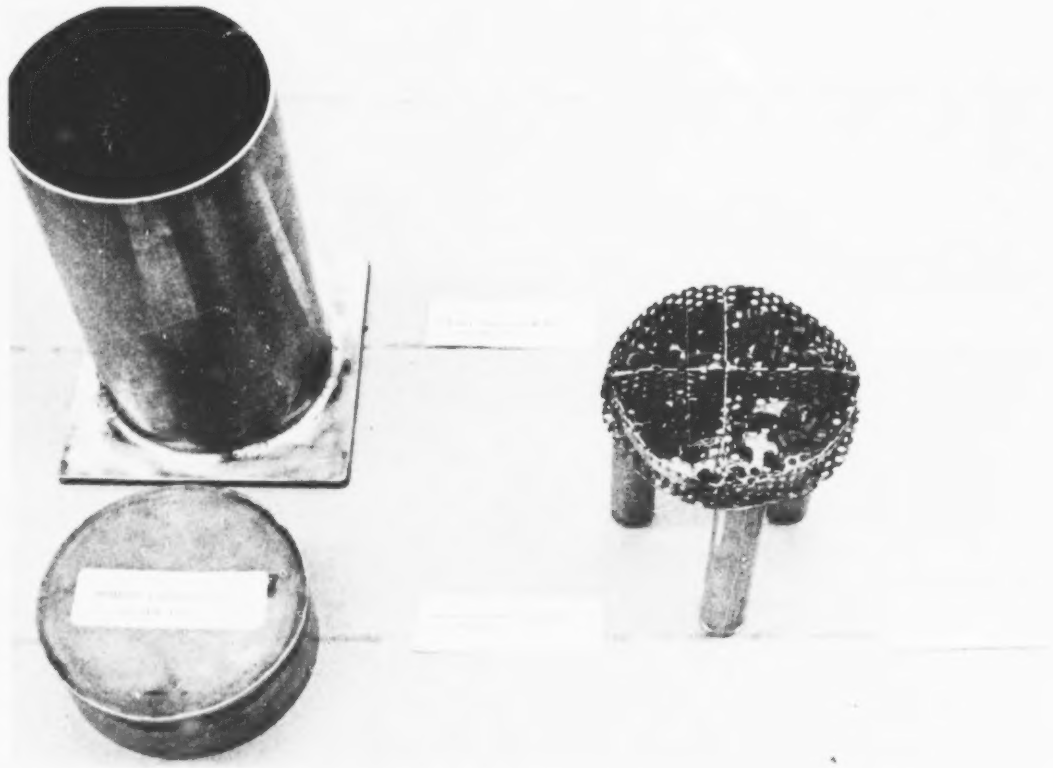

FIGURE C-2. COMPONENTS OF THE HUMIDITY CHAMBER

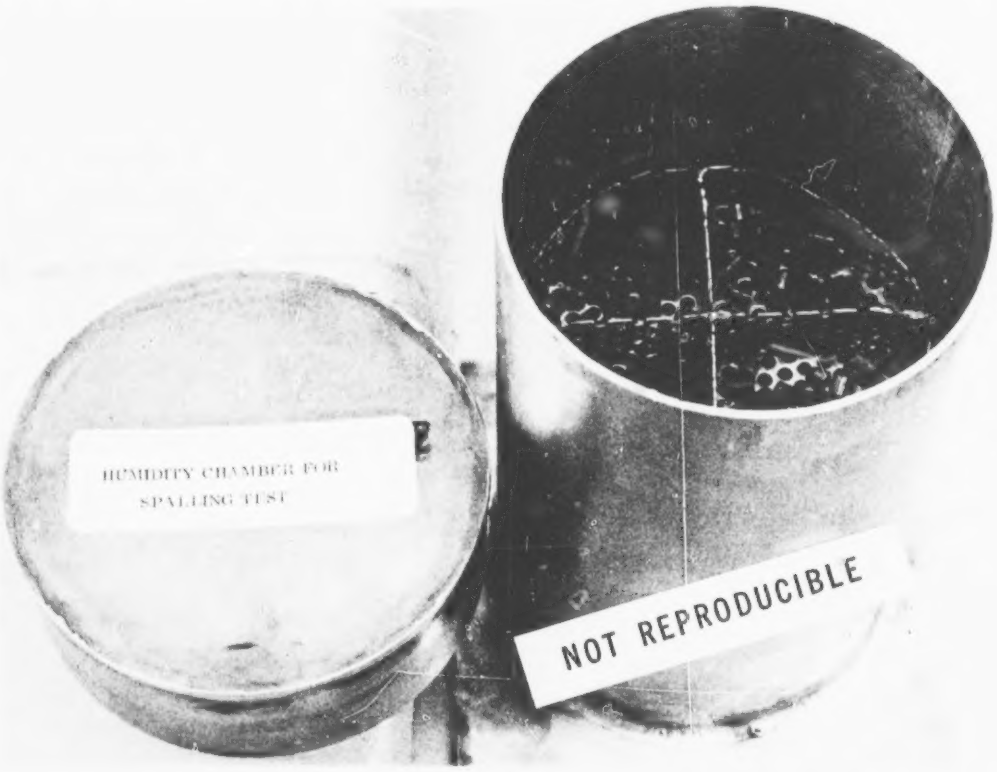

HUMIDITY CHAMBER FOR
SPALLING TEST

NOT REPRODUCIBLE

FIGURE C-3. CATALYST FORMULAS INSERTED INTO HUMIDITY CHAMBER

TABLE C-I

WEIGHTS OF CATALYSTS BEFORE, DURING AND AFTER SPALLING TEST

Formula	Weight Before Test g	Weight During Test g	Weight After Test g
RE(23)75	9.819	9.828	9.806
RE(23)75-P	9.112	9.280	9.025
RE(M3)75	10.033	10.199	10.016
$CuCr_2O_7$	10.050	10.232	9.925

Figure C-4 gives a view of all four catalysts after the spalling test. For the copper dichromate no change in appearance was noted. The results for the other three catalyst formulations are as follows:

- Solar Catalyst Formula RE(23)75-P: No change in appearance noted.
- Solar Catalyst Formula RE(M3)75: Only minor changes in the surface noted. Small longitudinal cracks, which were present in the original pellets before the spalling tests, became slightly enlarged. These cracks were a function of the preparation of the catalysts and have now been eliminated by improving the preparation procedures, therefore, it can be said that the spalling test had no effect on the formula RE(M3)75 either.
- Solar Catalyst Formula RE(23)75: Small cracks which were present in the pellets before the test became noticeably enlarged. This formula showed the least spalling resistance and can be expected to fall apart on the repeated humidity-and-heat treatment.

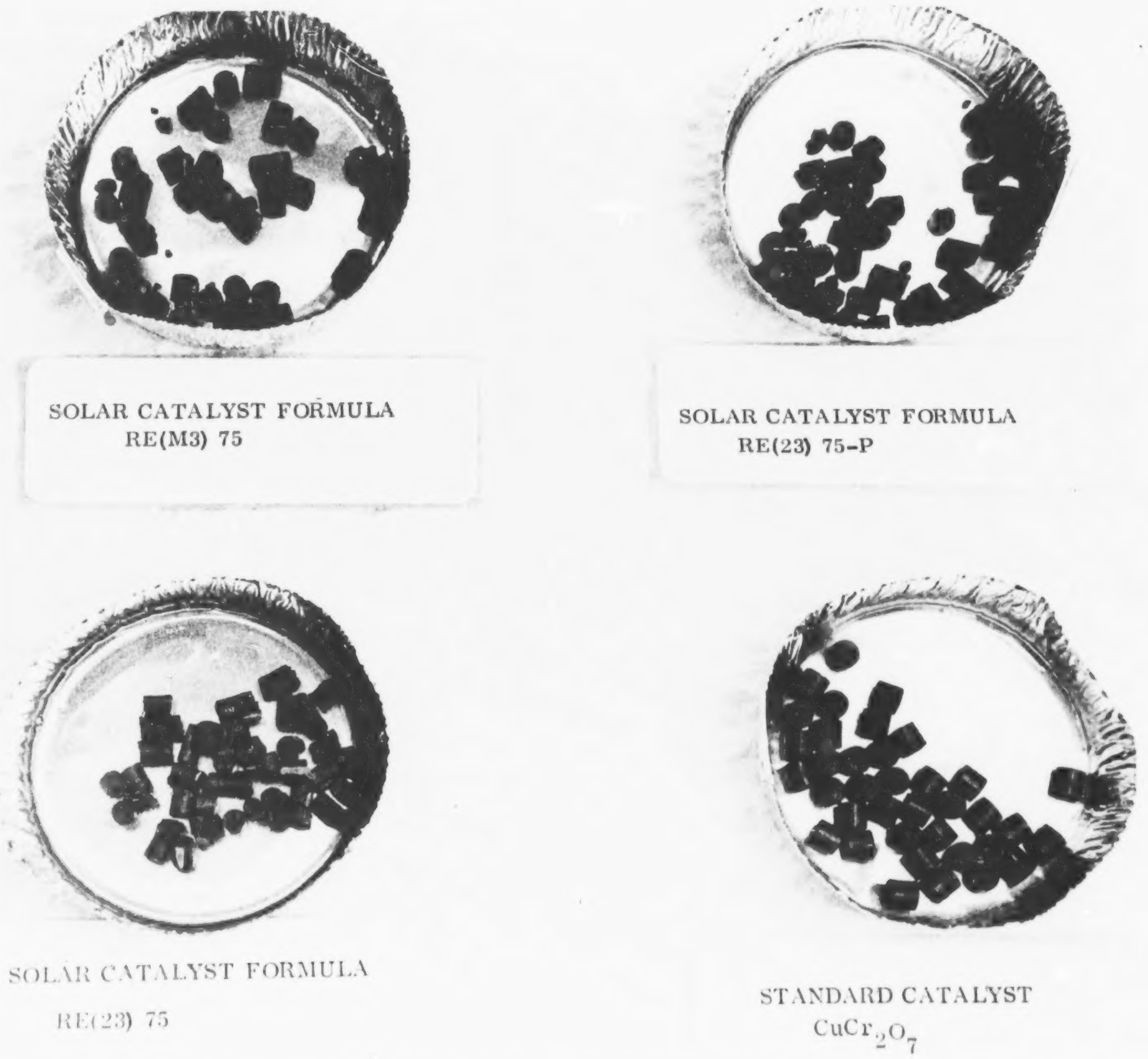
SOLAR CATALYST FORMULA
RE(M3) 75
SOLAR CATALYST FORMULA
RE(23) 75-P
SOLAR CATALYST FORMULA
RE(23) 75
STANDARD CATALYST
$CuCr_2O_7$

FIGURE C-4. SOLAR CATALYST FORMULAS AS THEY APPEARED AFTER SPALLING TEST

NOT REPRODUCIBLE

APPENDIX D

Preceding page blank

APPENDIX D

RARE EARTH OXIDE CATALYST CHEMICAL PROPERTIES - LEAD POISONING AND REGENERATIVE STUDY OF CATALYST FORMULAS RE(23)75-P and $CuCr_2O_7$

The object of this test was to show that the rare earth oxide catalyst, once it is covered by lead deposits, can be regenerated by chemical means, while the copper dichromate catalyst and others in its class would be lost. The nature of this study was preliminary, since no catalytic efficiency studies after the restoration of the pellet, were made. This experiment was not completed in that respect due to the change of emphasis in the program, since it is now expected that unleaded fuels will be widely available in 1975, if required by catalytic systems, which will prevent the lead poisoning of catalytic systems.

For the lead-poisoning and regeneration study described in this appendix, we selected

10 grams of catalyst RE(23)75-P, which was 25 pellets, and

10 grams of copper dichromate - 38 pellets,

both of which were dessicated in order to remove the moisture adsorbed onto it. The following figures graphically describe the experimental procedure followed in this catalyst poisoning and regeneration experiment.

(a) Poisoning of the Catalysts

The view of these catalysts as they appear before the test, after the bakeout, is seen in Figure D-1. The purpose of these photographs is to give a comparison of the catalyst appearance before and during the lead poisoning test. Figure D-2 shows the retort in which the lead poisoning is taking place and its components. A stainless steel tube with a double bottom is seen in the background and in front of it a ceramic beaker, containing 10 grams of lead bromide and 12 grams of lead oxide, to yield the mixture $2PbO-PbBr_2$. A sieve-like boat for the two catalyst formulas is placed on top of the ceramic vessel containing the lead oxide and lead bromide, and the thermocouple is attached to the former to show the inside temperature of the retort. The Solar catalyst formula has been placed into the left cell of the boat

Preceding page blank

NOT REPRODUCIBLE

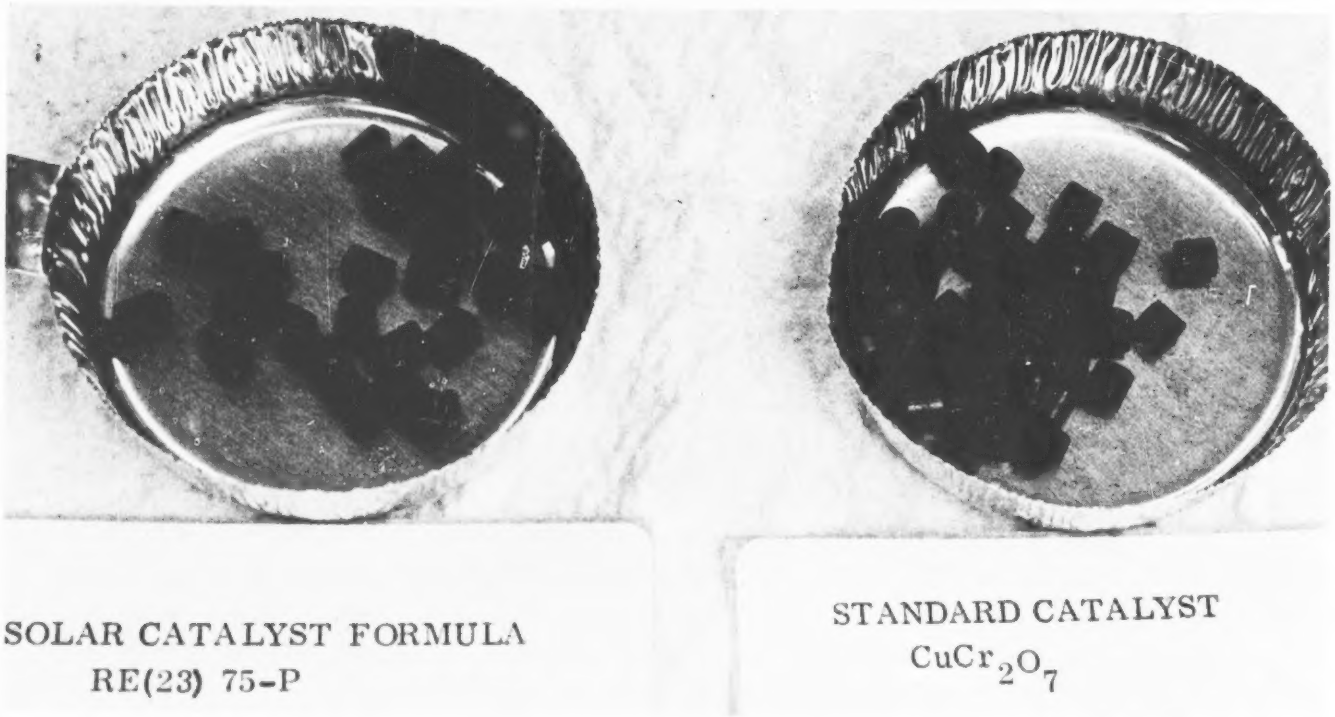
SOLAR CATALYST FORMULA
RE(23) 75-P
STANDARD CATALYST
$CuCr_2O_7$

FIGURE D-1. SOLAR CATALYST RE(23)75-P AND STANDARD CATALYST $CuCr_2O_7$ BEFORE LEAD POISONING TEST

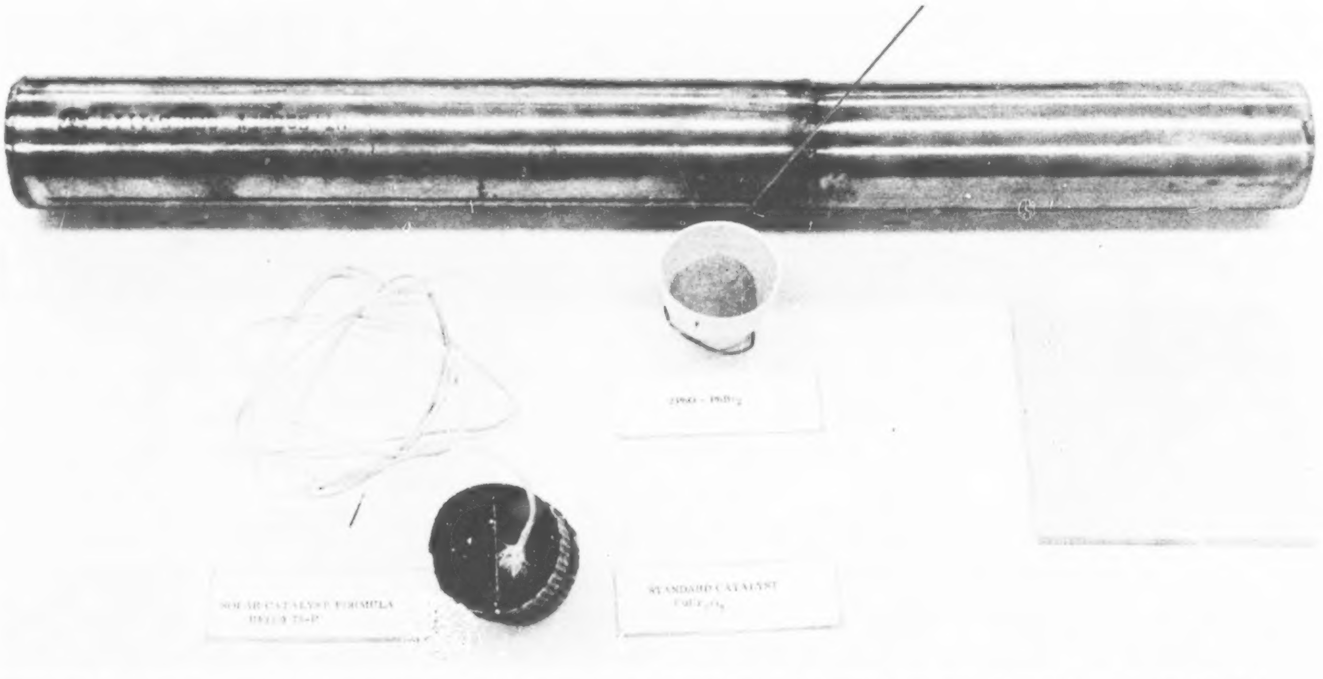
SOLAR CATALYST FORMULA
RE(23) 75-P
STANDARD CATALYST
$CuCr_2O_7$

FIGURE D-2. THE RETORT AND ITS COMPONENTS FOR THE LEAD POISONING TEST OF THE CATALYST and the standard catalyst into the right cell. Figure D-3 shows the operator, placing the ceramic boat containing the lead oxide-lead bromide into the retort, and Figure D-4, the placing of the catalyst boat on top of the lead salts. The retort is then placed into the furnace, as pictured in D-5, which is the same furnace being used for our gas flow apparatus.

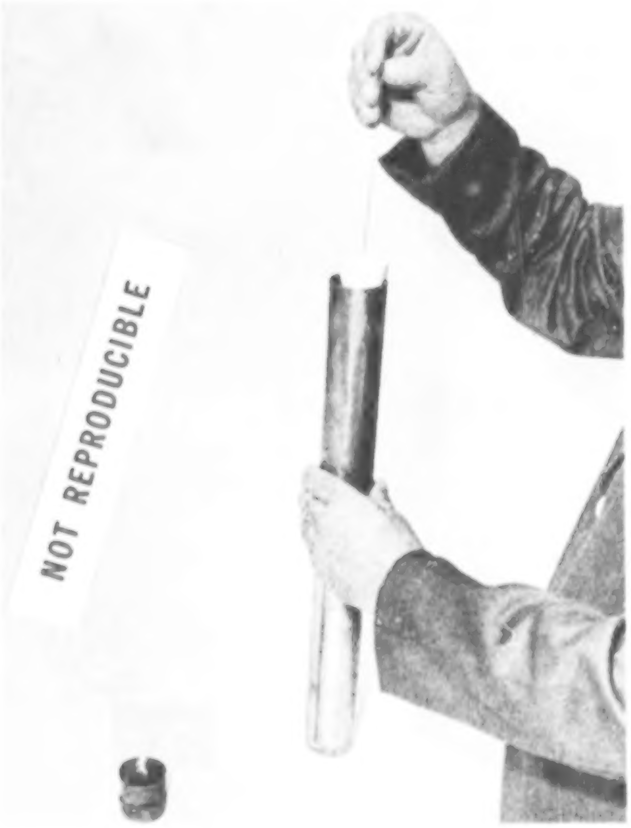

FIGURE D-3. THE BOAT WITH THE $2PbO-PbBr_2$ IS INSERTED INTO THE RETORT

The retort was heated for 2 hours and the catalyst was then removed, weighed and returned into the heated fumes for 3 more hours. After that the poisoning phase of the test was completed.

Figure D-6 shows the dissembled retort after the test. All components were found to be coated with lead. The lead salts in the ceramic boat were completely boiled out. Table D-I will summarize the weights of the two catalysts as originally selected, as they appeared after the bake-out, as they appeared after 2 hours of exposure to lead vapor, then after 5 hours exposure, and finally after the washing.

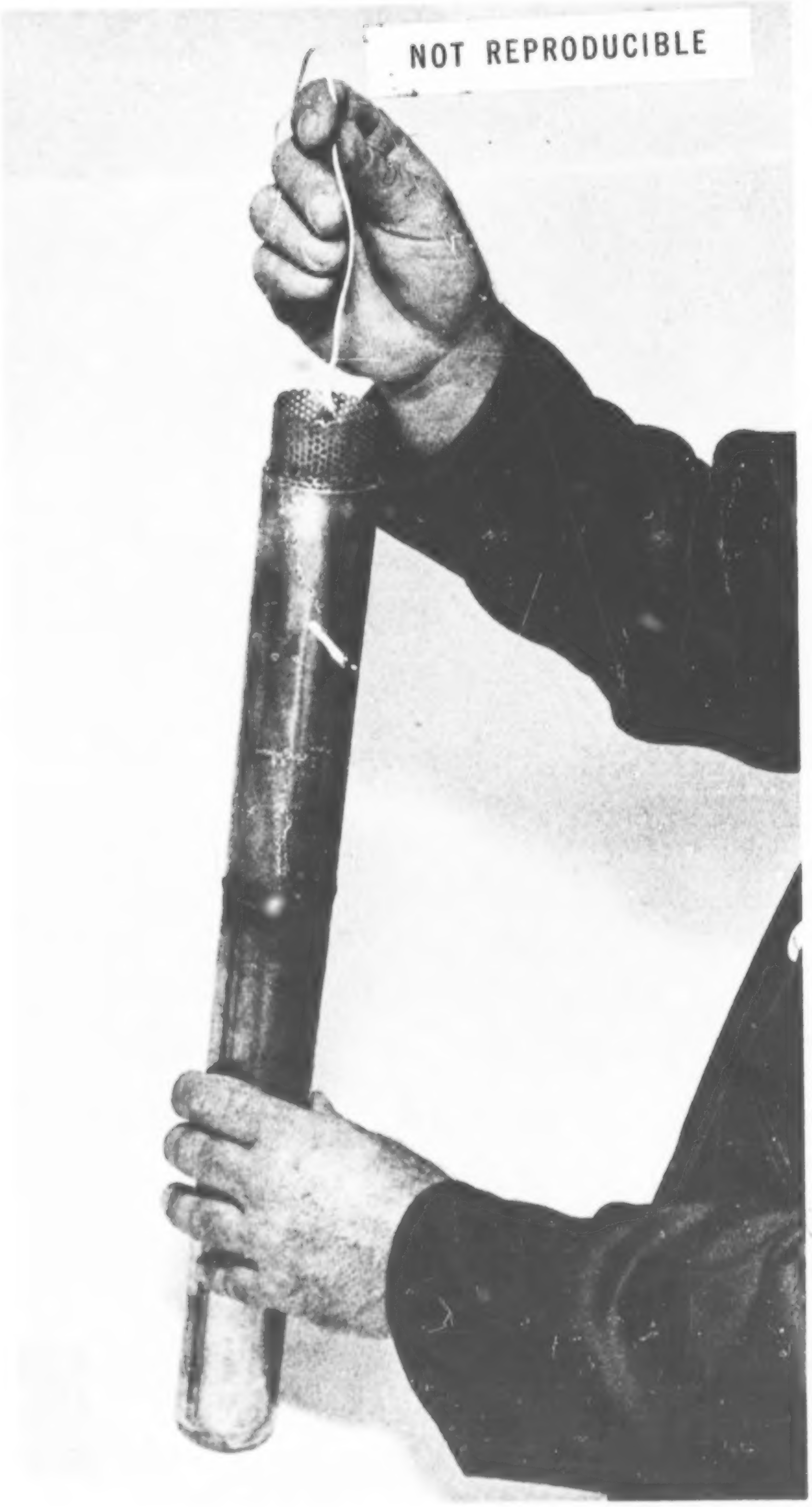
NOT REPRODUCIBLE

FIGURE D-4. THE CATALYST BOAT IS PLACED ON TOP OF THE BOAT CONTAINING THE LEAD OXIDE-LEAD BROMIDE, AND THE RETORT IS THEN COVERED WITH THE CERAMIC BLOCK AT LEFT

NOT REPRODUCIBLE

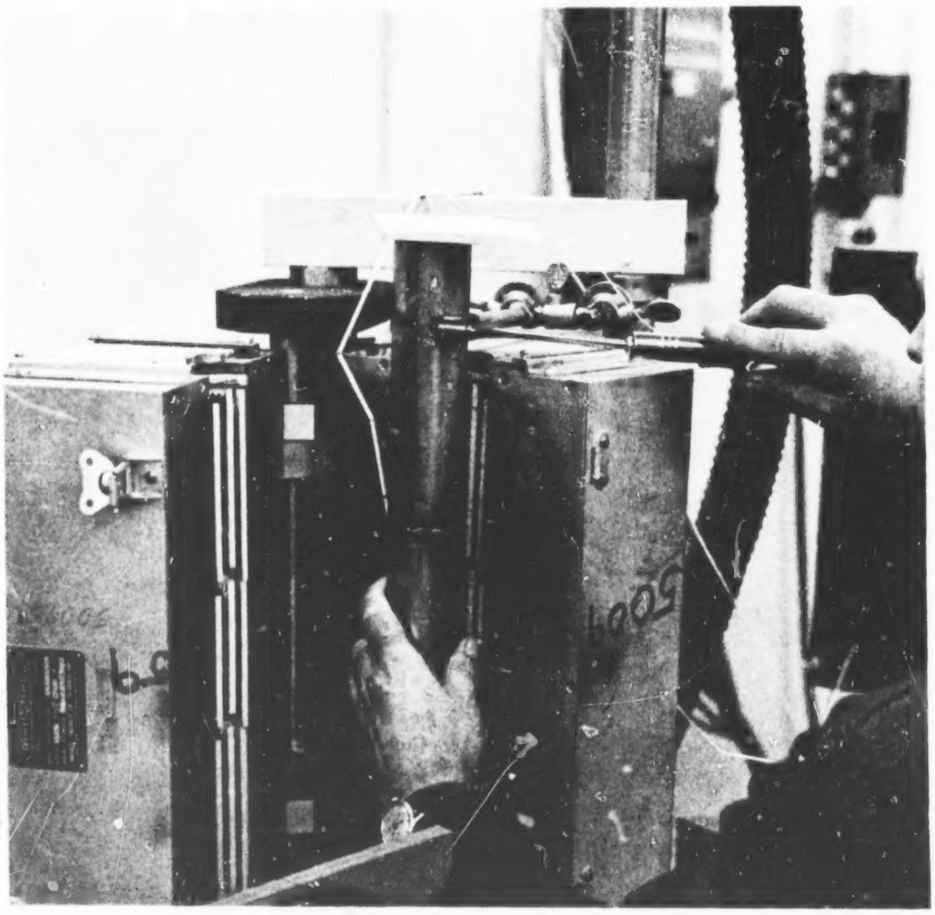

FIGURE D-5. OPERATOR PLACES RETORT INTO FURNACE TO MELT THE LEAD COMPOUNDS

The appearance of the catalysts, after being coated by the lead vapors, is shown in Figures D-7A and 7B, which are close-ups of the poisoned catalyst formulas. Of special interest here was the observation that the copper dichromate did not gain any weight but instead lost some. This is ascribed to be due to possible reactions of the copper oxides and chrome oxides with the lead vapors. A check of the dimensions of the copper dichromate pellets showed that there was no change from those prior to the test in spite of the loss of weight.

(b) Restoration of the Catalysts

After the poisoning test was completed, both catalysts were placed in test tubes to which diluted nitric acid was added. This is seen in Figure D-8. Note the immediate discloration of the washing liquid containing the standard copper dichromate catalyst. Figure D-9 shows that the catalysts in their nitric acid baths are heated, though not over the flame as indicated in the picture, but in boiling water baths. During this procedure the liquid containing the copper dichromate turned green, while the liquid containing the rare earth oxide catalyst remained clear.

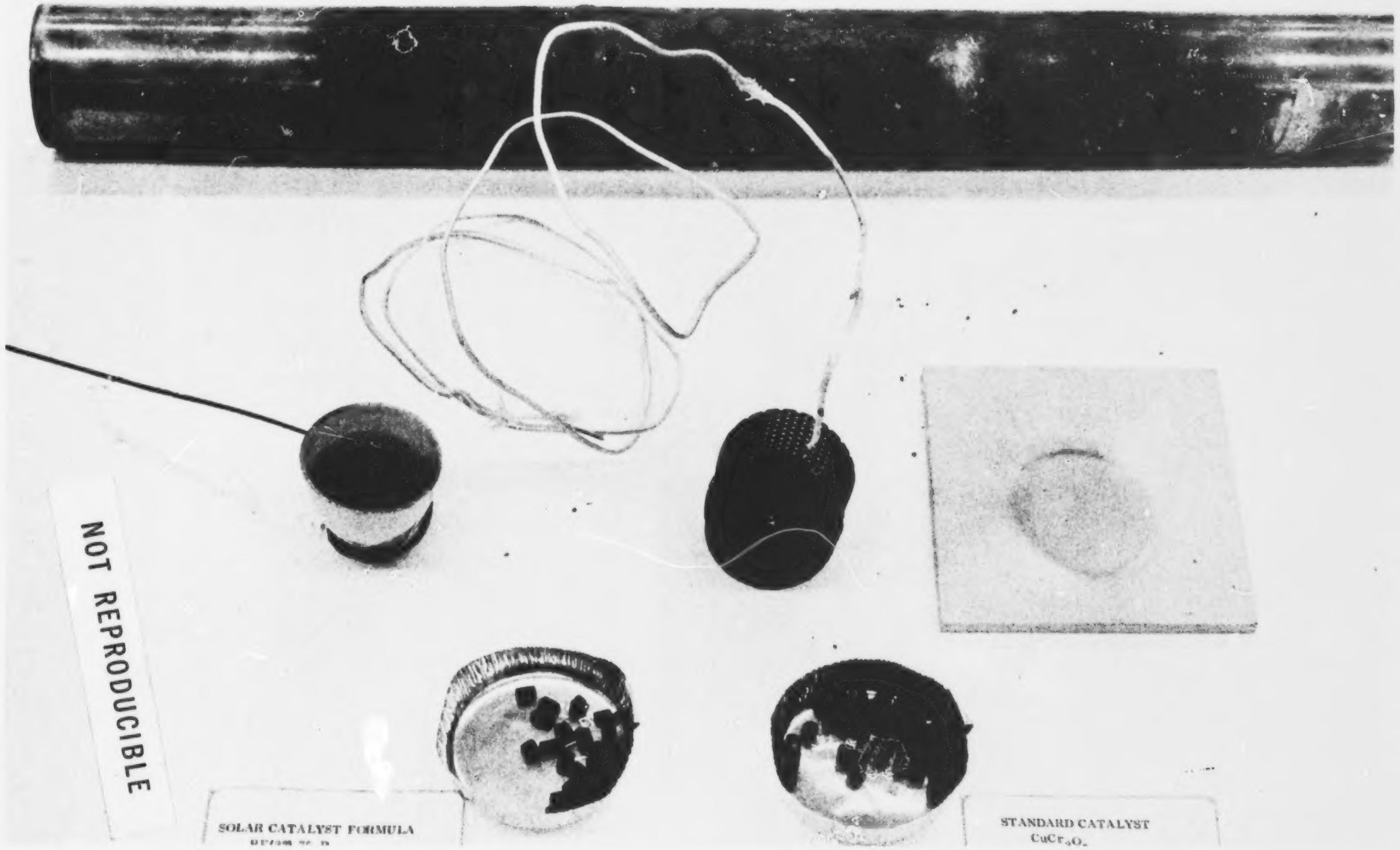
SOLAR CATALYST FORMULA
STANDARD CATALYST
CuCr₂O₄

NOT REPRODUCIBLE

FIGURE D-6. RETORT AND ITS CONTENTS AFTER THE LEAD POISONING TEST. NOTE DEPOSITS ON CATALYST BOAT AND CERAMIC TOP

TABLE D-I

CATALYST WEIGHTS DURING POISONING AND REGENERATION EXPERIMENTS, IN GRAMS

Date	Condition	RE(23)75-P net weight	CuCr$_2$O$_7$ net weight
11-20	Original weight	10.0049	10.1144
11-23	Weight after dessication, start of exp.	10.0016	10.0996
11-23	Weight after 2 hours exposure to Pb	9.9846	9.6651
11-24	Weight after 5 hours exposure to Pb	9.9942	9.5963
11-25	Final weight, after restoration	9.5904	None
	Remarks	4% loss	100% loss

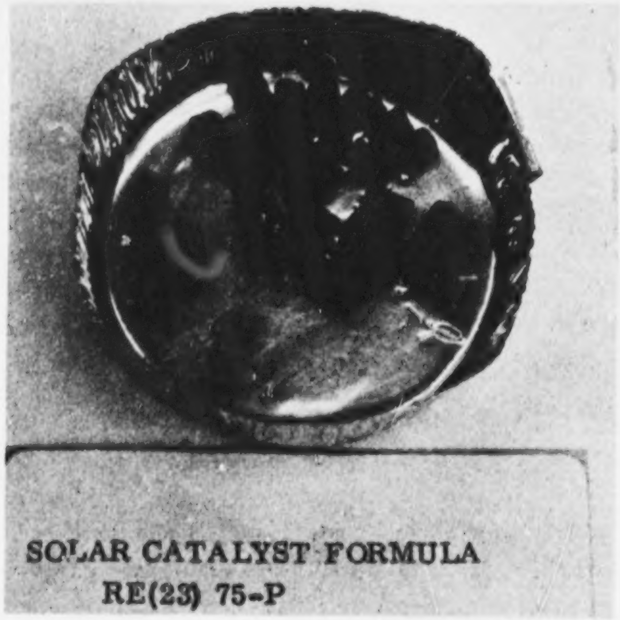

FIGURE D-7A. CLOSE-UP OF LEAD POISONED SOLAR CATALYST FORMULA RE(23)75-P

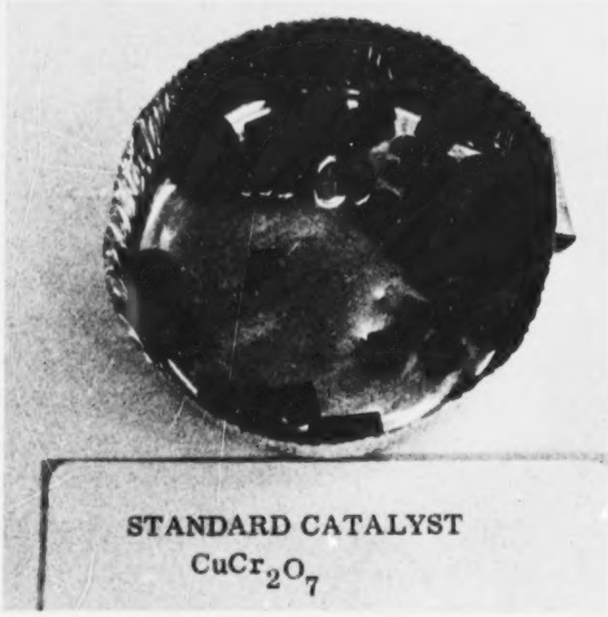

FIGURE D-7B. CLOSE-UP OF LEAD POISONED STANDARD CATALYST CuCr$_2$O$_7$

NOT REPRODUCIBLE

NOT REPRODUCIBLE

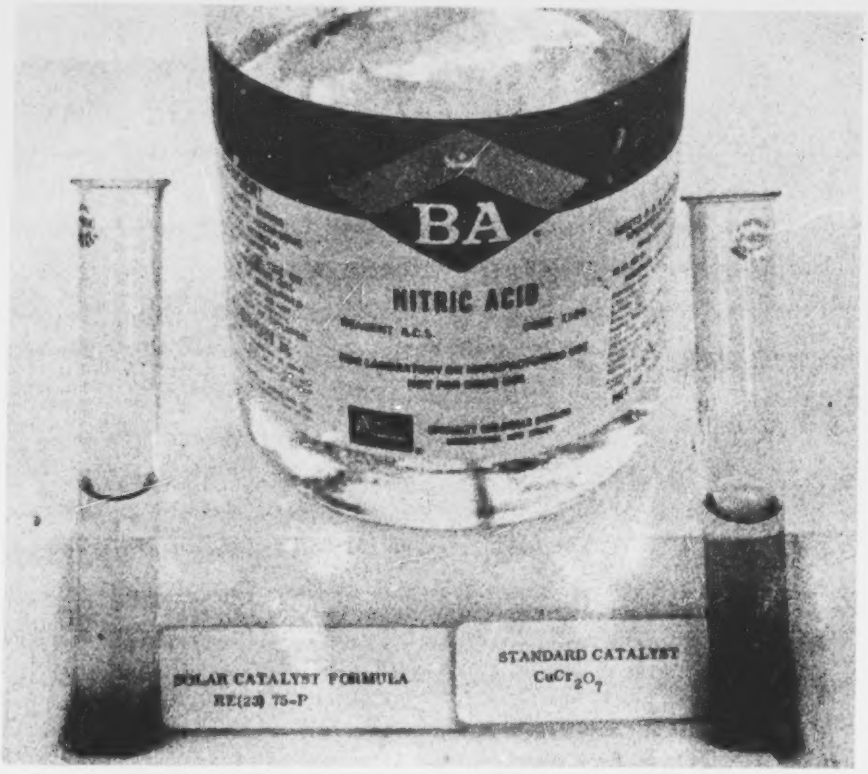

FIGURE D-8. BOTH CATALYSTS ARE IMMERSED IN DILUTE NITRIC ACID (DILUTION 1:1) TO WASH OFF POISONING LEAD DEPOSITS. NOTE DISCOLORATION IN LIQUID OF $CuCr_2O_7$ BATH

After 75 minutes boiling time the copper dichromate-containing test tube showed advanced dissolution of the pellets. The liquid of the test tube containing catalyst formula RE(23)75-P had turned slightly yellow. The yellow liquid from the REO catalyst was then recovered and fresh dilute nitric acid substituted. The copper dichromate containing test tube was left unchanged and the boiling continued. The liquid recovered from the REO catalyst was tested for contents of lead by the following method:

To the washing liquid dilute sulfuric acid is added. The precipitation of white crystals indicate the presence of lead sulfate. In this case the washing of the pellets at 250° F in diluted nitric acid was continued, until no precipitate in the new washing liquid was found. The result of this procedure is shown in Figure D-10. Here we have the REO catalyst formula, which has been washed in two nitric acid baths and then rinsed in distilled water, dried and placed on a Petrie dish. The lead sulfate precipitate from the first washing water is shown in the test tube appearing behind the rare earth oxide dish. On the other hand, the copper dichromate completely dissolved in its nitric acid bath, and its test tube is shown along with the empty Petrie dish for the standard catalyst. This result then shows that standard commercial catalysts and those in their class cannot be recovered once they have been poisoned by lead oxides and sulfur oxides, while the REO based catalysts can be regenerated.

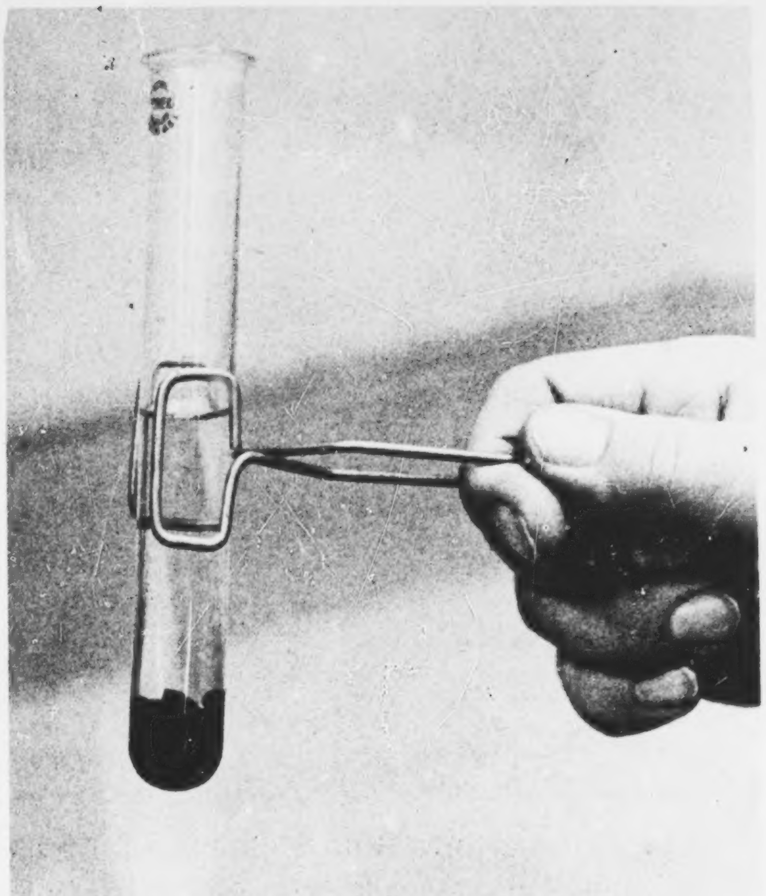
NOT REPRODUCIBLE

FIGURE D-9. SYMBOLIC REPRESENTATION OF HEATING STEP FOR WASHING OF POISONED CATALYSTS

NOT REPRODUCIBLE

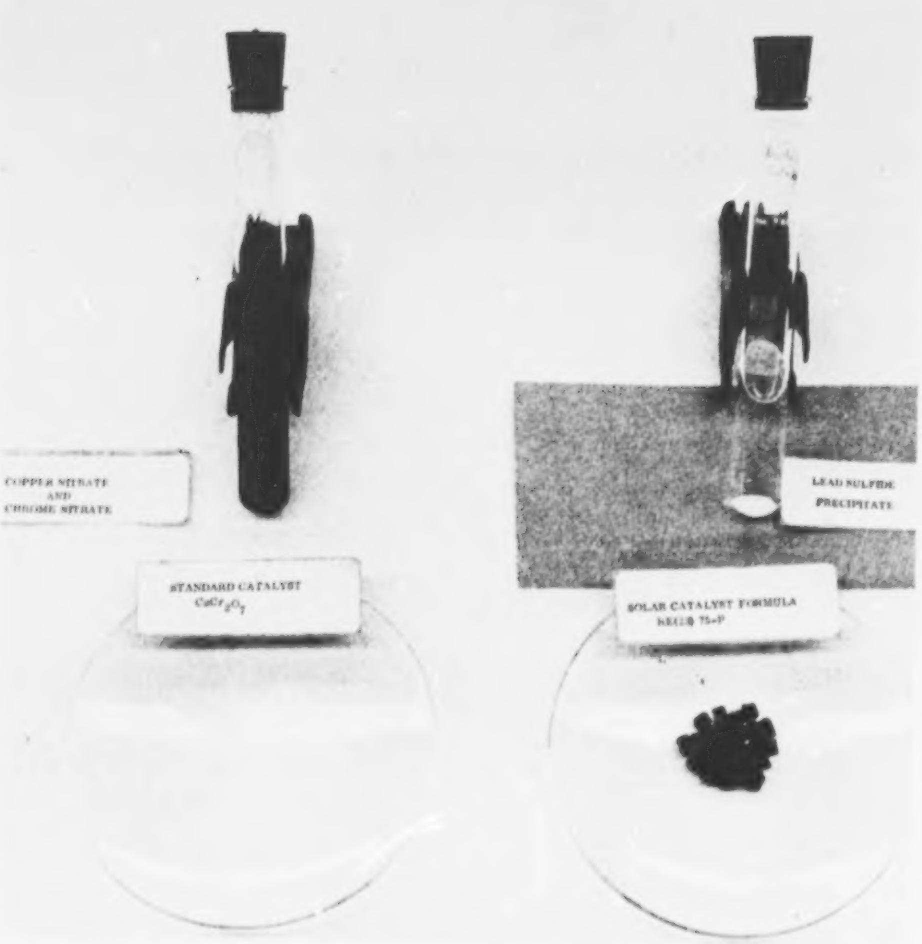
COPPER NITRATE
AND
CHROME NITRATE
STANDARD CATALYST
$CuCr_2O_7$
LEAD SULFIDE
PRECIPITATE
SOLAR CATALYST FORMULA
RE(23) 75-P

FIGURE D-10. RESULTS OF RESTORATION OF POISONED CATALYSTS. LEAD DEPOSIT FROM RE(23)75-P WASHED RIGHT OFF, FORMING A WHITE DEPOSIT WITH ADDITION OF DILUTE SULPHURIC ACID. $CuCr_2O_7$ PELLETS DISSOLVED IN WASHING LIQUID

Figure D-11 is a close-up view of the REO catalyst after the lead poisoning and restoration test. All 25 pellets are restored. As seen from Table D-I there was a four percent loss in weight in this catalyst after the described procedure.

The conclusion of the experiments shows that copper dichromate cannot be regenerated by this procedure from lead poisoning and thus is lost. The high purity REO catalyst, RE(23)75-P, can be regenerated from lead poisoning and can be reused.

NOT REPRODUCIBLE

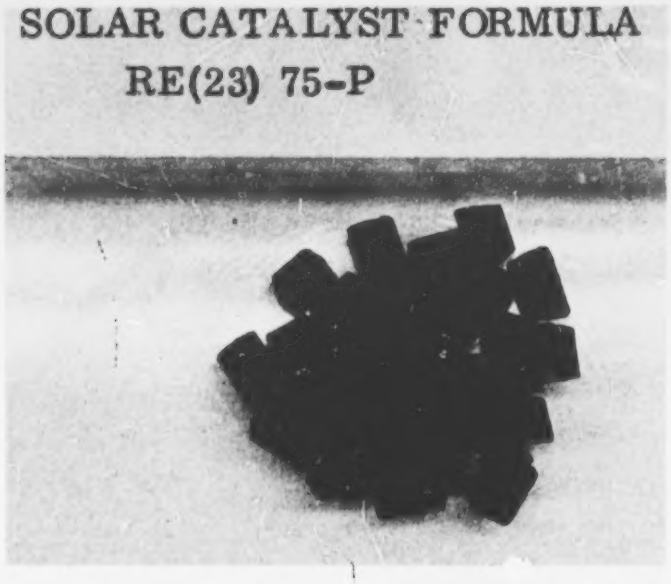
SOLAR CATALYST FORMULA
RE(23) 75-P

FIGURE D-11. CLOSE-UP OF RESTORED SOLAR CATALYST FORMULA RE(23)75-P AT CONCLUSION OF TEST

APPENDIX E

Preceding page blank

APPENDIX E

THE ECONOMICS OF THE REO CATALYSTS

Availability of Rare Earth Oxides

In any applications contemplating the use of rare earths because of their unique properties, the first thing one should do is dispel the notion that these elements are rare, when as a matter of fact, this group of elements, including scandium and yttrium, comprise about 25 percent by weight of the metallic elements in the periodic table. (Ref. 23). Cerium is more abundant than tin, and yttrium and neodymium are more abundant than cobalt. Even the scarcest of the rare earths are more abundant than the more commonly known metals such as silver, gold, and platinum.

Of the various sources of rare earths, as euxenite, xenotine, monozite, and bastnasite, the bastnasite source is the most significant. The United States is fortunate in this respect as it possesses the world's largest bastnasite deposit at Mountain Pass, California, which is located in the Sierra Nevada Mountains near Las Vegas, Nevada. This particular orebody supplied 60 percent of the 1969 world shipments of the "light" rare earth oxides, which include oxides of lanthanum, cerium, neodymium, praseodymium, samarium, and europium. Present production of rare earth oxides from this particular source is 25,000 tons annually, with the capability of increasing this to a 50,000 ton annual capacity. It is reported that proven reserves for the Mountain Pass deposit are five billion pounds of REO (rare earth oxides), with indicated reserves of several times that amount (Ref. 24). Thus it appears that an ample supply of "light" rare earth oxides is assured for some time to come.

Analysis of Requirements and Cost of REO for Automotive Catalysts

Two forms of rare earth oxide catalysts for use in automotive exhaust systems are contemplated:

- Pressed and sintered pellets of varying porosity
- Relatively thin coatings of the oxides upon some sort of support medium exhibiting a large active surface area.

Preceding page blank

Because of convenience, preliminary studies at Solar have made use of the pellet form. But of the two, for reasons of economy and effectiveness, the supported catalyst would appear to have the greatest potential in the long run.

The following cost analysis is based upon the latest and best price information available to date, and upon the assumption that automobile sales will average about 10 million annually. Historically, the price of rare earths has decreased approximately 10 percent per year over the past several years. The figures obtained for this study have taken this factor into account and were projected into the near future, using the best facts and judgment available to the industry. (Ref. 25).

Another fact which must be kept in mind in any cost analysis is the saleability of the byproducts when considering the use of a single oxide, or say a mixture of just two oxides. For example, the distribution of the rare earths in bastnasite is given below. If we were only interested in praseodymium oxide, it would mean the production of 25 times that amount of cerium, lanthanum, and neodymium oxides as byproducts. Unless these were saleable, the entire cost would have to be borne by the praseodymium oxide. This, of course, is another incentive for the use of the mixed oxides, if at all possible. Preliminary investigations at Solar indicated that the proper blend of oxides may indeed provide a satisfactory automotive catalyst for NO reduction.

Rare Earth	Percent in Bastnasite
Cerium	50
Lanthanum	34
Neodymium	11
Praseodymium	4
Samarium	0.5
Gadolinium	0.2
Europium	0.1
Others	0.2

Pelletized REO Catalysts

Assuming a production of 10^7 automobiles per year, a requirement of 15 pounds of oxide catalyst per unit, and use of the maximum amount of any one of the oxide constituents, the question of supply and availability would appear as follows:

- REO (Mixed RE Oxides) - Proven reserves of bastnasite deposits in the U.S. indicate 5 x 10^9 lb of REO or, on the basis of 1.5 x 10^8 lb/yr, a supply for at least 33 years.

- Cerium Oxide (CeO_2) - Bastnasite contains 50 percent, which translates to about 2.5 x 10^9 lb total. This amounts to at least a 20 year supply.

- Lanthanum - Neodymium - Praseodymium Oxides ("Didymium") - Since this mixture comprises 47 percent of bastnasite, the supply situation will be roughly the same as the cerium oxide above.

- Praseodymium Oxide (PrO_x) - At four percent of bastnasite, the requirements of 4 x 10^7 lb/yr would mean a supply of about five years.

Figure E-1 summarizes the results of a cost analysis based upon the presently proposed Solar formulations. Depending upon the purity of the component oxides or mixtures of the RE oxides, the cost of the catalytic agent would vary from a high of $4.08/lb for RE(23)75 of 99 percent purity to a low of $0.45/lb for RE(M) of a 90 percent purity level. It would be well to remember at this point, that the cost of the higher priced formulations could no doubt be lowered substantially by optimizing and refining the compositions of the present catalytic agents.

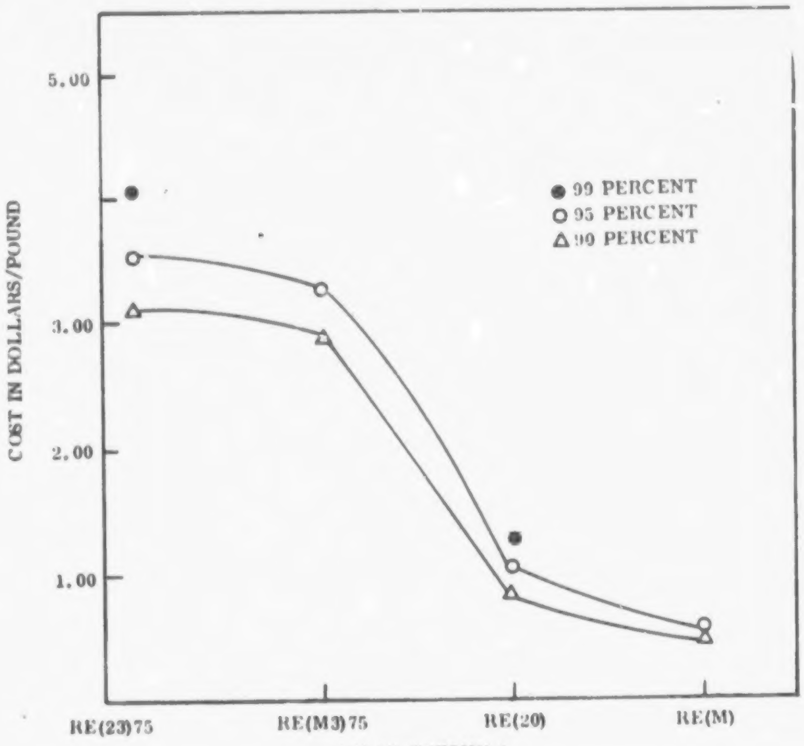

FIGURE E-1. COST OF CATALYTIC AGENTS OF VARYING PURITY

REO Coatings on Support Medium

Estimated requirements for a supported catalyst call for approximately one pound of rare earth oxides per automobile, or 10^7 lb annually. Although the required supply is roughly an order of magnitude smaller than what is needed for the pelletized form of catalyst, the cost of the raw materials is not expected to be any different. Using the same approach as before, the supply picture would appear as given below.

- REO (Mixed RE Oxides) - Bastnasite reserves of 5×10^9 lb of REO and a need for 10^7 lb annually would translate to a supply of the mixed oxides that would last at least 500 years.
- Cerium Oxide (CeO_2) - At 50 percent of 5×10^9 lb, a supply would be assured for a minimum of 200 years.
- Lanthanum - Neodymium - Praseodymium Oxides ("Didymium") - As in the case of cerium oxide, enough of the material should be available for approximately 200 years use.
- Praseodymium Oxide (PrO_x) - At the lower level of use, we could count on at least 50 years supply.

In summary, it is apparent that the supply of rare earth oxides is more than adequate to serve the needs of an automotive catalyst based on 10^7 new cars per year for some time to come, without any consideration at the present time for reactivating used catalytic material.

Life Cycle Aspects of REO Catalysts

The foregoing discussions were based on the assumption that there would be no need to reuse the catalytic material, because the supply appears adequate at this time. In reality, however, the national concern for environmental pollution, including the generation of solid wastes, would dictate that serious consideration be given to the recycling of the catalytic agents.

It is generally known that lead and lead compounds tend to poison catalysts and thus render them useless. Furthermore, lead and its compounds are extremely corrosive to most metals and their oxides, particularly at elevated temperatures.

Studies at Solar with the copper dichromate and REO pellets in a molten $2PbO\text{-}PbBr_2$ mixture indicate a drastic deterioration of the copper dichromate catalyst, whereas the REO pellets appeared to be fully resistant to this highly corrosive environment.

Another aspect which is also worthy of consideration is that of conservation of relatively scarce and critical materials. (Ref. 26). Copper dichromate would certainly fit into this category, as copper occurs to the extent of only 64 ppm average in the earth's crust and the chromium supply is located in areas which are inaccessible to the U.S. for political reasons. Although it is true that the relative average abundance of an element such as cerium (46 ppm) is less than that of copper, the reactivation aspect mentioned above could minimize this apparent shortcoming. In addition, there are so many other applications requiring the use of copper and chromium that the demand could conceivably exceed the supply of these materials.

The Comparative Economics of the Rare Earth Oxide Catalysts With Common Noble Metal Catalysts

In our study on the cost per pound of catalysts, we are comparing the various catalyst materials considered earlier with platinum metal catalysts, both in pure and supported and in pellet forms, and with the commercial copper dichromate catalysts. Figure E-2 gives a schematic view of the costs of the various catalysts starting from the most expensive one, osmium powder, down to the least expensive one. The cost ranges between $3,300 for the most expensive pure noble powder per pound to $1.20 per pound for copper dichromate or pure supported cerium oxide catalyst. Figure E-2 divides the catalysts into several groups. Group 1 is the pure noble metal powders, which are of course the most expensive, ranging in cost from $3,300 to $540 per pound.* Next follows the noble metal powders supported on carbon. These range from $230 per pound to $68 per pound.* Then follow the supported noble metal catalyst pellets which range between $135 and $36 per pound. Next down in cost is the category of the high purity rare earth oxide catalyst pellets, whereby the high purity is 96 or 99 percent rare earth oxide. Here the high goes from $30 per pound for praseodymium oxide down to a low of $6 per pound for cerium oxide. (Ref. 25). In between these two are costwise the didymium oxides and the pure Solaform 8 and the pure Solaform 10 formulas. The commercial mixed oxides, unenriched with anything, are comparable in price with the commercially available copper dichromate. The rare earth oxides as such, cost $2.40 per pound and the didymium oxide $1.85 (Ref. 25); the copper dichromate in comparison is $1.20. If we support our catalyst formulas on alumina pellets, which come to about 60 cents per pound, using the approximation that for a supported catalyst, only 10 percent of the quantity of the unsupported catalyst is needed, the cost for the pure praseodymium catalyst supported is $4.60, while the pure cerium oxide supported catalyst would be equal to the copper dichromate cost of $1.20. The range of all these catalysts in cost per pound is shown on Figure E-2, which also shows the acceptable upper limit for the catalyst material cost of $8.30 and the mean catalyst cost per pound

---

* Phone conversation with Mr. T. Romeo of Engelhard Co., 6001 Bandini, Los Angeles, California, week of September 20, 1970.

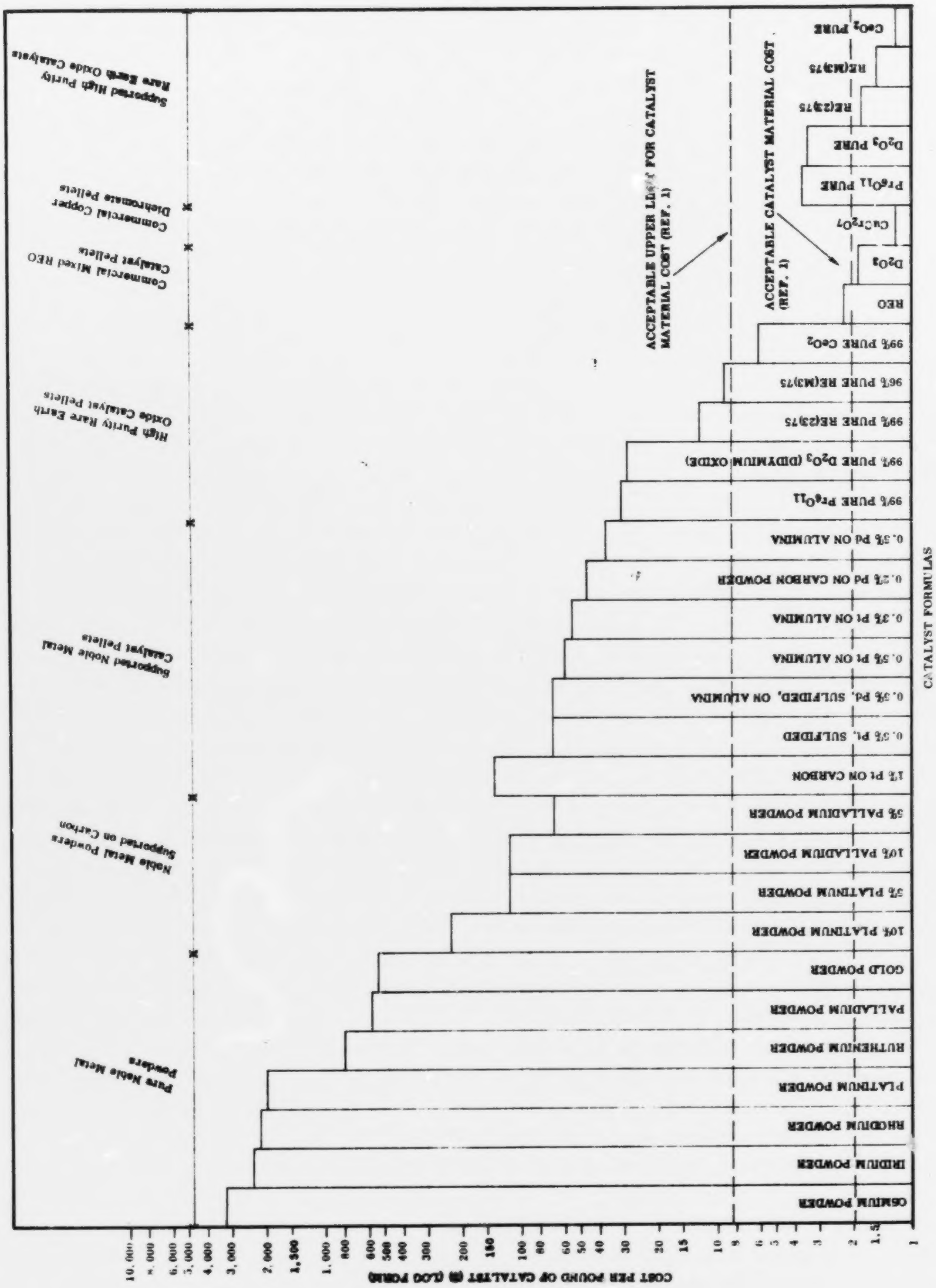

FIGURE E-2. ECONOMICS OF CATALYSTS

of \$2.00 (obtained from Ref. 6). If a catalyst is more expensive than this upper limit, it would be economical to support it on alumina pellets or on carbon. Catalysts, which by themselves cost less, could be used in their pure state. It has to be considered here, however, that with the decrease in the purity of the rare earth oxides, the price of the rare earth oxides will decrease. The prices for the rare earth oxides are based on 100 pound quotations. For quantities in the amounts of tons, the prices might decrease by 50-70 percent. Therefore, it appears reasonable that Solar Formulas 8 and 10 both could be economically used in large quantities and lower purity in the unsupported state as well as the supported state.

APPENDIX F

Preceding page blank

APPENDIX F

AMERICAN OIL COMPANY EVALUATION OF SOLAR NO_x CATALYST BY PULSE-FLAME METHOD

AMERICAN OIL COMPANY

RESEARCH AND DEVELOPMENT DEPARTMENT 2500 NEW YORK AVENUE WHITING, INDIANA 46394

H. R. TALIAFERRO
Coordinator-Automotive
Emissions Research

July 1, 1971

AIR MAIL--SPECIAL DELIVERY
Mr. W. A. Compton
Assistant Director--Research
Solar
2200 Pacific Highway
San Diego, California 92112

Dear Sir:

Re: Evaluation of Solar NO_x Catalysts

Your Solar catalysts were evaluated using the pulse-flame apparatus developed by Dr. Meguerian and described in some detail in the attached paper.* Isooctane was used as the fuel. The results of our evaluation are listed in the attached tables.

We wish to make the following observations based on these data and visual examination of the catalysts:

(1) Both catalysts are mechanically very weak. During shipment to us, considerable pellet break-up occurred. The attached photograph shows the condition of the catalysts as received.

---

* Reference 5

(2) At 650°C and 800°C, significant NO_x reduction was obtained at a CO concentration of about 1% (Tables I and II). However, higher CO levels were required to obtain a NO_x reduction level of 90% or more. Because this level was attained at a lower CO concentration with catalyst No. 2 than with No. 1,** No. 2 is the better catalyst. At 550°C, both catalysts were not active except at very high CO concentrations.

(3) A substantial fraction of the NO_x was reduced to NH_3 over both catalysts. Although less NH_3 formed over catalyst No. 1 than over No. 2, NH_3 is unacceptably high in both cases. At 800°C, we have observed 10% or less conversion to NH_3 with some catalysts.

We are returning both the used and unused portions of your catalysts under separate cover.

If you have any questions with regard to our data, please call me.

Very truly yours,

HR Taliaferro

H. R. TALIAFERRO

Attachments

** Catalyst No. 1 is Catalyst RE(M3)75, here denoted also M3
Catalyst No. 2 is Catalyst RE(23)75-P, here denoted also 75-P

TABLE F-I

CATALYST EFFECTIVENESS

Solar No. 1 N-3

Space Velocity = 33,000 hr.$^{-1}$

% O_2	% CO	NO_x, ppm Inlet	NO_x, ppm Outlet	% NO_x Reduction
		550°C		
1.04	0.70	560	550	2
0.99	0.82	560	515	8
0.64	1.50	560	540	4
0.57	1.98	550	480	13
0.54	2.86	520	190	64
		650°C		
0.74	1.11	540	535	1
0.65	1.23	585	345	41
0.58	1.55	570	85	85
0.57	2.01	560	125	78
0.55	2.78	535	85	84
		800°C		
0.88	0.65	630	560	11
0.97	0.78	560	545	3
0.85	0.91	580	500	14
0.68	1.12	630	260	59
0.76	1.18	555	245	56
0.64	1.32	520	185	64
0.61	1.38	675	150	78
0.70	1.40	550	185	66
0.60	1.83	540	5	99

Note: Space velocity is volume of gas per volume of catalyst per hour.

FWR/ac
7/1/71

TABLE F-II

CATALYST EFFECTIVENESS

Solar No. 2 75-P

Space Velocity = 26,000 hr.$^{-1}$

% O_2	% CO	NO_x, ppm Inlet	NO_x, ppm Outlet	% NO_x Reduction
		550°C		
0.98	0.59	670	575	14
0.77	0.89	595	560	6
0.73	1.01	605	560	7
0.73	1.28	550	475	14
0.64	1.36	590	455	23
0.57	1.80	520	375	28
0.67	2.32	650	170	74
0.54	2.60	610	225	63
0.58	3.67	565	190	66
		650°C		
1.04	0.57	610	600	1
0.75	1.11	530	240	55
0.74	1.13	580	330	43
0.61	1.61	610	90	85
0.58	2.24	620	45	93
0.57	2.30	560	15	97
		800°C		
0.90	0.59	615	580	6
0.83	0.89	550	270	51
0.76	1.02	550	220	60
0.69	1.27	600	125	79
0.66	1.43	560	60	89
0.63	1.50	510	15	97
0.61	1.69	600	15	98

FWR/ac
7/1/71

TABLE F-III

NH_3 PRODUCTION OVER SOLAR CATALYSTS

Space Velocity = 27,000 hr.$^{-1}$
Inlet NO_x = 1,350 ppm

Catalyst	Temp., °C	% O_2	% CO	% NO_x Conversion Overall	% NO_x Conversion To NH_3
No. 1 - M3	550	0.33	2.12	8	4
	650	0.32	2.39	52	37
	800	0.36	1.81	62	17
	800	0.33	1.63	80	16
No. 2 - 75P	550	0.42	1.72	7	5
	650	0.32	1.72	44	29
	800	0.42	1.85	83	63
	800	0.37	1.72	86	64
	800	0.41	1.72	82	58

FWR/ac
7/1/71